FEARS STRUCTURAL ENGINEERING LABORATORY

SEISMIC PERFORMANCE EVALUATION OF LIFELINES

by

Leon Ru-Liang Wang
and
Yaw-Huei Yeh

Sponsored by the National Science Foundation
Earthquake Hazard Mitigation Section
Civil and Environmental Engineering Division

Final Report for Grant No. CEE-8025172

Technical Report No. LEE-005
in Lifeline Earthquake Engineering Research Series

November 1982

School of Civil Engineering and Environmental Science
University of Oklahoma
Norman, Oklahoma 73019

50272-101

REPORT DOCUMENTATION PAGE	1. REPORT NO. NSF/CEE-82112	2.	3. Recipient's Accession No. PB84 184175
4. Title and Subtitle: Seismic Performance Evaluation of Lifelines, 1982 Final Report			5. Report Date: November 1982 6.
7. Author(s): L.R.L. Wang, Y.H. Yeh			8. Performing Organization Rept. No. LEE-005
9. Performing Organization Name and Address: University of Oklahoma, Fears Structural Engineering Laboratory, Norman, OK 73019			10. Project/Task/Work Unit No. 11. Contract(C) or Grant(G) No. (C) (G) CEE8025172
12. Sponsoring Organization Name and Address: Directorate for Engineering (ENG), National Science Foundation, 1800 G Street, N.W., Washington, DC 20550			13. Type of Report & Period Covered 14.

15. Supplementary Notes

16. Abstract (Limit: 200 words)

Experimental methods suitable for either overall or parametric seismic performance evaluation of lifeline systems are summarized. Ground motion characteristics, called the most influential parameter of all lifeline systems, are examined. Active field testing methods, passive field testing methods, and laboratory testing methods of below-ground systems are described. Parameters of importance to buried lifeline systems, such as lateral and longitudinal soil resistance characteristics and joint resistant behavior, are discussed. For above-ground lifeline systems, seismic observations, field testings, and model testing of bridges, above-ground pipelines, and communication lifelines are presented. It is said that above-ground lifeline systems can be evaluated by a multiple system table system; such a system is not yet available in the United States.

17. Document Analysis a. Descriptors

Earthquakes
Evaluation
Tests
Pipelines
Bridges
Communication cables

b. Identifiers/Open-Ended Terms

Lifeline systems
Ground motion
L.R.L. Wang, /PI

c. COSATI Field/Group

18. Availability Statement: NTIS

19. Security Class (This Report)

20. Security Class (This Page)

21. No. of Pages 122

22. Price

TABLE OF CONTENTS

ACKNOWLEDGEMENT

This is the fifth in a series of the technical reports under the general title of "Lifeline Earthquake Engineering"(LEE) research at the University of Oklahoma. This report serves as the final report under the Research Grant No. CEE-8025172 sponsored by the Earthquake Hazard Mitigation Section, Division of Civil and Environmental Engineering of the National Science Foundation for the period from June 1, 1981 to November 30, 1982. Dr. S.C. Liu and Dr. W. Hakala are the program managers for the project. Dr. Leon Ru-Liang Wang, Professor of Civil Engineering and Environmental Science, is the Principal Investigator.

The research has been carried out by Professor Leon R.L. Wang, and Research Assistant, Mr. Yaw-Huei Yeh, a Doctoral Student under the supervision of Dr. Wang. Mr. Yuan-Chen Lau, a Master Student and Mr. Farrokh Jalalvand, a senior, have participated, in parts of the research. The typing is done by Ms. Lori Creech.

Please note that although the project is sponsored by the National Science Foundation, any opinions, findings, conclusions and/or recommendations expressed in the report are those of the authors and do not necessarily reflect the view of NSF.

CHAPTER I

INTRODUCTION

1.1 Preface

Lifeline earthquake engineering is a branch of earthquake engineering that studies the adequacy, safety, analysis and design of lifelines due to earthquake effects. A lifeline is defined as any structure, facility or system that extends to a long distance over a large area and provides services and supports to human needs.

By their functional use, lifelines may be classified as public work lifelines, such as water and sewer lines; energy lifelines, such as oil, gas and power transmission lines; transportation lifelines, such as highways, railways, waterway, tunnels and long span bridges etc. and communication lifelines, such as telephone, telegraph, TV, transmission lines. From construction point of view, these lifelines may be classified as below-ground lifelines, above/on ground lifelines and concentrated facilities.

Because of the importance of lifelines to the health, supply and safety of the populace, lifeline earthquake engineering, although its development came much later than the seismic building design, is now beginning to draw the attention of the engineering profession. Currently, researchers in the United States[47], Japan[28] and others around the world are actively engaged in research on lifelines under various seismic environments. Among them, most are analytical studies. Very few experimental data to verify or improve the analytical results. In the United States, experimental data on lifeline performance are particularly limited.

Before the mathematical models developed can be implemented for practical applications, field and/or laboratory verifications are absolutely necessary. Other than the seismic input data, several important parameters that will affect the behavior of buried lifelines are empirical in nature. They are the joint resistance characteristics between pipe segments, soil resistance and wave propagation velocity characteristics of the surrounding soil and geological environments.

Lacking specific experimental data on these parameters, most investigators have adopted a parametric study approach in order to compensate for the absence of specific empirical data. To aid future design of buried pipelines to resist earthquake ground shaking, these experimental parameters must be obtained.

1.2 Objective and Scope

To aid the future development in the field of lifeline earthquake engineering, this report is to summarize and synthesize the existing experimental methods that are suitable for either overall or parametric seismic performance evaluation of various lifeline systems.

The discussions will be divided into below-ground and above-ground lifelines. However, the most influential parameter of lifeline systems, either below-ground or above-ground is the ground motion characteristics. In this report, Chapter II will discuss the measurements and investigations of the characteristics of the ground motion due to earthquakes. The experimental studies of below-ground lifelines will be given in some details in Chapter III; above-ground lifelines in Chapter IV. Finally, Chapter V gives the summary and discussions of various evaluation methods on the performance of various lifeline systems in terms of their operation and cost effectiveness.

CHAPTER II

GROUND MOTION CHARACTERISTICS

2.1 Preface

Seismic waves, which are generated when an earthquake occurs, travel in every direction away from the source and are manifested as ground motions that may be recorded at a station where an instrument has been placed. The instrument usually has a device that can record the time history of accelerations, velocities or displacements imposed by the passage of the ground waves. For accelerographs, typically three components of acceleration are recorded, two orthogonal horizontal components and the vertical component.

Earthquake ground motions are very complex. Evaluation of the characteristics of these motions and the identification of key ground motion parameters from past and future earthquakes are very important for engineering applications. It is essential in all areas of earthquake engineering, particularly the lifeline earthquake engineering, to familiarize these characteristics and the factors that affect them.

The ground motion characteristics are affected by many parameters. These parameters include geology, seismology, geotechnical engineering, structural engineering and others. In general, it is widely recognized that earthquake ground motion parameters are affected by (1) source factors, (2) travel path and (3) local geological and topological conditions[27,43].

Recent studies[31,48] have shown that the seismic behavior of lifeline systems is predominately controlled by the ground displacement/strain characteristics. Lifeline system includes buried pipelines, long suspension

bridges, submerged tunnels and water supply networks, etc., all of which are extending to long distance and/or over a large service area. For the aseismic design of lifeline network facilities, it is necessary to estimate rational input of ground motion. In order to study the local variations of strong ground motions induced by earthquakes, the deployment of dense instrument array at the interested area is required. For examining the seismic behaviors of buried pipelines, a lineal extending array may produce proper observation data of the ground displacement for the seismic analysis.

2.2 Lineal Seismometer Array Observation

Most lifeline systems are linearly extended structures along extremely long lines, and also large facilities are often built at the nodal points of a lifeline system. One of the major seismic hazards to lifelines[31] is ground shaking which induces soil strains in the vicinity of pipelines.

To appreciate the influence of the relative displacement between two separated points in the free field and traveling seismic wave, one needs to know not only the maximum displacement at one point but also the wave length and the wave propagation speed of the ground. For the purpose of observing these characteristics, Suzuki[45] had conducted a lineal seismometer array observation along a gas pipeline during the Miyagi-Ken-Oki earthquake.

The observation site is located along a buried gas pipeline which connects two thermal power stations in Chiba Prefecture east of metropolitan Tokyo. The seismometer array is shown in Figure 2.1, and the positions of each accelerometer are described in Table 2.1. The soil profiles of two points near the observation station and the distribution of elastic wave velocities are shown in Figure 2.2.

The observation array consists of five horizontal component accelerometers and an observation house. Every accelerometer records two components of ground or pipeline motion, i.e., transverse (X) and longitudinal (Y) components along the axis of the pipeline. All the accelerometers are of servo type whose frequency ranges from 0.2 Hz to 50 Hz. Contained in the observation house, are amplifiers and magnetic tape recorder with twenty tracks.

The observed earthquake records were taken from the magnetic tape recorder, and the records of twenty tracks were stored in the memory of a digital computer using an on-line A/D converter at regular interval of 0.01 sec.

The observed seismic data are listed below:

i) Location of Epicenter: 142^{o} 24' E, 38^{o} 06' N

ii) Richter Scale: 7.4

iii) Epicentral Distance: 340 KM

iv) Depth of Origin: 30 KM

v) Maximum Acceleration (at S5X): 29.6 gal.

vi) Date: June 16, 1978

The observation results are described briefly as follows:

1) Wave length is 7300 m.

2) Wave propagation speed is 1465 m/sec.

3) Traveling wave during earthquake seems to be Love wave.

4) The maximum amplitudes of the ratios of acceleration, velocity and displacement of the pipe (at point S3Y) to those of the surrounding ground (at point S4Y) are 0.81, 0.99 and 0.93 corresponding respectively.

5) The predominant period is 1.7 sec.

6) Figure 2.3 shows the spectrum ratio of the Fourier Spectrum of acceleration at the pipeline (S3X) to that of the surrounding ground (S4X). In this figure, the spectrum ratio is nearly unity except in the low period region less than 0.2 sec.

7) The momentary distribution of displacement during the earthquake at the points S1, S4 and S5 along a gas pipeline at intervals of 0.1 sec. is shown in Figure 2.4. This figure gave a visual evidence that the traveling wave is "caught" by this array.

8) There exists relative displacement wave between S5 and S1, but the amplitude of displacement was small.

According to the results of seismic observations and analyses, it is concluded that during the Miyagi-Ken-Oki earthquake, the pipeline behaved in the same way as the surrounding ground, and the long period wave can be elucidated by Love wave theory.

2.3 Dense Instrument Array Observations

To be used for the development of earthquake resistant design of structure, the primary objective for the deployment of dense instrument array is to collect and analyze the engineering data on the response of the ground to strong shaking. The secondary objective is to study the effects of variation of local geological conditions along the path of wave propagation on the frequency content and amplitude of strong ground motions.

At the present time, several strong-motion instrument dense arrays have been deployed in Taiwan[10], Mainland China[11], Japan[42], United States[51] and other countries around the world[28]. Among them, only the Japanese deployment, in which some recorded data have been analyzed for lifeline application[48] will be described.

The recent Public Works Research Institue (PWRI) deployment is a local laboratory array consisting of 20 accelerometers at PWRI site, Ibaraki Prefecture, Japan. The deployment of dense instrument array is shown in Figure 2.5. The main specification of the accelerometers employed are summarized in Table 2.2. The triggering of the signals is activated either when

maximum acceleration of vertical component exceeds 3 gals. or when the induced acceleration in any horizontal components is larger than 5 gals.

In the recording and processing systems, the computer system has played an important role for signal transmission and data analysis. A flowchart for data processing system is shown in Figure 2.6(a). For analyzing the recorded seismic excitation, a computer system with a core memory of 192 KW is provided as shown in Figure 2.6(b).

In application to lifeline system, the free field motion on the surface of the ground would be sufficient to represent the ground motion input, because for buried lifelines, the buried depth in general is rather shallow, say 1m to 2m deep as compared to subsurface soil layer. Wang et al[48] have conducted a study to investigate ground strains from strong motion array data for lifeline application.

Since December 1980, three earthquakes, one in Chiba Prefecture and the other in Ibaraki Prefecture, have been recorded at PWRI, denoted as EQ-13, 14, and 15. Due to the fact that the magnitudes of EQ 14 and 15 are too small to give meaningful results, the study uses EQ 13 data only. Figure 2.7 shows the location of the array and Table 2.3 gives the maximum accelerations of the channels that were functioned properly during the earthquake.

The determination of ground velocity and ground displacement can be obtained by integrating the originally recorded acceleration data once and twice through Fourier transformations. The maximum velocities and displacements are also given in Table 2.3. In examining the maximum ground displacements at PWRI site from Table 2.3, one can find that the displacements on the surface in general are larger than those underground as expected. It is interesting to note, however, that the amplification due to the depth effect in

the EW direction is more than in the NS direction. Since the epicenter of EQ 13 was located at 71 km south of PWRI, such amplification in the direction normal to seismic wave propagation direction may be attributed to the shear wave. The analysis of ground strains can be achieved by using finite element method. The configurations for the pyramids used in the finite element analysis are shown in Figure 2.7(b) and (c).

In consideration to evaluate the depth effects on ground strains, 10 observation stations were selected to form 8 different tetrahedrons as shown in Figure 2.8 for strain analysis and the results of the strains are given in Table 2.4.

The amplification on ground strains can be seen in Table 2.4 and similar conclusions are observed. To quantify the amplification due to depth effect, the magnification ratios, which is defined as the maximum upper level strain divided by the lower lever strain, are given in Table 2.5. It is found that the amplification of axial strain in EW direction ranged between 3 to 4. For NS direction, however, there was little amplification.

In addition, Wang[48] et al. have investigated the ground strain at Ashitaka area which is only a simple extended array on the surface of the ground crossing Ukishimagahara. The strains, which were calculated over a distance ranged from 400 m to 1275 m, were too low to represent the peak ground strains for lifeline application. Furthermore, the simple extended array could not provide adequate information to account for the effects of transverse wave during the examination of ground strain. Thus, to be useful to lifeline application, it is suggested that more strong motion accelerographs apart no more than 50 m must be installed.

Table 2.1
Positions of Sensors

Sensor	Position
S1 X/Y	On the ground surface
S2 X/Y	G.L. -26.6 m
S3 X/Y	G.L. -1.5 m; fastened to the pipeline
S4 X/Y	G.L. -1.5 m, 2 m from pipe center
S5 X/Y	Same as S4 X/Y

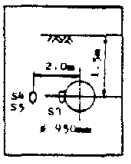

Table 2.2
Main Specification of Accelerometer
used by Local Laboratory Array at PWRI

No. of Component	3
Type	Velocity Feed Back
Natural Frequency	5 Hz
Frequency Range	0.1 - 50 Hz; within 1 β
Maximum Acceleration	± 650 gals.
Diameter, Length	φ 13 cm, 125 cm
Weight	50 kg

Table 2.3

Maximum Accelerations (gal), maximum velocities (kine) and Maximum Displacements (cm) of EQ 13 at PWRI Site

point	comp.	Max. Accel.	Max. Vel.	Max. disp.
1	NS	39.47	2.40	-0.299
	EW	40.08	-2.48	0.342
	UD	-12.64	-0.79	-0.112
2	NS	13.05	-1.19	0.242
	EW	-14.94	1.03	0.189
	UD	-5.94	0.54	-0.081
3	NS	15.20	-1.22	0.233
	EW	-13.95	1.00	0.180
	UD	-	-	-
4	NS	12.61	-0.99	-0.212
	EW	14.48	1.29	0.208
	UD	-5.86	0.56	0.085
5	NS	11.81	-1.04	-0.206
	EW	14.59	1.32	0.224
	UD	-	-	-
6	NS	-14.41	-1.03	-0.243
	EW	-13.58	-1.11	-0.206
	UD	6.81	0.46	-0.074
7	NS	43.04	-2.43	-0.282
	EW	44.15	3.52	0.473
	UD	-11.61	-0.77	0.102
8	NS	25.29	-1.54	-0.202
	EW	23.76	1.57	0.247
	UD	7.35	-0.40	0.061
9	NS	32.58	2.24	0.328
	EW	35.49	2.78	0.446
	UD	-	-	-
13	NS	-22.51	-1.20	0.152
	EW	28.00	-1.81	0.242
	UD	-6.75	-0.43	-0.052

* No data due to mal-function of instrument

Table 2.4

Maximum Ground Strains [$\times 10^{-6}$]

at PWRI Site for EQ 13

Zone	Strain	Lower Level	Upper Level
I	ε_x	9.4	-27.2
	ε_y	-14.5	15.4
	ε_z	-12.4	-12.4
	γ_{xy}	-13.4	-46.4
	γ_{yz}	-	-54.2
	γ_{zx}	59.7	68.2
II	ε_x	12.1	52.4
	ε_y	-14.5	15.4
	ε_z	-12.4	-12.4
	γ_{xy}	15.8	66.4
	γ_{yz}	-	-54.2
	γ_{zx}	60.4	47.3
III	ε_x	12.1	52.4
	ε_y	17.3	14.2
	ε_z	-12.4	-12.4
	γ_{xy}	20.1	81.4
	γ_{yz}	-	-
	γ_{zx}	60.4	47.3
IV	ε_x	9.4	-27.2
	ε_y	17.3	14.2
	ε_z	-12.4	-12.4
	γ_{xy}	-19.1	32.2
	γ_{yz}	-	-
	γ_{zx}	59.7	68.2

Table 2.5

Magnification Ratio (Max. Upper Level Strain/Max. Lower Level Strain)

Zone	Strain	Magnification
I	ε_x	2.90
	ε_y	1.07
	ε_z	1.00
	γ_{xy}	3.47
	γ_{yz}	-
	γ_{zx}	1.14
II	ε_x	4.33
	ε_y	1.07
	ε_z	1.00
	γ_{xy}	4.19
	γ_{yz}	-
	γ_{zx}	0.78
III	ε_x	4.32
	ε_y	0.82
	ε_z	1.00
	γ_{xy}	4.05
	γ_{yz}	-
	γ_{zx}	0.78
IV	ε_x	2.90
	ε_y	0.82
	ε_z	1.00
	γ_{xy}	1.69
	γ_{yz}	-
	γ_{zx}	1.14

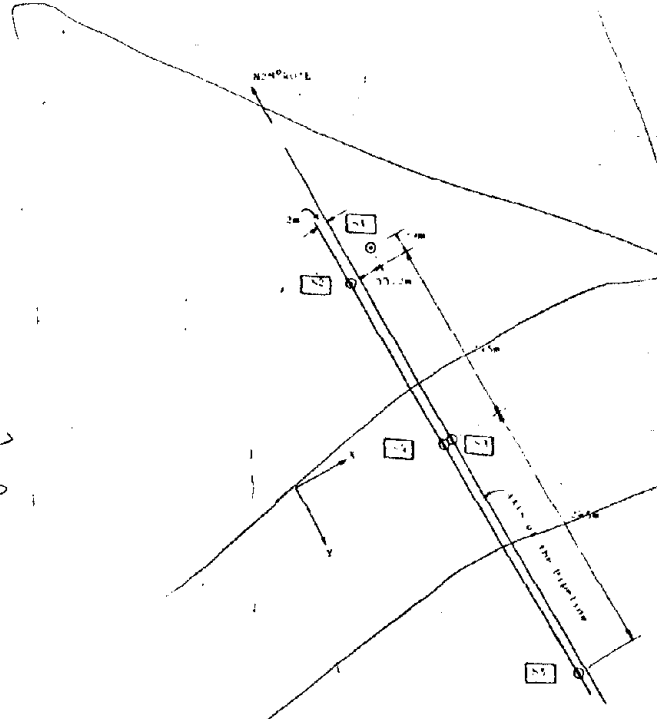

Figure 2.1 The Seismometer Arrays

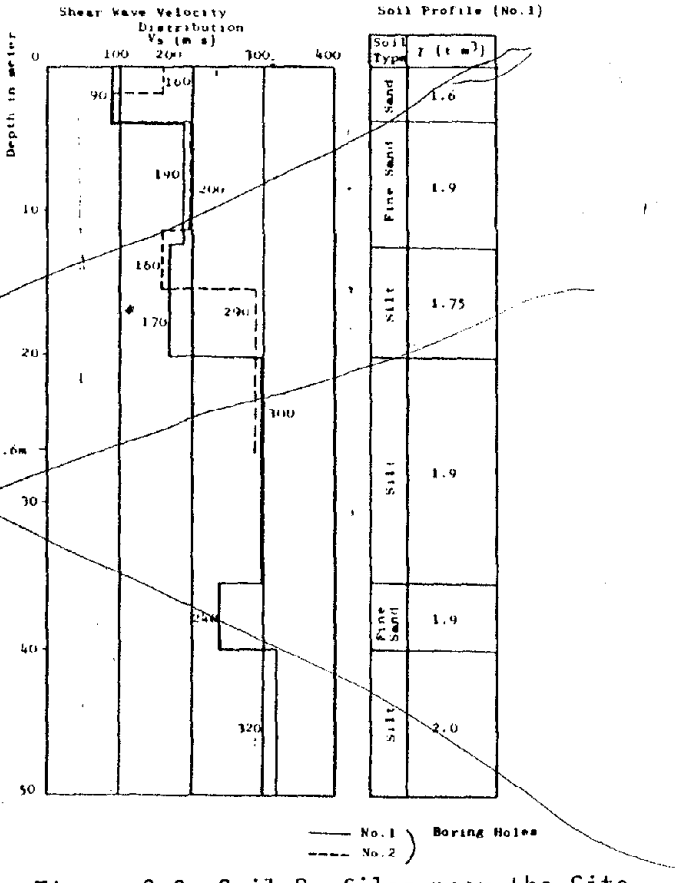

Figure 2.2 Soil Profiles near the Site

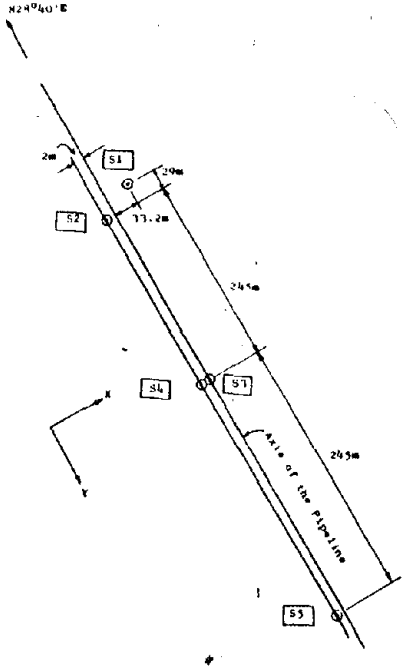

Figure 2.1 The Seismometer Arrays

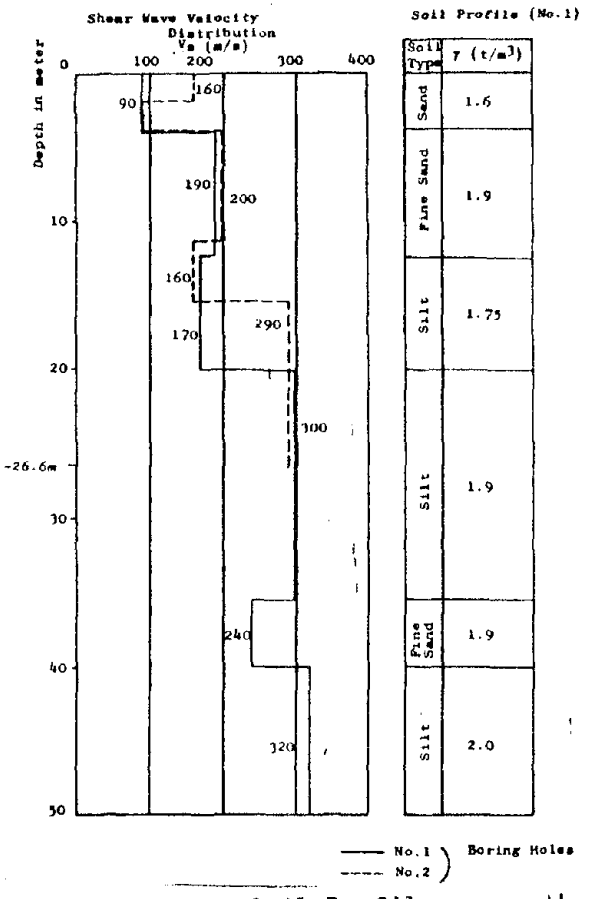

Figure 2.2 Soil Profiles near the Site

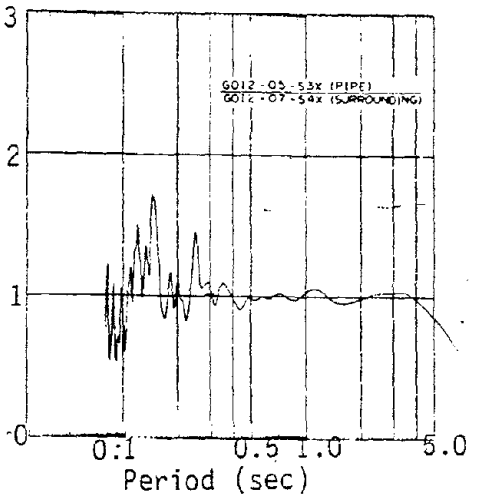

Figure 2.3 Spectrum Ratio of the Pipeline to the Surrounding Ground

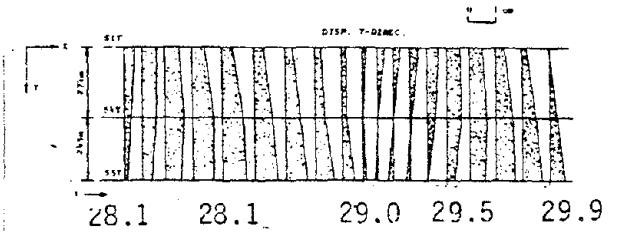

Figure 2.4 The Momentary Displacement Distribution along the Pipeline

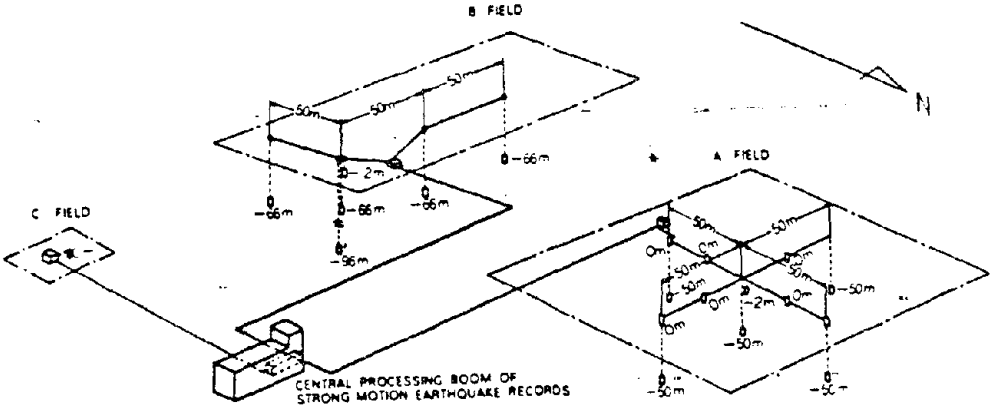

Figure 2.5 Local Laboratory Arrays at PWRI

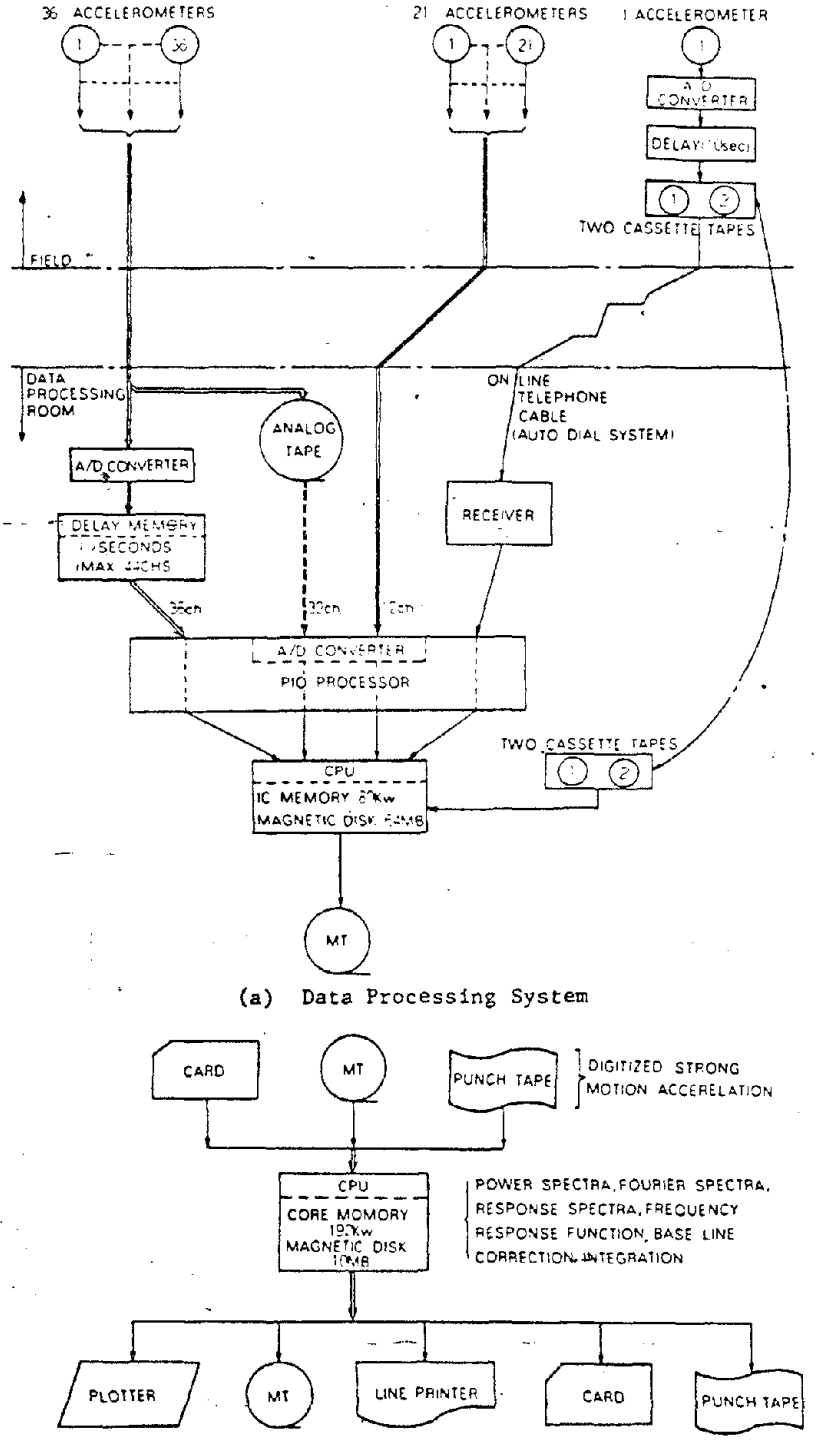

(a) Data Processing System

(b) Data Analyzing System

Figure 2.6 Data Processing and Analyzing System

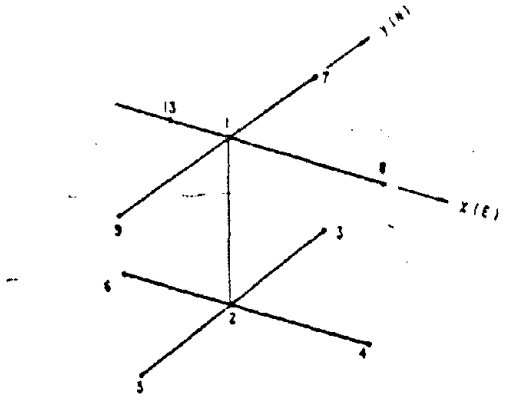

(a) The Deployment of Both Vertical and Horizontal Arrays

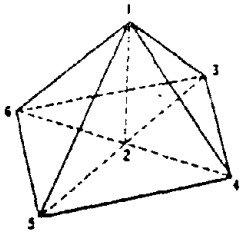

(b) Configuration of Lower Pyramid

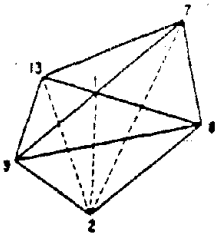

(c) Configuration of Upper (inverse) Pyramid

Figure 2.7 Dense Array Arrangement at PWRI

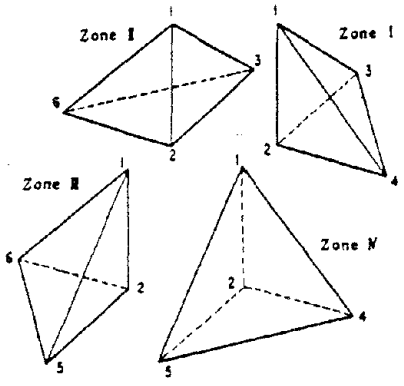

(a) Tetrahedrons for Calculating Lower Level Strains

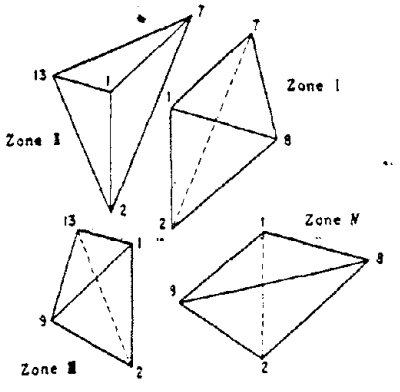

(b) Tetrahedrons for Calculating Upper Level Strains

Figure 2.8 Tetrahedrons for Finite Element Analysis

CHAPTER III

BELOW GROUND LIFELINE SYSTEMS

3.1 Introduction

The seismic behaviors of buried lifelines during earthquakes may be achieved by statistically analyzing the past damage records and/or by conducting some experiments for certain specific purposes.

Through investigation of past damage records, it may be possible to establish statistical relationships between various failure mechanisms and parameters such as the type and size of pipe, soil conditions, and joint details. But most of the existing literature concerning buried pipeline damage due to earthquake give a qualitative rather than quantitative description of the damages. This is due to the fact that a complete quantitative survey of buried pipeline damages is rather difficult and expensive.

Recently several experiments have been undertaken to investigate the dynamic behaviors of buried lifelines during earthquakes. This chapter is to synthesize these experiments in terms of experimental procedure, apparatus and application, etc.

Generally, experiments currently conducted for studying the behavior of buried pipelines in an earthquake can be divided into four main branches: (1) active field testings, (2) passive field testings, (3) scale models testings and (4) testings on influential parameters. They are discussed below:

3.2 Active Field Testings

The seismic effects to lifelines are much different than that of building structures because of the spatial distribution of the seismic wave. Building structures require only single point source ground motion with only temporal vibration. However, lifelines which cover a large area require ground motion inputs with both temporal and spatial variations. Thus, for lifeline investigations, it is necessary to generate the earthquake - like ground motion for the purpose of studying the seismic effects to lifelines. Several methods generating earthquake-like ground motion will be discussed.

3.2.1 Explosion

A small experiment, assigned the test name MINI-SIMQUAKE by C.J. Higgins et al.[25,26], was conducted to verify the technical feasibility of sequentially detonating closely spaced planar arrays of high explosives for the purpose of simulating earthquake-like ground motions, although trial blasts were used earlier[14].

Figure 3.1 provides an elevation view of the MINI-SIMQUAKE experiment. The back array was loaded with a total of 347 lbs. of PETN explosive in 12 holes, 40 inches on center. The explosive was located between the 5 and 20-foot depths giving an array height of 15 feet and an areal explosive loading density of 0.58 lbs. PETN/ft^2. The front array contained 232 lbs. of PETN explosive in 16 holes, 30 inches on center. The array dimensions were the same as those of the back array and the areal explosive loading density was 0.39 lbs. PETN/ft^2. The arrays were 15 feet apart and were designed to fire with a 300 millisecond separation.

A small cylindrical reinforced concrete structure with a height of 3.75 feet, an outside diameter of 2.5 feet and a total weight of 1218 lbs. was embedded to 25% of its height at a range of 25 feet from the front array. The structure walls were 3 inches thick.

The apparatus for instrumentation includes accelerometers, velocity gages, angular displacement gages, magnetic tape, mobile field instrumentation van and fast technical photographic tool.

The ground motion results can be observed after detonation. The results are indicated as follows.

1. There are two peak outward acceleration ranging from 3.4g to 10.3g recorded at depth of 2.5 ft. and 12.5 ft. respectively.
2. There may exist a near-surface effect on ground velocities and displacements as indicated that the higher values appear at near-surface in both of ground velocities and displacements after integration of accelerogram.
3. The peak upward vertical velocities are about 40 to 50% of peak outward velocities.
4. The vertical displacement is upward at all times and seems to contain little permanent set.

From observation, various phenomena concerning the structural horizontal response can also be obtained during testing.

1. The peak outward accelerations at the structure top due to the back and front array pulses are only about 60% of those at the base (Figure 3.2).
2. The top acceleration has little similarity to the base acceleration after the first outward acceleration pulse and undergoes

significant free vibration as the base acceleration approaches quiescence.

3. The velocity and displacement at the top of the structure overshoot the base response throughout their time histories.
4. The velocity and displacement at the structure top also clearly show the free vibration phase.
5. The shock spectrum at the structure base is very similar in shape to that at the 30-foot range and 2.5-foot depth in the free-field.
6. The amplitude difference is about what would be expected due to motion attenuation and, hence, the structure base is responding closely with the free-field.
7. The spectral peak at a period of 0.25 sec the structure top is about 55% greater than the corresponding spectral peak at the base.
8. The top spectrum has a peak at a period 0.11 seconds (9HZ) which does not appear in the base spectrum. The peak corresponds well to the free vibration frequencies evident in the time history data.

In a similar task, Bruce Lindberg et. al at the Stanford Research Institute[12,13] have developed a technique to generate earthquake-like motions with contained explosions. The technique produces earthquake-like ground motion by simultaneous detonation of a planar array of vertical line sources placed in the soil near the structure to be tested, as shown in Figure 3.3. Each line source shown in Figure 3.4 produces ground motion through an expandable rubber bladder rugged enough to withstand repeated tests with expan-

sions as large as twice the initial bladder diameter. The explosive is detonated inside a steel canister within the bladder, and the explosion products flow out of the canister through vent holes to pressurize the bladder at a controlled rate. In this way, both amplitude and frequency are controlled at levels suitable for testing with the source arrays close to the test structure, and the array sources are re-usable. This opens the possibility of in-situ testing at strong shock levels to test any structure effectively and economically.

The following results for 1/3 scale array were observed:

1. The ground motion is uniform along the 12 ft. length of the instrumented area.
2. The ground motion attenuates about 30% across the 10 ft. width of the instrumented area.
3. The ground motion at the mid-depth of the array has a slightly faster-rise time and is slightly lower in amplitude than that near the surface.
4. The soil displacement and stress follow the source pressure-time history.
5. The primary frequency of the ground is in the 8 to 15 Hz range.

3.2.2 Moving Loads

A field testing on a full-scale pipe by varying the depth of the soil backfill and moving loads has been done by Niyogi[38]. The test program was designed to evaluate the deformation and strain behavior of 30-inch diameter Aluminum Bronze piping subjected to backfill, surcharge and live loadings.

The apparatus used for instrumentation contains extensometer (linear potentiometer), tilt meter (pendulum type, Model No. CP17-0601-1), strain gage (micro-measurement type), volt meter and a controlling computer.

The test procedures are described as follows:

1. The pipe is embedded in granular backfill at depth ranging 6 to 14 feet.
2. Install the extensometer disk inside pipe as shown in Figure 3.5.
3. Tiltmeters are installed with the extensometer disk as shown in Figure 3.6.
4. Strain gages are located at twelve positions, at the exterior and interior surfaces of the pipe at an interval of 30^{o}. Gages are water proofed as shown in Figure 3.7.
5. Lead wire sets are attached to each disk following initial placement.
6. Initial baseline radial measurement is made with an inside precision micrometer following disc placement and gaging.
7. Potentimeters, tiltmeters and strain gages are run with a 6.0 DC power source.
8. Power is checked and logged twice daily during testing.
9. During testing, data is obtained utilizing an automatic scanning integrating digital voltmeter and controlling computer.

The load type and their results are tabulated in Table 3.1. In load type 2, compaction from the sides of the pipe shortens the horizontal axis of the cross-section and the point "a" on the crown moves up. The point "a" starts to move downward due to subsequent increase in load. Due to this irregularity, there is a wide variation between the theoretical and experimental values of stress and deflection in the beginning. Experimental hoop stress at "a" also varies widely in other load types. This attributes to experimental errors. Otherwise experimental and theoretical results should agree within certain extent.

3.2.3 Vibrators

Vibrators used to generate ground motion to test buried pipelines have been described in Reference 4 and 46. In general, two techniques were used: one is indirect and the other is direct vibration.

In indirect vibration tests, the buried pipe is deformed by propagating waves generated by a large-size vibrator which is installed on a concrete footing on the ground surface at a distance from the pipe. Figure 3.8 shows an example of an indirect vibration test, in which a 320 mm diameter steel pipe was buried in reclaimed sandy soil. The vibrator which had a capacity of 50 tons was installed in a concrete pit which was 12.5 meters away from the buried pipe. The indirect vibration test can approximate incident seismic waves reasonably well, however, the amplitudes of the pipe motion and strain were much smaller (for example, below 30-40 x 10^{-6}) than those associated with earthquakes because the vibrator has to be installed far away from the pipe. Furthermore, the amplitude of the vibrator's motion had to be set at a low level to avoid liquefaction of the sandy soil around the vibrator's pit. Finally, an expected slip between the pipe and the surrounding soil did not occur.

In the direct test, the pipe was excited by a small vibrator which is attached at the end of the pipe, as in Figure 3.9. In this case, the strain of soil and the amplitude of the pipe motion was as large as that during earthquakes and the slippage occurred between the pipe and soil. The test can be very useful in finding restoring large strains. But it is noted that there is disagreement whether the input motion realistically approximates that of an earthquake.

The tests were carried out for a frequency range of 3.0-12.0 Hz. For

this range the restoring force properties of soil depend not on the frequency but on the displacement amplitude of the forced vibration. When the displacement amplitude of the test pipe became much more than 0.4-0.6 mm, the slippage occurred between the pipe and soil and the displacements were independent of the frequency of the forced vibration. Furthermore, at the onset of movement, the ratio of the maximum shear stress on the pipe surface to the vertical earth pressure was 0.5-0.7.

From vibration tests on pipe elements buried in the field, the following conclusions were obtained:

1. The natural vibration of the buried pipe due to its inertia force cannot be recognized and the pipe vibrates in the same manner as the ground.
2. Strain due to axial deformation is dominant for straight pipes, while the circumferential strain due to bending deformation is large in bent pipes. This result suggests that the conventional beam model is not suitable to analyze the strain of pipes at the bent pipes and a shell model is necessary.
3. The dynamic properties of the restoring force of the surrounding soil (such as the coefficient of reaction force, the friction coefficient and the relative displacement when slippage begins) depends little on the frequency of the input motion. The coefficient of subgrade reaction largely effected by the relative displacement between the pipe and ground.

3.2.4 Air-gun and Board-striking (Shear) Process

Nasu[35] conducted vibration tests on a stright pipe of diameter 1.2 m and length of 84.0 m buried in reclaimed silty ground, shown in Figure

3.10. The main objects of the test consisted in the studies of (1) the vibrational characteristics of the ground and the pipe, and (2) the strains and their distributions in the pipe during the vibrations.

Two different processes were employed to generate the ground vibration, i.e., the shear (or board-striking) and air-gun. The measuring instruments for vibration measurement consists of (a) transducer (pick-up), (b) amplifier and (c) recorder. As to the instruments for strain measurement contains (a) strain gage transducer (b) Wheatstone bridge box: 10-channel, DC-current, gage and three arms (each of 1 kilo-ohm), input voltage = 24 volt, (c) Amplifier, (d) data-recorder, (e) Analog computer and (f) other devices for measuring the input voltage of Wheatstone bridge, and for checking the gain of amplifier.

The test procedures are described as follows:

1. Welding of seven segments of the pipes.
2. Laying the pipes in a trench and overlying with soils.
3. Making CBR test to the original ground and the fill.
4. Installing the sensors (pick-up and strain gage) in pipe, on ground surface or in underground.
5. Generating the ground vibration
   a) Shear: ingot (15 tons) struck by metal bob
   b) Air-gun: firing chamber 2000 cc, at 140 atmospheric pressure, laid at (-5m) in boring hole (full of water)
6. Determining the velocities of P and S waves by recording the readings of the travel-times of the waves at various distances from the origin of the wave.
7. Recording the data of strains and displacement in the pipe and ground.

8. Analyzing the resulting data during tests.

In order to study the vibrational characteristics of the ground and pipe, the bandpass-filters can be used to pick out the predominant periods of waves; and the Fourier analysis can be employed to obtain the response spectra for vibrations of ground and pipe. Figure 3.11 shows the Fourier spectra for vibrations of ground and pipe.

From the results of tests, it is observed that the vibrations of the pipe and the ground in the shear test are different to that of the air-gun test. Note that in both tests, there can be seen no appreciable relative displacements between the pipe and the ground. The axial strain produced in the pipe during the ground shaking is proved predominant. The results of stress analysis are shown on Table 3.2.

3.2.5 Pile Driving (Standard Penetration Test)

In the standard penetration test an impact at the bottom of a bore hole is produced by weight dropping and may be expected to generate seismic waves. This test is performed by dropping a weight to drive a sampler. The weight hits the knocking head that is fixed to the rod, and thus the sampler is driven in the borehole. The weight is 63.5 kg and falls freely 76 cm to the knocking head.

The impact at the bottom of the borehole due to dropping generates several types of waves. Ohta[39] et al. has used this method to measure shear wave velocity of soil. A schematic representation of this method is shown as Figure 3.12. The waves generated at the bottom of the borehole are detected by a geophone set at the ground surface. Two examples of wave signals recorded by geophone are shown in Figure 3.13.

The whole observation system was composed of conventional instruments.

A set of three-component, moving coil type geophones, with a natural frequency of 28 cps, was installed on the ground surface at a distance of several meters from the borehole. Otherwise, a 4-channel magnetic tape recorder is also required.

Nasu[35] has conducted a test to determine the pipe strain by using pile driving method. The motion generated by this method seems to be random in nature as in actual earthquake; however, the frequency is higher and the duration shorter than earthquakes. The analysis for resulting data of tests is similar to that of last section. The strain of pipes caused by the artificial vibrations was always very small (below 10×10^{-6}).

3.3 Passive Field Testings

In order to confirm the current analytical findings, field verifications or prototype testings on the response behavior of buried lifelines due to or simulated earthquakes are needed to be done. The passive field experimental method is to install response gages to measure strains and/or displacements, etc. of buried lifelines due to actual earthquakes. Such kind of preliminary experiments have been done in Japan, an extremely seismically active region. Note that the field experiments in Japan have effectively yielded qualitative response behavior of submerged tunnels, buried pipelines and communication lines.

In the United States, seismic instrumentation for a few selected tunnels in California has been proposed[8]. The objective of the study has been to provide guidance for an early installment of relatively simple instrumentation in a few selected tunnels in California. No data have been published yet.

Generally, in many field observations, the accelerations and displacements of the pipe and the surrounding ground, axial and circumferential strains of pipe (or tunnels) and the deformation of pipe joints due to seismic excitations were measured simultaneously. The description of those field observations will be depicted in three categories, (1) buried pipelines, (2) tunnels and (3) communication lines.

3.3.1 Buried Pipelines

During the Matsushiro swarm earthquakes in 1965-67, several studies[36,40] which consisted of measuring strains and displacements of pipelines during earthquake were conducted by actually burying pipelines in the ground.

One experiment was on steel pipe in which a pipe with an outer diameter of 27 cm, thickness of 6.6 mm and length of 90 m was buried at a depth of 1.5 m below the surface. The area around the pipe was packed with sand. A manhole was provided and insulated from the pipe. The main objective of the experiment was to ascertain whether or not the pipe would move completely with the ground. Within the indicated period, various earthquakes with acceleration up to a maximum 120 gal were occurring and the observed results were:

1. Resonance vibration of the pipe did not occur.
2. The deformation of the pipe was more or less identical to the deformation of the ground.
3. The axial strain is predominant. The relation between strain and seismic ground motion is given by

$$\varepsilon = \frac{\mu}{2\pi} \cdot \frac{Ta}{C} \tag{3.1}$$

where ε = strain

μ = constant (nearly unity)

a = seismic acceleration

T = period of seismic wave (sec)

C = propagation velocity of seismic wave (cm/sec)

4. Bending strain is occurred in curved pipe, but there is no tendency for it to be greater than the strain along the straight pipe. Meanwhile, the strain at pipe connection with a manhole is not significantly high.

Another experiment was made on concrete pipe[40]. The pipeline consisted of four asbestos-cement pipes with inner diameter of 12.5 cm. One end of the pipeline was connected to the manhole. The connection between manhole and pipe was made to withstand a considerable amount of bending. The results obtained are given below.

1. The manhole and the ground within at least 5m from the manhole showed roughly identical movements.
2. During vibration, there is a phase difference between manhole and the far end of pipeline.
3. During an earthquake, a seismic wave associated with large acceleration and large displacement will result a large strain in the pipeline. The larger the seismic acceleration the greater the strain is.
4. On examination of the strain distribution over the entire length of the pipeline, the strain becomes larger near a joint and is rapidly reduced with increased distance from the joint.
5. At joints, bending stress is more significant than the axial

stress. At the mid-section of the pipe, the reverse is true.

6. According to the result of investigation, in the vicinity of a joint, the strain is increasing to a certain limit as the acceleration becomes larger.
7. For a strong earthquake with the acceleration up to 120 gal, the resulting maximum stress in the concrete pipe was approximately 15 kg/cm^2 at a joint and 5 kg/cm^2 at middle point of the pipe; but the maximum stress induced in the steel pipe was almost 10 times the stress in the concrete pipe.

Based on these two studies, it can be concluded that the buried pipeline moves roughly with the surrounding ground during seismic excitation. It also shows that the axial stress was predominant for both cases of steel and concrete pipes. Note that the existence of a manhole does not make much difference in the case of steel pipe, but for a concrete pipe the stress distribution was affected significantly.

Nishio et al.[36] conducted field observations of buried pipelines behavior during earthquakes at three sites in Japan. The first observation was made at Yokahama, from October, 1972 to December, 1973. Three pipelines with diameters of 150 mm were buried in the ground to the depth of 1.2m. The arrangement of pipelines and sensors is as shown in Figure 3.14. Table 3.3 shows the seismic data and the results observed from dynamic response of buried pipelines during earthquakes. From the time history of pipe strain as shown in Figure 3.15, it is noted that the bending stress is very small compared with axial stress (compare the strain records of A1 and A2). In addition, no evidence of a travelling wave along the pipeline could be found by observing the strain records at C and D from Figure 3.15.

The second observation was carried out at Soka, from April of 1974 till March of 1976, using steel pipeline of 400mm in diameter which is actually used for gas transmission. The set-up of sensors and layout of pipeline are shown in Figure 3.16. Table 3.4 is a list of observed earthquake and the resulting data.

The third site of observation was at Omori and the period of observation was from December 1976 till December 1978. A steel pipeline of 200mm diameter was laid in T-shape as shown in Figure 3.17. The recording data of earthquakes and seismic responses of the pipe are listed in Table 3.5.

Based on the observed results, one finds that the traces of traveling wave which causing the pipe strain could not be detected during earthquakes. Note that in each field observation, the dynamic behavior of a pipeline is almost the same as that of the surrounding ground.

Figure 3.18 shows the relationship between the maximum acceleration of the observed earthquakes and the maximum strain in the pipeline. An approximate relationship between the axial strain of pipe and the ground acceleration by analyzing the data of twenty-four earthquakes can be expressed as

$$\varepsilon = 1.85a^{0.55} \times 10^{-6} \qquad (3.2)$$

where ε is the maximum axial strain of pipe and a is the maximum acceleration (cm/sec^2) on the ground surface.

Authors conclude that the wave propagation along a buried pipeline has little significance in explaining the pipeline behavior and that, on the contrary, the model of an upwardly incident earthquake motion with respect to the bottom of the surface soil layer is important.

3.3.2 Tunnels

In 1973, Okamoto et al,[40,41] studied a sub-aqueous tunnel provided for crossing the Tama River by a railroad near Tokyo City as shown in Figure 3.19. The tunnel has 6 submerged tubes each 13m wide, 7.35m high and 80m long. Tube No. 1 is on diluvial silt while Tubes No. 4 to 6 are on the transient zone between the two. Tubes No. 2 and No. 4 are each provided with accelerograms and strain gages. The strain gages are installed at either sidewall of the cross sections 30m apart and are set to measure strain in the axial direction (Figure 3.20).

During the period from April to October 1970, several earthquakes were recorded at the tunnel, as listed in Table 3.6. Although severe seismic motions have not yet been observed at this site, the records obtained to date are thought to indicate the general nature of the earthquake behavior of sub-aqueons tunnels.

Figure 3.21 shows one of portions of the accelerograph and strain gage records obtained from a small nearby earthquake. The earthquake occurred on September 30, 1970, its magnitude was M = 4.8, its hypocenter was right beneath the tunnel and its intensity at Yokohama (about 15 km from the epicenter) was VI on the Modified Mercalli scale.

Study of these records leads to several significant conclusions regarding the dynamic earthquake response of the soil-tunnel system, as follows:

(a) The generally "in phase" nature of the strain readings demonstrates that the tunnel is subjected primarily to axial straining rather than flexural; this is particularly evident for the distant earthquake.

(b) The distant earthquake produces relatively lower accelerations but higher strains as compared with the nearby earthquake.

(c) The variation of ground motion depends on the location and seismic wave form.

(d) Bending moments and shear forces are large at joints between ventilation tower and submerged tube.

(e) The stress values along a sub-aqueons tunnel are varying greatly with the seismic waveform.

Hamada[24] has conducted a program to measure accelerations and strains due to the after shocks of Miyagi earthquake for a railroad tunnel and thus to investigate the characteristics of wave propagation in bed rock. Figure 3.22 shows the general view of the tunnel and the location of instruments. The tunnel is constructed in bed rock with a length of 4670m. It has a horse-shoe shaped cross section of 4.8 x 6.1m with a 0.3m thick concrete lining.

The observations from the Miyagi earthquake will be described as follows:

1. The accelerations recorded at the places of A1 and A5 in the rock area are quite similar to each other, but the acceleration at the entrance (A4) is about 2 or 3 times larger than those in the rock, as shown in Figure 3.23.
2. According to Figure 3.24 the amplification ratio (a_{A4}/a_{A1}) of the acceleration at the entrance can be estimated to be about two:
3. As shown in Figure 3.25(a) and 3.26(a), the axial strain of the tunnel lining ε_x is uniform along the axis and displays a reasonably good similarity to the calculated rock strain in the axial direction. ε_x was obtained as the ratio of the seismic wave velocity in the rock to the apparent propagation velocity along the axis. This is based on the assumptions that the recorded wave consisted of only body waves and the propagation velocity

was constant.

4. Using the time lag between two observation points (A1 and A5), the apparent wave propagation velocity along the axis was estimated about 3500 m/sec. This is rather larger than that of the shear wave velocity of the rock which is about 200 m/sec.
5. The axial strain of the tunnel lining is about 30% of the rock strain. It should be considered that the joints (at intervals of 12m) in the concrete lining have an effect of reducing the strain of the tunnel.
6. The circumferential strains at two observation points of S7, S10 as shown in Figure 3.25(b), which are located at 45^{o} of arch, have a similar wave form but almost opposite phases to each other.
7. The shear strain γ_{yz} was calculated by the multi-reflection theory under the assumption that it was caused by the seismic motion that vibrated in the y-direction and propagated in the z-direction. Furthermore, the normal strains of the rock ε_z and ε_y were calculated on the assumption that the seismic motion in the y and z directions propagated in the y and z directions, respectively. The circumferential strain at 45 degrees points of the arch is about 60% of the shear strain of the rock.
8. The apparent wave propagation velocities, estimated from the time lags between two observation points, were 2900 m/sec and 4500 m/sec in the y and z directions, respectively.
9. The strain at the arch crown (S9) has a good similarity with the composite strain of the normal strain ε_z and ε_y with the rate 0.8:0.1, while the strains at side wall (S6, S11) are very similar to that with the rate 0.5:0.5.

10. The rate of the strain composition is considered to be influenced not only by the location of the observation point but also the stiffness of the tunnel lining and rock.

3.3.3 Communication Lines

During the Matsushiro swarm earthquake in 1957-67, a study[40] on measuring strains and displacements of buried communication lines has been made at ductways for high-voltage lines in the downtown districts of Tokyo (See Figure 3.27). The communication line is a circular steel shield with an outer diameter of 3m covered by soil around 12m deep. The nature of the soil is silt and silty soil with a high water table 1m under the ground surface. There are two manholes 78m apart and seismometers have been installed inside the duct between the manholes. According to the results obtained from the measurement, the records show the axial and transverse acceleration in the duct are lower than that of the ground surface. The acceleration ratio of at the duct and ground surface is 70-80% in the axial direction and 60-70% in the direction perpendicular to the axis.

According to displacement records, displacement at a period of approximately 0.9 sec is prominent, and this might be the predominant period of the ground. Axial displacements are measured at cross section C, Q and E. As shown in Figure 3.27, the point C is midway between the two manholes, Section Q is 14m away from C, and Section E is 14m away from Q and 6m to the manhole. Based on the records obtained from measurement, there are no phase difference among these three points, but the displacement at point C is about 70% of displacement at point E. Note that the movement of point Q is the same as that of point E. According to these observations, there is a 1 mm difference produced every 14 m long in the duct, it shows that the average

strain is 7×10^{-4}. The accelerations have been observed up to 70 gals., but the displacement only up to 3mm. Under such kind of environments, the influences of differential ground movement and manholes may not be significant.

3.4 Laboratory Testings

Vibration tests of scale models of buried pipe segments have been conducted for the purpose of obtaining the fundamental characteristics of pipe-soil interaction phenomena. In most of these vibration tests, the scale model of a buried pipe with the surrounding soil was made of elastic material with a slightly viscuous nature, such a silicone rubber (pipe), gelatine gel or high polymer (soil). Generally, the reduction scale of the model was about 1/100 - 1/500. The scale is naturally largely dependent on the size of the available shaking table.

As to the vibration tests of scale models of tunnels, it can be conducted in similar way like as that of buried pipes in the laboratory.

As indicated, a description on model tests of buried pipes and tunnels will be narrated as follows:

3.4.1 Buried Pipelines

Figure 3.28 shows one example of such a scale model utilized by Nishio et al.[36] It is known that the non-uniformity or discontinuity in soil properties is one of the major causes of damage to buried pipelines in earthquakes. Therefore, the authors made a model of discontinuous soil structure with a pipeline buried in it and observed its behavior due to the excitations on a shaking table.

The model was made by gelatine and a rubber string to simulate soil and pipe respectively. The model is in the scale of 1:100 and the shear wave

velocity in the actual soil is assumed to be 100 m/sec which corresponds to the case of soft soil deposit while the bed rock is assumed to be so hard which is regarded as a perfectly rigid body. The specific weight of the soil is assumed to be 1.6 t/m^3. A dimensional analysis on the relationship between the model and the prototype is listed in Table 3.7. They were calculated according to the similarity law based on the equation of motion assuming soil layer as a perfectly elastic body. Steel pipe of 750 mm diameter was simulated by a rubber string of 10mm diameter in which its elastic modulus permits to keep the similarity in static balance of the pipe-soil interaction. A number of marks were made on the surface of the model so that the displacement of the ground can be observed and measured. Three accelerometers were placed on the surface of the simulated ground and five strain gages were utilized on the simulated pipeline as shown in Figure 3.28.

The model was placed on a shaking table which vibrated in the horizontal direction in a harmonic motion with varying frequency, as well as in random motions. The elastic modulus of the model material was chosen as low as possible to easily obtain the resonant frequency of modeled ground within the test frequency range. Therefore, conventional accelerometers and paper strain gages, which may change the stiffness of the model, were not too suitable to use. Thus, in most cases, the deformation of the buried pipe and the surrounding soil was measured by optical methods such as a high-speed photography. It was rather difficult to obtain details of pipe-ground interaction such as the reaction force of the ground and pipe strains from these vibration tests alone. However, this kind of test is quite effective in determining the fundamental characteristics of buried pipes and surrounding soil.

The dynamic behavior of buried pipes observed from the model tests using shaking table can be described below:

1. The pipe vibrates with natural frequency of the surrounding ground and the resonant frequency of ground is barely affected by the existence of the buried pipe.
2. The pipe moves almost the same as the ground. Figure 3.29 shows an example of the distribution of displacement of the soil and the pipe when excited sinusoidally in the direction of pipeline axis.
3. The maximum strains take place where the thickness of surface layer changes sharply.
4. The occurrence of maximum strain may not correspond to that of maximum acceleration at the same location, but always take place at the portion of discontinuity of the surface layer.

Usually the straight pipes can be considered as moving almost the same as the surrounding ground. However, in case of curved pipelines, axial forces and bending moments are both produced during earthquakes. As an experimental study of this problem, a model test[40] was carried out. A model of the ground and pipeline with bent was made with gelatin and a teflon rod, and the displacement and strain of curved pipe was measured as applying shear waves from one end of gelatin.

As described earlier, the model (Figure 3.30) was placed on a shaking table which vibrated in the horizontal direction in a harmonic motion with varying frequency. The instrumentation and measurement to the deformation of the pipe bent and the surrounding soil is similar to that of Nishio's experiment. An optical method of the high-speed photography was used to measure the displacement of the

buried pipe and the ground during the vibration test.

The results are shown in Figure 3.30(a) in which axial force is produced in the pipeline in the direction coinciding with the direction of application of vibration, while bending moment is produced at the portion of bend. In the pipeline along a direction perpendicular to application of vibration, almost no bending moment of axial force occurs. When a coupling (Figure 3.30(b)) connected to the joint between a bend and the pipe is allowed to rotate, the axial force, produced in the direction coinciding with that of application of vibration, is reduced. Note that bending moment at the portion of bend and straight pipe in the direction orthogonal to the direction of application of vibration is increased, in contrast. Based on the results observed from test, it can be concluded that the axial strain is dominant in the straight pipe while the bending strain is overwhelming in the bent pipes.

3.4.2 Tunnels

Okamoto and Tamura[40,41] have carried out an experimental test that a three-dimensional models of a subaqueous tunnel were built on a shaking table and vibrated for the purpose of investigating the dynamic behavior of the tunnel.

The small scale dynamic models of tunnels were built with cross-section 2.8 cm in height and 8.4 cm in width, and submerged in model of soft ground 2.2 m in length, 1.0 m in width and 10.4-17.8 cm in thickness. The scale of the model is 1/250. The material of the soft ground was gelatin and that of the tunnels was silicone rubber. Both materials have extremely low moduli of elasticity. This is good for producing states of resonance at low frequencies in models mentioned previously. The vibration tests were performed in the linear elastic domain and only inertia forces were considered.

The ground was comprised of four different layers, and those thickness and modulus of elasticity of each layer was given in Table 3.8. The ratio of the modulus of elasticity of the softest ground to that of the hardest ground was 1:6.

The total thickness of the model of ground layer was 10.4 cm at the bottom of the water with the thickness gradually increased at the slopes until on land it became 17.8 cm. The modulus of elasticity of the model material of tunnel is roughly 500 times that of the soft ground.

The shaking table, on which the model was tested, was of a mechanical excitation type in which the frequency could be controlled at any desired constant amplitude. The excitation waveform was simple harmonic with the frequency range being 0 to 20 Hz.

Measurements of displacement were achieved from the records of still photograph and motion picture. Black lines are rubber bands embedded to determine displacements of ground above or below the submerged tube and the white spots are targets of paper placed for measurement of displacements of the ground surface. The displacements of tunnel elements were measured by the movements of lines on the surfaces of the elements. The frequencies at the times of measurement were between 2.5 and 14 Hz. It was possible to make the measurements to an accuracy of about $\pm$ 0.1 mm.

During the vibration tests, a series of resonance vibrations were arranged to occur in land, slopes and bottom of channel respectively. The conclusion on the observations from the vibration tests were described as follows:

1. The resonance phenomena are comparatively localized. For instance, in the case of resonance occurred on the land, the

displacement distribution of the ground along tunnel axis is significant, the slope regions are only displaced slightly due to some effect from the resonance on the land. But there is almost no influence at the bottom area of channel.

2. A subaqueous tunnel will vibrate at the frequency of the surrounding ground, and deforms correspondingly to the deformation of the ground.
3. Both of bending and axial deformations are visualized in the subaqueous tunnel during vibration tests. The deformations are much significant in the slope regions.
4. There is an effect of buried depth to the dynamic behavior of a subaqueous tunnel.

3.5 Testings on Influential Parameters

Earthquakes in Japan, Alaska, and California have demonstrated the vulnerability of underground piping systems to strong ground shaking. The failure of buried pipes in water supply, natural gas distribution, and sewage disposal systems presents severe hazards and difficult and expensive repair problems in urban areas after an earthquake.

The response of buried pipelines during earthquakes is governed by factors different from those usually considered in other areas of earthquake engineering. In most application of lifeline earthquake engineering techniques, first, the lengths of the pipes are comparable to seismic wave lengths, and thus spatial, as well as temporal, variation in the excitation must be considered. Second, since the pipe is completely surrounded by soil, soil-pipe interaction is a crucial factor in determining pipe response to earthquakes.

Thus, pipe conformance to ground-distortion from traveling seismic waves is more important than the loading of the pipe from its inertia. Further, it appears that axial strain in the pipe caused by differential axial displacements and the response near elbows and other discontinuities will be more critical than response to transverse or oblique waves that travel past straight lengths of pipe.

Numerous dynamic and static tests of pipe elements have been conducted in order to obtain the restoring force characteristics of the surrounding soil, the flexibility, and the ultimate strength of various types of joints.

3.5.1 Lateral Soil Resistant Characteristics

Large abrupt differential ground movements that might result at a pipeline crossing of an active fault probably represent the most seismic effect on a buried pipe. The soil resistant characteristics plays a very important role in the design of buried pipelines crossing an active fault. In this respect, Audibert and Nyman[5,6,7] have conducted an experimental test to deal with the soil restraint on buried rigid conduits subjected to a horizontal motion. The testing was designed with the following purposes: (a) To study the pipe-soil interaction, (b) to reveal the failure mechanisms at shallow and large depths of embedment, (c) to determine the load-displacement (p-y) curves, and (d) to investigate the influence of such parameters as depth, embedment ratio, pipe diameter, and soil density.

All model tests were run in a testing box, shown in Figure 3.31. The box was filled with air-dried Carver sand, a clean medium sand of glacio-fluvial origin. As shown in Figure 3.31, a horizontal load was applied to the model conduits by a hydraulic jack pulling on cables secured at the ends of model conduit. The load was measured directly by a proving ring, and the horizontal movement was recorded by two dial indicators mounted on the sides of

the testing box.

The laboratory testing program was designed to investigate the influence of soil density, depth of embedment, and pipe diameter. Three sizes of model conduits were used (a) A 1-in. outside diameter (O.D.) model conduit was tested at cover ratios (depth of cover/pipe diameter) of 1, 3, 6, 12 and 24; (b) a 2.45-in. O.D. model conduit was tested at cover ratios of 1, 3, and 6; and (c) a 4.5-in. O.D. model conduit was tested at cover ratios of 1 and 2.

Almost all tests were run as strain-controlled tests, but at the beginning of the testing program a few were run as stress-controlled tests. During each test the horizontal load applied at the ends of the model conduit and the corresponding horizontal displacement of the conduit were recorded.

Although the pressure distribution around a buried rigid pipe may resemble that presented in Figures 3.32 (a) and (b) for conditions before and after horizontal translation, the equivalent resultant pressure has been simplified to the uniform pressure of 3.32(c). The unit pressure, p, is thus defined as

$$p = \frac{P}{L \times D} \tag{3.3}$$

where P is total horizontal load on conduit; L is length of conduit; and D is outside diameter of conduit.

The soil pressure p was plotted versus the horizontal pipe displacement y. The p-y curves obtained with the 1-in. model conduit for cover ratios varying from 1D-24D are shown in Figures 3.33(a) and (b) for loose and dense sand, respectively. It is apparent that the soil pressure-displacement relationship is nonlinear, and it could be approximated by a normalized equation shown as below:

$$\bar{p} = \frac{\bar{y}}{0.145 + 0.855\bar{y}}$$

where $\bar{p} = p/p_u$ for $p \leq p_u$, $\bar{y} = y/y_u$ for $y \leq y_u$.

Audibert and Nyman have concluded that the determination of p_u from the experimental p-y curves is relatively simple because in most cases the p-y curves reach a well defined plateau. However, y_u is not precisely defined, and only a range of values can be obtained from the p-y curves. By plotting the ratio of y/H_e versus the depth of embedment, H_e, for both the loose and dense sand cases as shown in Figure 3.34, the following conclusions emerge. In loose sand, the ratio y_u/H_e varies from about 6% for 1-in. pipe to about 3% for the 4.5-in. pipe, and appears to tend toward an asymptotic value of 2% for the large diameter pipes. A similar trend is also observed for dense sand, y_u/H_e decreasing from 3.5% to an apparent asymptotic value of 1.5%. These values are in close agreement with the results of Das[16] on vertical anchor plates for which y_u/H_e varies between 2% and 2.4%.

3.5.2 Soil-Pipe Transverse Interaction (X-ray Technique)

An X-ray detective technique was utilized by N. Nishio et al.[37] and Wataru[50] to clarify the earth pressure around a buried pipe and surrounding soil behavior due to the settlement of the adjacent soils. The earth settlements may be caused by earthquakes.

Due to the extended buried pipe, a plane strain condition was considered in this test. Figure 3.35 shows a test installation with a sand container made of iron. Two aclylic plates were inserted in the windows of both front and rear walls of sand box. A plastic pipe and an iron flat bar were used for a buried pipe. The X-ray film was attached behind the rear aclylic plate to detect the soil rupture plane around the buried pipe. The lead shots spreading as shown in Figure 3.35 were used to display the surrounding soil behavior. Several other experimental conditions were listed in Table 3.9.

Four different experiments, three for plastic pipe and one for flat bar, were executed to seek the interaction between the buried pipe and the surrounding soil. The earth pressures were measured by a proving ring which fixed to a vertical rod. The X-ray pictures were taken before and after lifting the pipe during test. Note that it is important for strain analysis to determine the location of lead shot accurately. For this purpose, a special equipment called "X-ray film reader" has been designed for locating the images of lead shots on X-ray film. Figure 3.36 shows the graphical set-up of the "X-ray film reader".

From the X-ray film, the displacement of those lead shots is thus determined for strain analysis by using finite element method. As mentioned earlier, a plane strain case was considered for the extended buried pipe; thus it is adequate to apply constant strain triangles in the finite element method. Figure 3.37 shows the element of constant strain triangle. It is commonly known that the principal strain, the volmetric strain and maximum shear strain can be calculated from these three components of constant strains of ε_x, ε_y and γ_{xy}.

From observation of test, the relationship between the earth pressure and the relative displacement of buried pipe/soil, shows a peak pressure at very small relative movement as shown in Figure 3.38. The peak value of earth pressure is quite dependent upon the initial void ratio of backfill. In addition, the growth of rupture planes due to relative displacements between a pipe and sand can be described very clearly from the photos taken by X-ray. It is realized that the appearance of rupture planes also greatly depends on the initial void ratio of sand deposit.

The researchers have concluded that the method of using X-ray tecnnique is considered to be available in the researches of excavations, tunneling on geotechnical problems besides the soil-structure interactions.

3.5.3 Longitudinal Dynamic Soil-Pipe Axial Interaction

Recently, Colton et al.[15] conducted tests on a 12-inch diameter actual natural gas pipe, buried in a 15 ft. long and 5 ft. wide trench, and up to 27 in. high of sand. The buried test pipes were oscillated in the axial direction by a hydraulic actuator at frequencies from 0.01 to 12 Hz. From the measured steady state forces produced on these pipes, the force-time history can be determined for a similar pipe buried in sand when the surrounding earth is subjected to an arbitrary displacement time history as in an earthquake.

Figure 3.39 shows the experimental set-up. The apparatus consists of three sections of natural gas pipe buried end-to-end in a trench. All three of the 12-3/4 inch outside diameter pipes were wrapped with the same plastic linings used in service. The pipe covering is soft and allows sand grains to become partially embedded in it. Also, the wrapped cover has ridges exposed to the sand. Therefore, for large pipe displacements slip actually occurs in the sand near the pipe. The middle pipe is the test pipe. An important feature of this configuration is the pipes on each end of the test pipe, which are stationary during the test. A gap was provided between the test pipe and each of the stationary end pipes to allow for the relative motion of the pipes during testing. As shown in Figure 3.39, the gap is sealed from the soil by a rubber tube wrapped around the end portion of the test pipe and the stationary pipe.

The pipes were placed in 2-foot-wide, 30-foot-long trench and back filled with Olympia No. 2 sand. In the first test series, the 15-foot-long

pipe was covered with sand 27 inches deep after compaction. In the second test series, the 5-foot-long pipe was covered with 12 inches of sand. The ratio of void volume to solid sand was in the range of 0.58 to 0.62. The moisture content of the compacted sand was about 4 to 5% by weight.

The test pipe was oscillated by a hydraulic actuator situated in a pit adjacent to the trench. Connected to the actuator is an aluminum push-rod attached to the cross-shaped aluminum link. The crosslink is bolted to the wall of the test pipe. During the tests, the displacement was controlled to follow a specified waveform and frequency, while the resulting load was measured.

Instrumentation consisted of displacement, force, and acceleration gages. One LVDT and one piezoresistive-type load cell was factory installed in the actuator to control or monitor the displacement and force exerted by the actuator piston. A second LVDT was used to measure directly the displacement of the test pipe relative to one of the stationary pipes. In the test pipe, two slip gages were mounted to measure the slip between the pipe and the surrounding soil as shown in Figure 3.39. Slip was measured by LVDT with its body mounted to the inside of the test pipe and its armature connected to a 1-inch square aluminum plate ¼ inch thick that acted as a vain which moves with the sand. An accelerometer was buried in the soil 4 inches above the top of the pipe to measure soil acceleration.

Two series of tests were performed. In the first series, only tests with displacement less than 0.015 inch were performed. In these tests, no slip or only small slip were produced between the pipe and the sand because the force delivered by the actuator and pump system was limited to 5500 pounds. In the second series, the pipe length was reduced to 5 feet and the soil cover was reduced to 12 inches so that both large-displacement and additional small-

displacement tests could be performed. The tests with large displacements are more typical of those produced in earthquakes that damage pipelines. In all tests, the inertia forces of the pipe are small compared to the resistance forces from the sand.

The force-displacement relations measured at different frequencies in tests of similar small displacements with no slip are shown in Figure 3.40. Figure 3.41 shows data for a test at 0.1 Hz with the displacement of the test pipe still small, but large enough to produce some slip between the pipe and the sand. For a large displacement test at 1.0 Hz on the 5-foot test pipe, the force-displacement curve (Figure 3.42) has a sudden, large change in the slop when slip occurs.

From observations obtained during tests, the conclusions made by researchers can be described as follows.

1. At displacements less than about 0.01 inch, no slip occurred between the pipe and the sand.
2. At larger displacements, the pipe slips relative to the sand. The zone of slip is actually in the sand near the pipe.
3. During loading, the force-displacement relation is linear at small displacements. At larger displacements, the slip zone is formed and the slope of the force-displacement relation decreases.
4. As the slip zone encompasses the pipe, the slope of the force-displacement relation decreases at increasing displacements until at large displacements, the force is almost constant.
5. During unloading, the nonlinear characteristic of the force-displacement relation is again a dominant feature.

Also, under the direction of the Senior author of this report, Jalavand[29] has performed some laboratory tests on the longitudinal soil resistance using the MTS dynamic actuator at the Fears Structural Engineering Laboratory of the University of Oklahoma. The set-up of the test system is shown in Figure 3.43 and the pipe specimen is embedded in a wooden sand box.

The steel pipe with diameter of 12" is buried under sand varying from no cover to an equivalence of 24" buried depth. The test frequency is varied from 0 Hz to 6 Hz. The time history of a test sample with 6 inch buried depth and frequency of 1 Hz is shown in Figure 3.44 and the load-displacement curve is shown in Figure 3.45.

The results obtained are quite similar to those obtained by Colton et al.[15] with only a fraction of the cost. The effectiveness of laboratory test is recognized.

3.5.4 Resistance Characteristics of Pipe Joints

For segmented lifelines, the flexibility or ductility of joints plays an important role in the seismic resistnace of a pipeline. Unfortunately, there are limited data on the joint resistant characteristics available.

Recently, Singhal et al.[44] at Arizona State University have performed some tests on joint resistance to axial load and bending. The objective of this study was to experimentally determine the structural behavior and stiffness characteristics of 'push-on rubber gasket' joints of ductile iron pipes. The test fixtures for axial and bending are shown in Figures 3.46 and 3.47, respectively. A sample test for axial force and bending moment are given in Figures 3.48 and 3.49. In conclusion, the paper provides an actual stress-strain curve for the rubber gasket materials. Static and cyclic moment-deflection curves are initially linear. Values of permanent deflections for bending tests

are also obtained. Initial and recycled slip loads were determined from axial pull-out tests and the rate of axial pull-out is load dependent.

Under the supervision of the senior author, Getaz[21] has performed tests to determine the force and elongation or shortening resistant characteristics for rubber gasket bell and spigot joint of concrete pipes as well as ductile iron pipe. The tests were done by an Instron Machine. The schematic of the test set-up is shown in Figure 3.50. A sample of load-elongation curve for an 8" ductile iron pipe joint is shown in Figure 3.51. In the study, the following specific parameters were investigated:

1. The modulus or spring constant of the rubber gasket joint.
2. The ultimate pull-out force.
3. The ultimate pull-out elongation.
4. The ductile stiffness.

The results of above parameters are given in the report[21] and thus will not be repeated.

Table 3.1

Results of Load Tests

LOAD TYPE	Ho Inch	MOVEMENT[1]		EXPERIMENTAL STRESS[2]					CALCULATED CROWN PRESSURE[3]	CALCULATED DEFLECTION		CALCULATED HOOP STRESS @ a
		H	V	MAXM.	MIN.	SHEAR	HOOP @ a[4]	MaxmHoop		V EMPIRICAL	V ANALYTICAL	
1. No Backfill	0	0	0	0	0	0	0	0	0	0	0	
2. Backfill only	35	-.160	.158	4182	-9015	3737	0	6364	0.39	.03	.001	82
3. Backfill only	85	.005	-.005	5492	-9292	5205	1196	5492	4.27	.32	.008	896
4. Backfill only	104	.017	-.002	3717	-12693	5471	1874	7474	5.75	.40	.011	1207
5. F-9000 Dump Truck	104	.003	-.003	3598	-12589	5406	1837	7304	2.76	.19	.005	1787
6. 350-Payhauler	104	.008	-.010	2988	-11699	5111	1345	6196	4.40	.30	.008	2132
7. 4600-S4 Crane	104	.067	-.078	7146	-12479	5416	1644	4982	7.728	.53	.015	2830
8. Backfill only	198	.054	-.039	4116	-6635	2391	2740	5760	13.0	.82	.025	2730
9. F-9000Dump Truck	198	0.0	-.002	6708	-5598	2439	-193	6812	0.92	.06	.002	2923
10.350-Payhauler	198	.001	-.002	6501	-5426	2707	-87	6526	0.88	.06	.002	2915
11. 4600-S4 Crane	198	.007	-.009	7156	-4268	3022	-667	6981	3.22	.20	.006	3406

Notes:
1. Movement of point 'a' for a loading is due to that loading only.
2. Stresses are Principal stresses acting @ a. These stresses are due to total load of the equipment and soil.
3. Crown Pressure is due to the particular load only.
4. Hoop stress is calculated by subtracting stress of load type 2 from other stresses

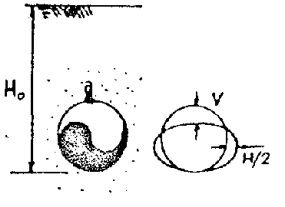

Table 3.2

Results of Stress Analysis

			Dynamite proc.		Shear proc.		Air-gun proc.	
			DI	DIII	SIII(x)	SIII(y)	AII	AIII
Vibration period (sec.)			0.3	0.3	0.5	0.4~0.8	0.03~0.08	0.05~0.08
Max. strain recorded ($\times 10^{-6}$)			4.0	3.0	0.2	0.5	0.8	1.2
Max. axial force (t)	S3	(+)	2.8	1.2	0.28	0.38	0.28	0.63
		(−)	2.5	1.0	0.19	0.24	0.66	0.80
	S36	(+)	2.35	1.2	0.24	0.28	—	—
		(−)	1.65	0.8	0.18	0.22	—	—
	S4	(+)	2.75	1.9	0.24	0.38	0.28	0.36
		(−)	2.75	1.5	0.19	0.25	0.19	0.36
Max. bending moment. (t·m)	S3		0.34	0.30	0.014	0.07	0.14	0.14
	S36		0.45	0.34	0.067	0.14	—	—
	S4		0.37	0.50	0.027	0.06	0.07	0.09
σ_A / σ_M	Horiz.		2 ~ 3	1	2~4	2	1	1
	Vert.		1.5	1	2	0.6	—	—

(+): Tension (−): Compression σ_A: Axial stress σ_M: Bending stress

Table 3.3 List of Earthquakes (YOKOHAMA)

Earthquake No.	Date	Location of Origin: Latitude (N)	Location of Origin: Longitude (E)	Depth (km)	Epicentral Distance (km)	Magnitude	Intensity at Tokyo (JMA)	Max. Acc. (gal): X	Max. Acc. (gal): Y	Max. Acc. (gal): Z	Max. Strain (×10⁻⁶): Axial	N. B.
1	1972 Nov.5	Northwestern Chiba Pref.		50	50	3.5	I	1.9	2.3	1.5	4.0	
2	Nov.6	Southwestern Ibaragi Pref. 36°12	139°48	40	65	5.1	III	17.5	10.0	5.6	17.0	Steel-Pipe 150 φ
3	Dec.4	Near Hachijojima 33°12	141°05	60	270	7.2	IV	26.0 over	26.0 over	11.5	28.4	
4	1973 Jan.17	Middle Saitama Pref.		60	60	4.1	I	–	–	–	12.3	Ductile Cast Iron Pipe (mechanical joint) 150 φ
5	Jan.21	Southwestern Ibaragi Pref.		70	65	4.8	I	3.3	6.8	1.5	6.7	
6	Mar.27	Northern Tokyo Bay 35°31	139°56	60	26	4.9	IV	73.7	38.8	16.5	10.3	Ductile Cast Iron Pipe (lead-yarn joint) 150 φ

Table 3.4 List of Earthquakes (SŌKA)

Earthquake No.	Date	Location of Origin: Latitude (N)	Location of Origin: Longitude (E)	Depth (km)	Epicentral Distance (km)	Magnitude	Intensity at Tokyo (JMA)	Max. Acc. (gal): X	Max. Acc. (gal): Y	Max. Acc. (gal): Z	Max. Strain (×10⁻⁶): Axial
1	1974 Oct.31	Southwestern Ibaragi Pref. 36°06	139°57	60	35.3	4.6	II	32.9	41.5	9.6	12.3
2	Nov.16	Off Choshi 35°45	141°15	40	129.6	6.1	III	29.5	29.0	4.5	11.0
3	Nov.30	South Off Japan 30°36	138°16	20	588.0	7.6	IV	33.8	19.0	6.6	18.7
4	1975 Feb.8	Middle Tonegawa 35°49	140°07	460	28.0	5.4	IV	43.8	16.4	10.2	13.6
5	Apr.12	Southwestern Ibaragi Pref. 36°10	140°01	50	44.1	4.0	II	36.7	39.0	8.8	12.5
6	Apr.18	Southwestern Ibaragi Pref. 36°08	139°51	50	36.4	5.0	II	37.0	49.5	13.4	7.3
7	Aug.12	Off Torishima 31°42	138°18	360	460.0	6.9	III	6.3	9.7	5.0	6.8

Table 3.5 List of Earthquakes (ŌMORI)

Earthquake No.	Date	Location of Origin		Depth (km)	Epicentral Distance (km)	Magnitude	Intensity at Tokyo (JMA)	Max. Acc. (gal)			Max. Strain (×10⁻⁶)
		Latitude (N)	Longitude (E)					X	Y	Z	Axial
1	1976 Dec.29	North Gunma Pref.		140	146	5.8	IV	15.5	15.9	7.2	6.3
		36°48	139°12								
2	1977 Jun.4	Northern Tokyo Bay		60	29	4.6	III	12.6	18.9	6.7	9.5
		35°31	140°03								
3	Oct.5	Southwestern Ibaragi Pref.		60	66	5.4	IV	19.8	20.5	8.5	14.7
		36°08	139°52								
4	Dec.17	Off Ibaragi Pref.		50	167	5.6	III	5.9	6.8	4.7	6.1
		36°35	141°05								
5	1978 Jan.14	Near Izu Oshima		0 5	100	7.0	IV	57.9	35.3	12.3	26.1
		34°46	139°15								
6	Jan.15	Middle Izu Peninsula		20	114	5.8	III	17.3	8.4	3.3	5.0
		34°50	138°53								
7	Jan.15	Middle Izu Peninsula		10	120	5.4	II	3.6	2.9	1.1	2.3
		34°48	138°50								
8	Mar.7	Far Off Tokaido		400	559	7.8	III	23.4	18.1	5.5	8.9
		31°36	137°48								
9	Mar.20	Southwestern Ibaragi Pref.		60	63	5.5	III	8.8	8.2	5.4	5.3
		36°06	139°54								
10	Apr.7	East Off Chiba Pref.		40	129	5.7	II	3.1	3.0	1.3	3.0
		35°12	141°06								
11	Jun.12	Off Miyagi Pref.		30	365	7.4	IV	27.0	21.7	7.5	17.0
		38°09	142°13								

Table 3.6 Earthquakes recorded at the Tama river tunnel—April to October 1970

Record No.	Date	Time h m	Epicentre N (deg)	Epicentre E (deg)	Focal depth (km)	*M*	Intensity	Epicentre location	Maximum acceleration at subaqueous tunnel (gal)
Record 1	17 May 1970	23 52	34·6	141·1	—		I	Off Boso peninsula	1·34
Record 2	27 May 1970	21 06	27·5	140·0	Deep		II	Ogasawara waters	3·0
Record 4	14 Sept. 1970	18 45	38·9	142·0	40	6·2	III	Off Sanriku coast	2·6
Record 5	30 Sept. 1970	4 26	35·6	139·7	50	4·8	III	Downstream Tama river	12·1
Record 6	30 Oct. 1970	8 14	36·0	139·9	60	4·9	III	Southwest Ibaragi prefecture	3·4

Released by the Japanese Meteorological Agency.

Table 3.7 Scale Factors of Model to Prototype

Note		Scale Factors	
Length	L	$Lm/Lp=\frac{1}{\lambda}$	$\frac{1}{100}$
Time	T	$Tm/Tp=\frac{1}{\lambda}\sqrt{\frac{Ep}{Em}\cdot\frac{\rho m}{\rho p}}$	0.389
Acceleration	α	$\alpha m/\alpha p=\lambda\cdot\frac{Em}{Ep}\cdot\frac{\rho p}{\rho m}$	0.066
Strain	ε	$\varepsilon m/\varepsilon p$	1.000
Young's modulus	E	Em/Ep	$\frac{1}{2,500}$
Mass	ρ	$\rho m/\rho p$	0.606

Table 3.8 Properties of soil layers for dynamic tunnel model

	Channel		Land	
	Thickness (mm)	Young's modulus (gm/cm²)	Thickness (mm)	Young's modulus (gm/cm²)
First layer	24	40	42	240
Second layer	40	90	96	90
Third layer	40	230	40	230

Table 3.9

Experiment Conditions

	Pipe	Flat Bar
diameter or width	8.9 cm	9.0 cm
length	18 cm	18 cm
depth	26.5 cm	26.5 cm
backfill	Toyoura dry sand	Toyoura dry sand
speed of lifting	0.5 mm/min	0.5 mm/min
initial void ratio	0.67 0.77 0.92	0.68

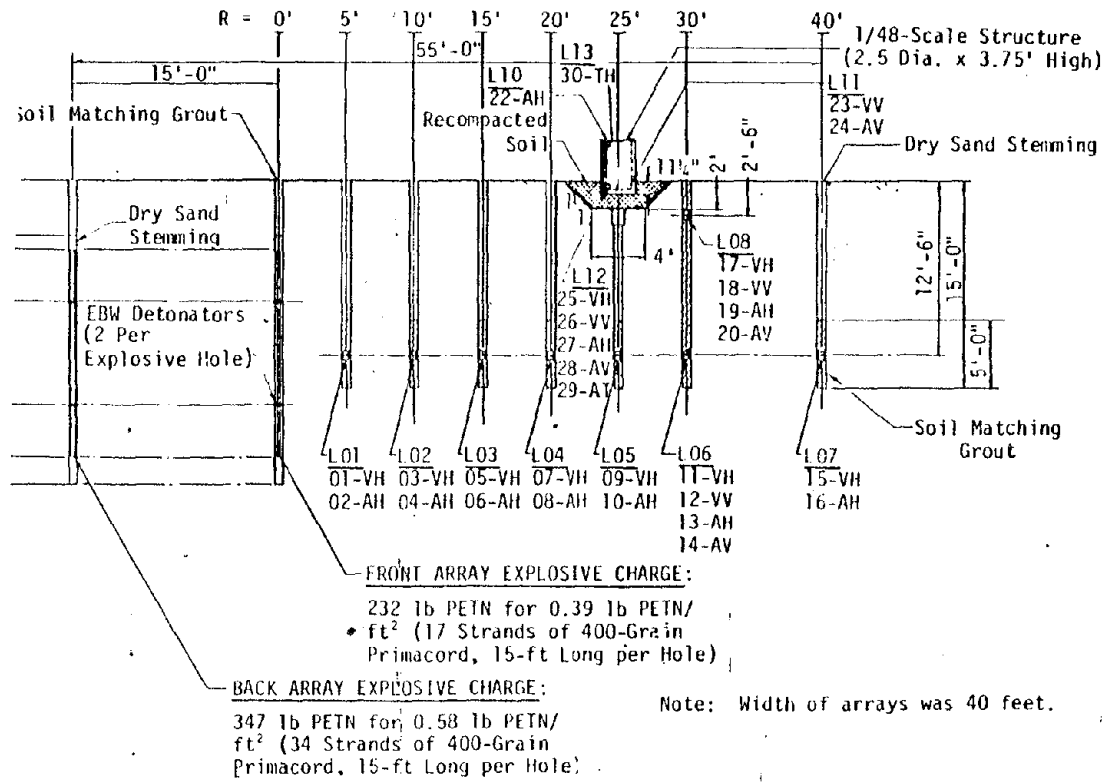

Figure 3.1 Mini-Simquake Elevation

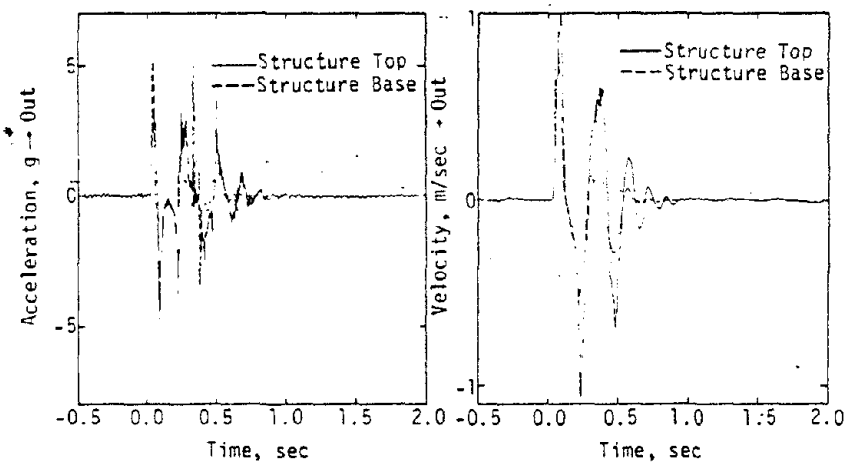

(a) Horizontal Acceleration (b) Horizontal Velocity

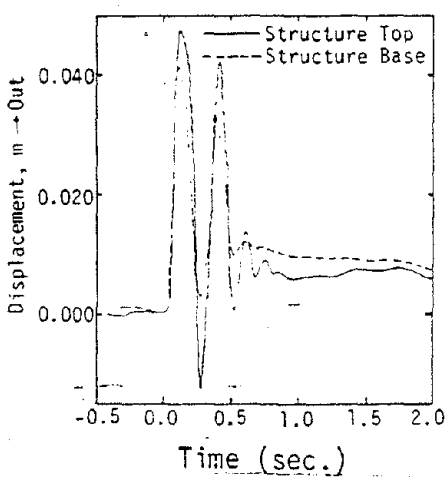

(c) Horizontal Displacement

Figure 3.2 Comparison of Horizontal Response of Base and Top of Model Structure

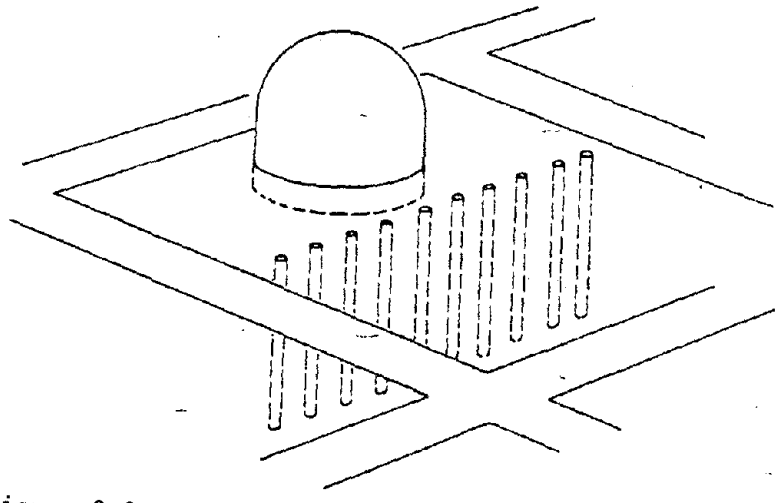

Figure 3.3 Scale Model Testing of Containment Building with Line Source Array

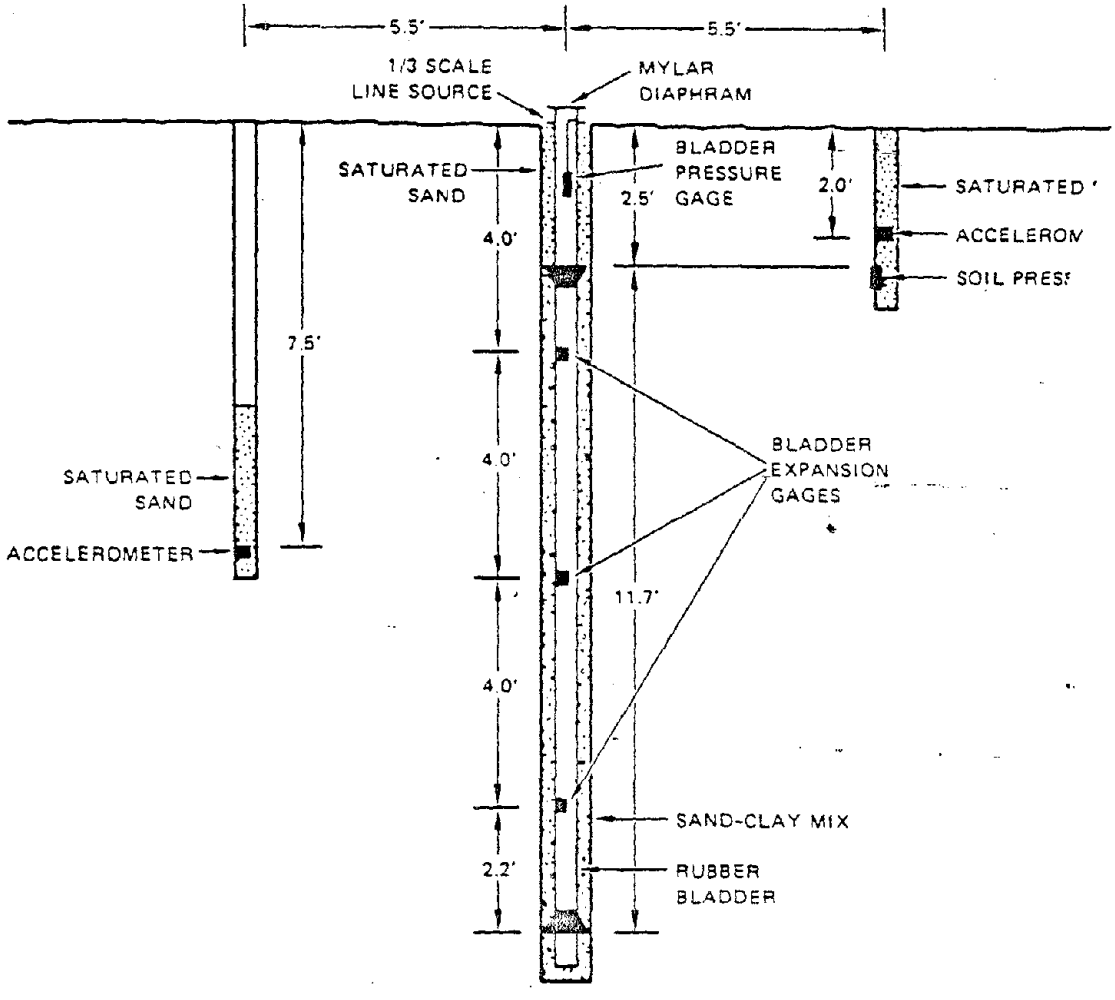

Figure 3.4 Schematic of 4-in.-Diameter Line Source in Soil

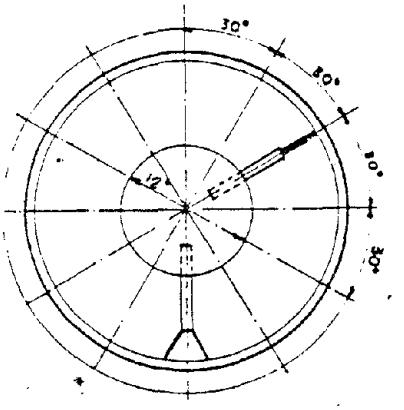

Figure 3.5 Extensometer Disk

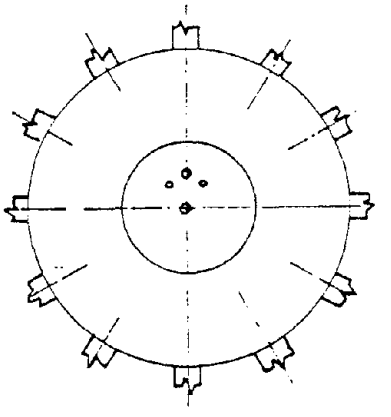

Figure 3.6 Tiltmeter Location

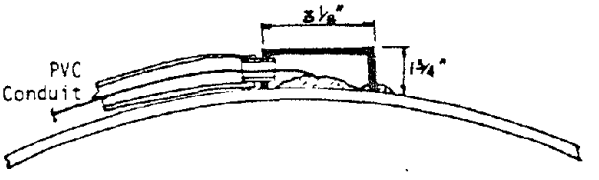

Figure 3.7 External Strain Gage Protection

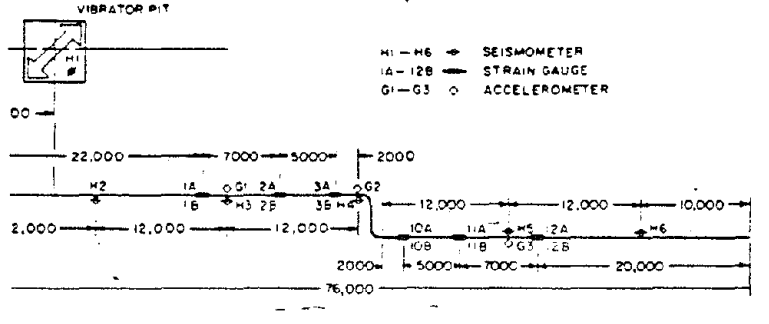

Figure 3.8 Indirect Harmonic Vibration Tests by a Vibrator

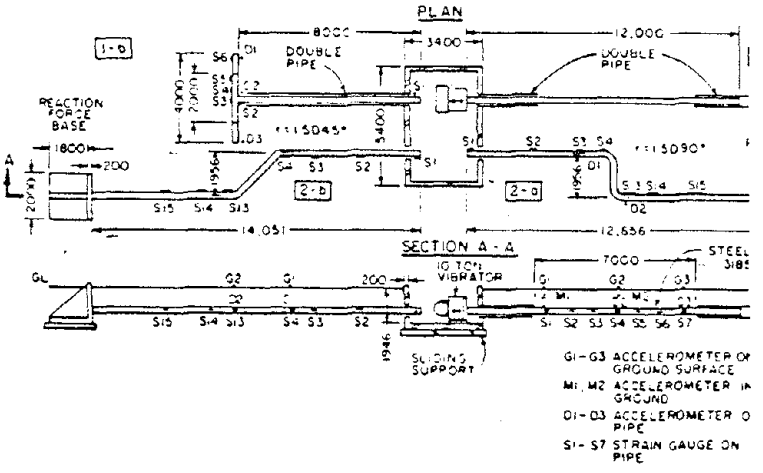

Figure 3.9 Direct Vibration Tests by a Vibrator

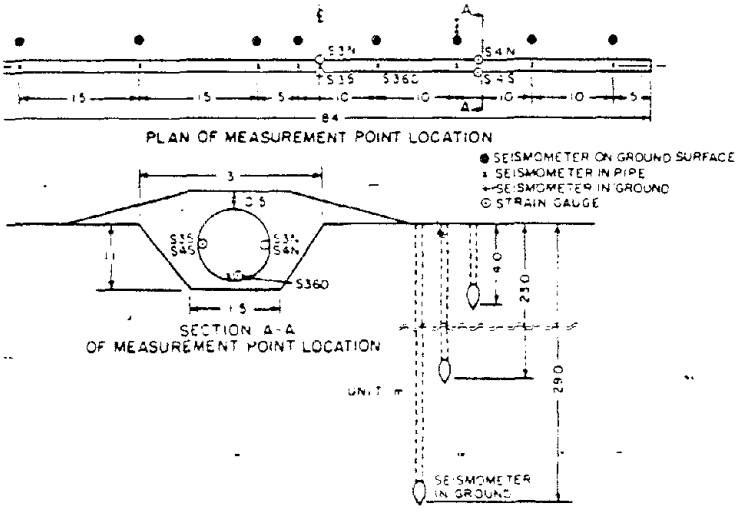

Figure 3.10 Transient Vibration Tests by Air-Gun

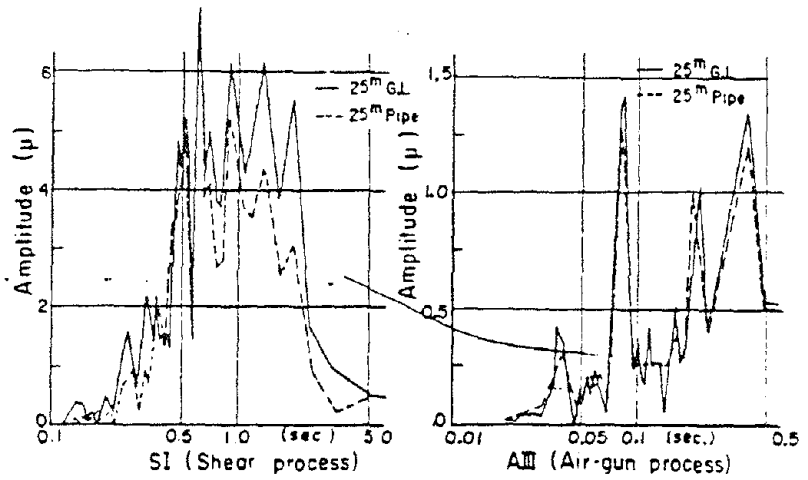

Figure 3.11 Fourier Spectra for Vibrations of Ground and Pipe

STANDARD PENETRATION TEST

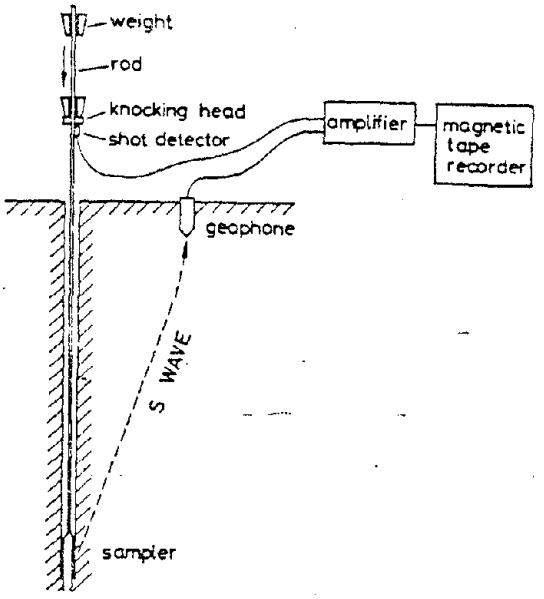

Schematic representation of simultaneous measurement of S wave velocity with standard penetration test. SV wave generated at the bottom of a borehole by a penetration sampler is detected on the ground surface near the borehole

Figure 3.12

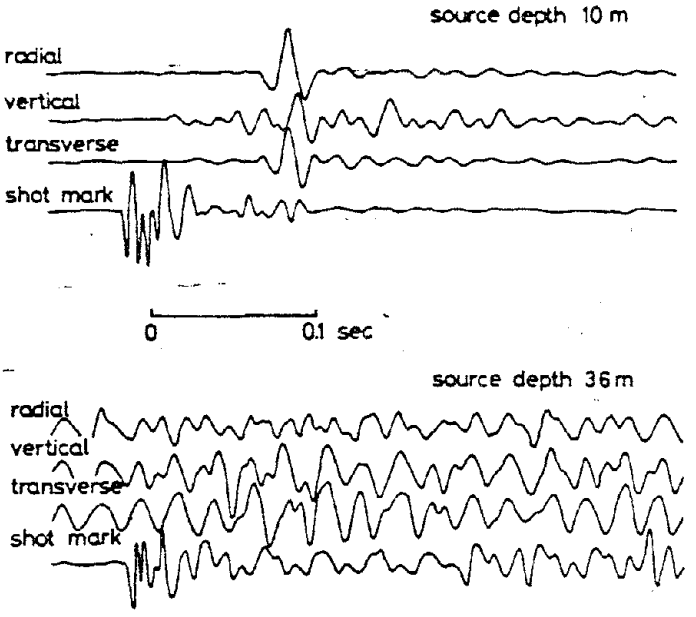

Examples of records with high and low signal to noise ratios

Figure 3.13

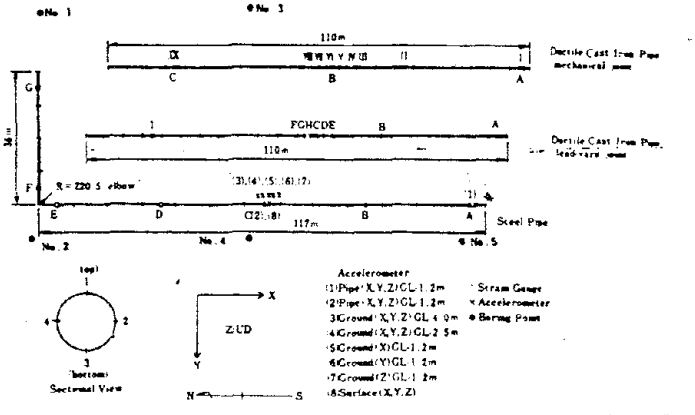

Arrangement of Instruments

Figure 3.14

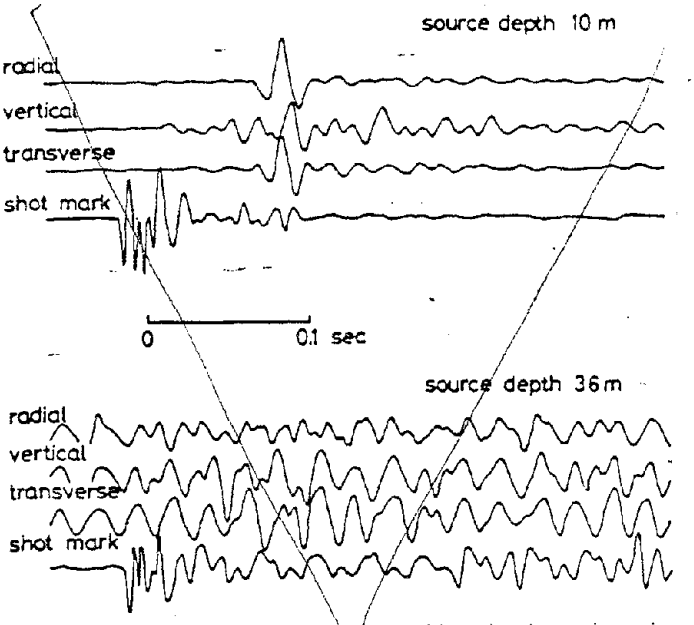

Examples of records with high and low signal to noise ratios

Figure 3.13

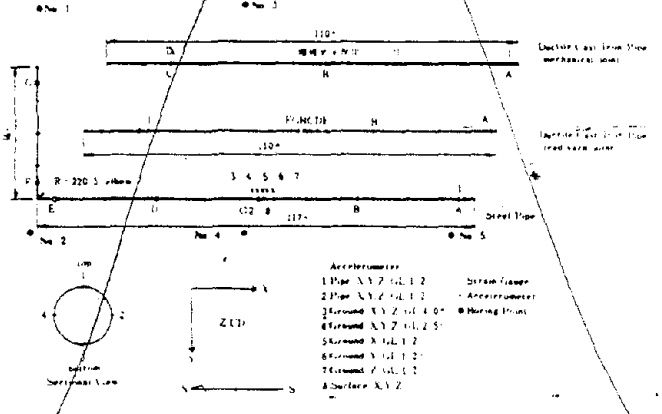

Arrangement of Instruments

Figure 3.14

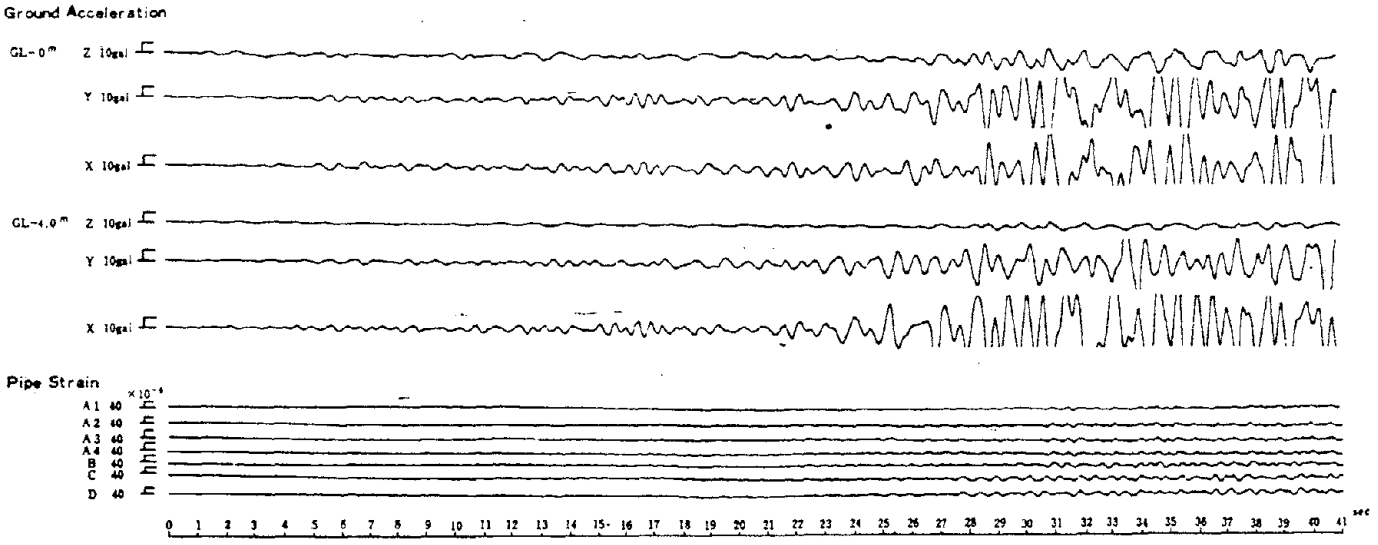

Records of the Near Hachijojima Earthquake, Dec. 4, 1972

Figure 3.15

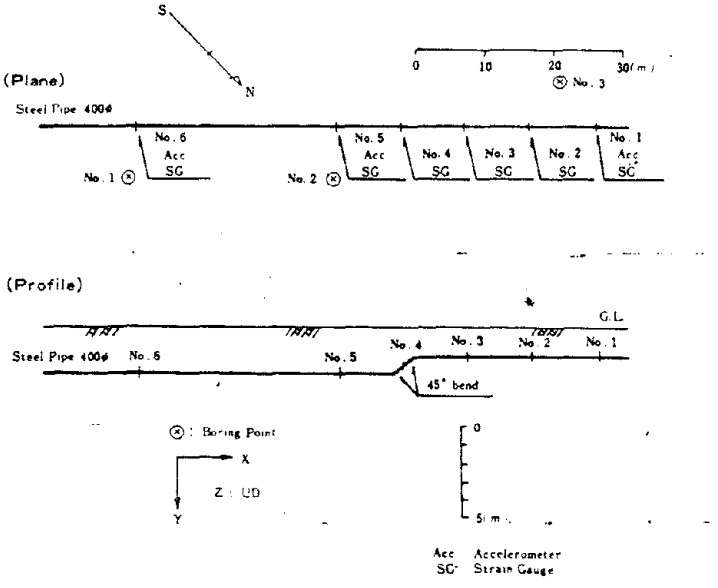

Arrangement of Instruments

Figure 3.16

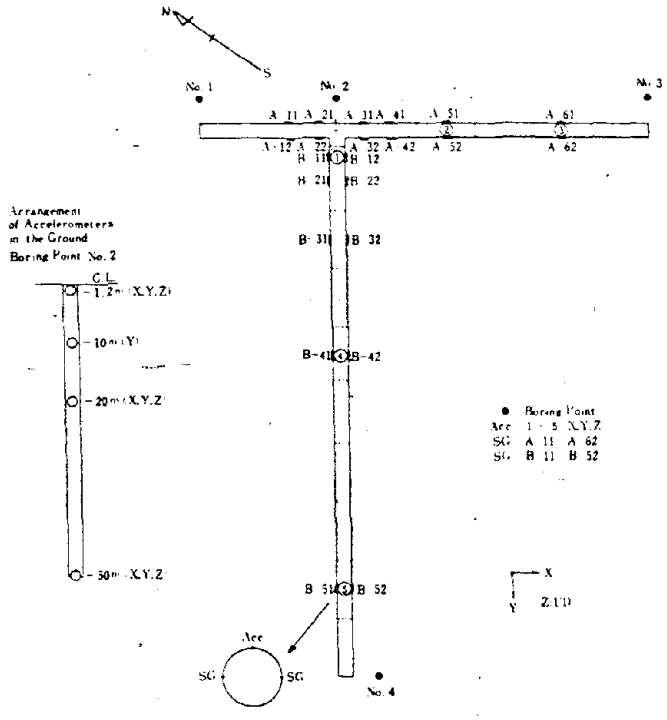

Figure 3.17 Arrangement of Instruments

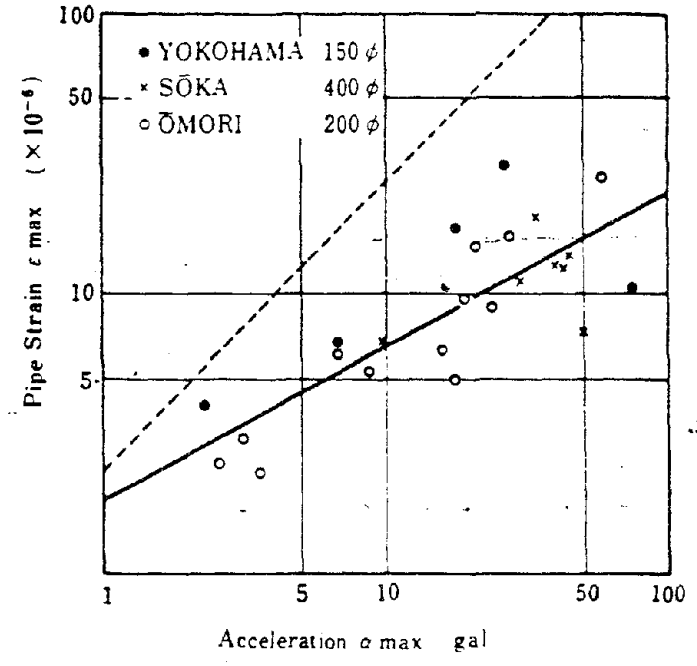

Relation between Max. Acceleration and Max. Strain

Figure 3.18

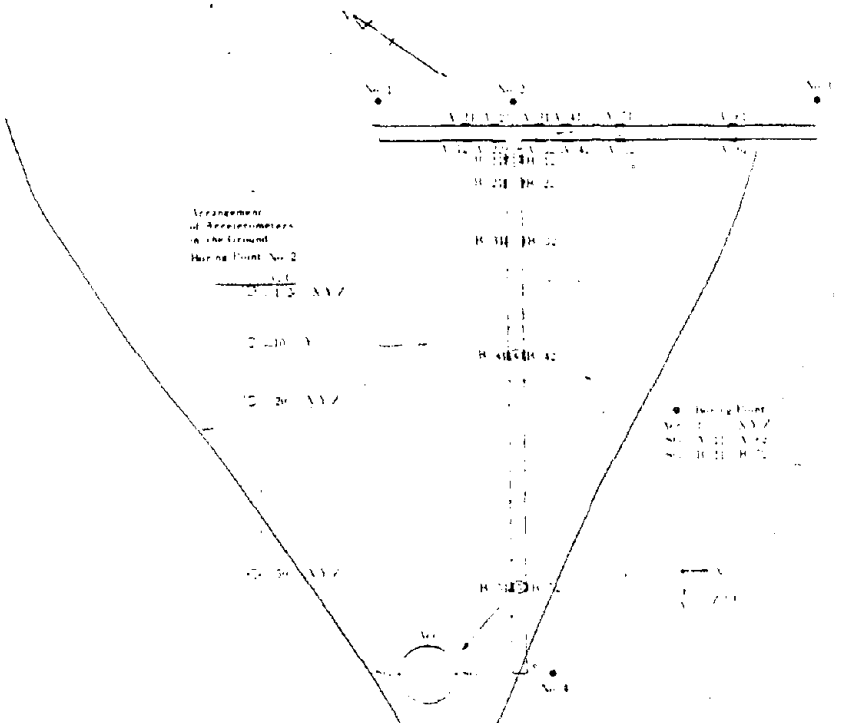

Figure 3.17 Arrangement of Instruments

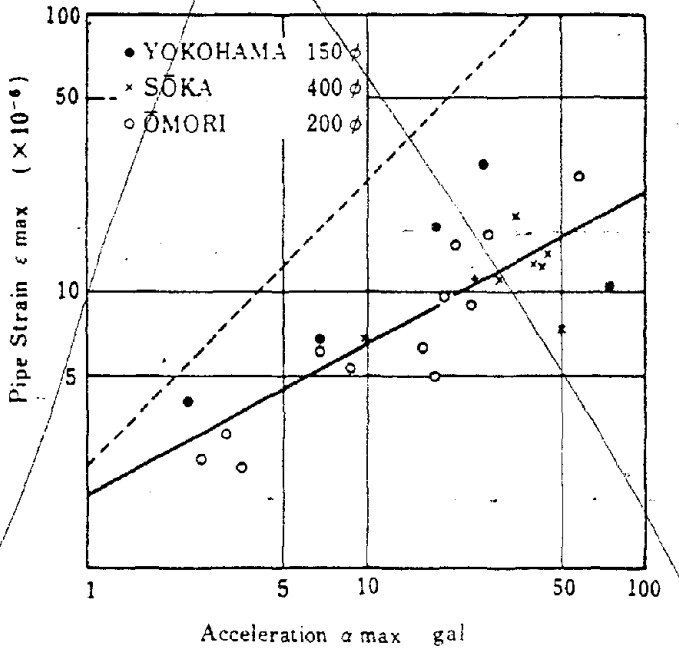

Relation between Max. Acceleration and Max. Strain

Figure 3.18

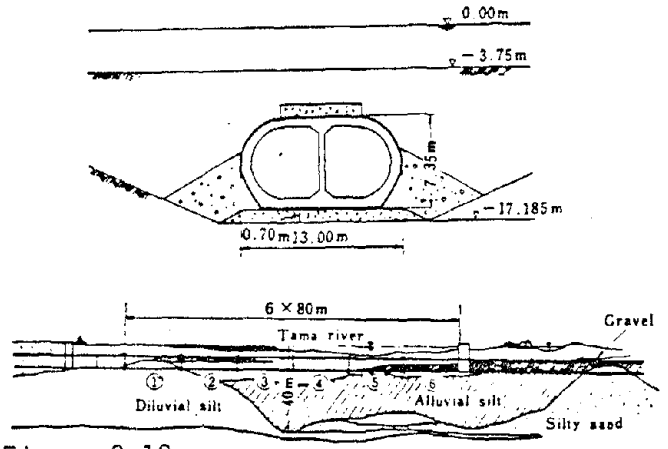

Figure 3.19 Tamagawa sub-aqueous railway tube.

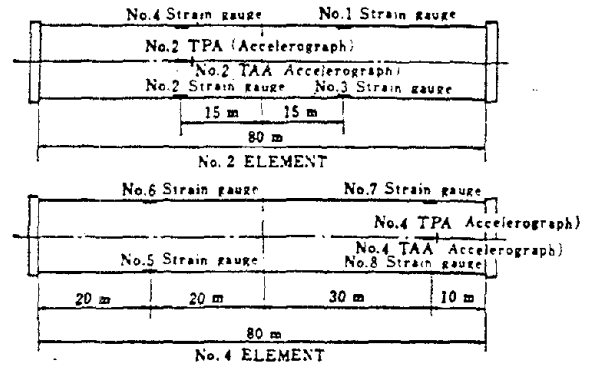

Figure 3.20 Plan of No. 2 and No. 4 elements of the tunnel.

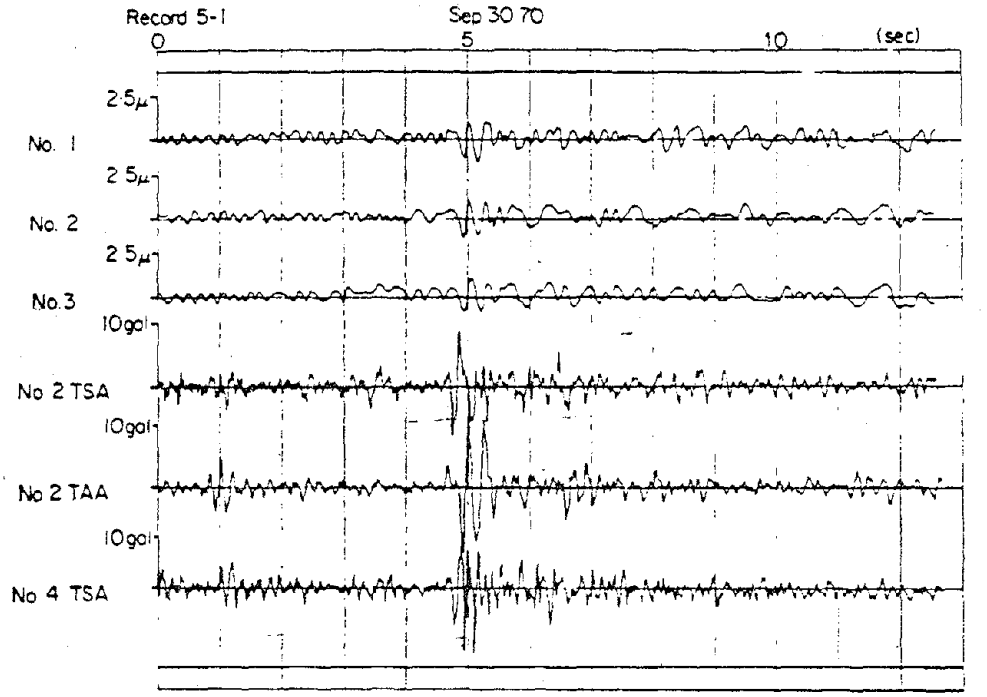

Earthquake record 5-1

Figure 3.21

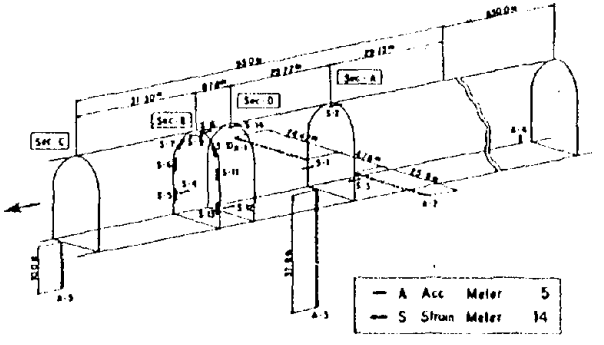

(a) Instrument location

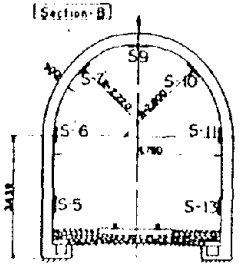

(b) Cross section B

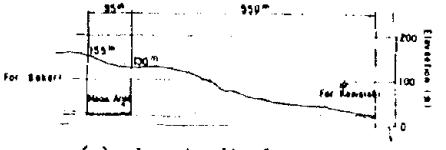

(c) Longitudinal section

General view of rock tunnel and location of measuring instruments

Figure 3.22

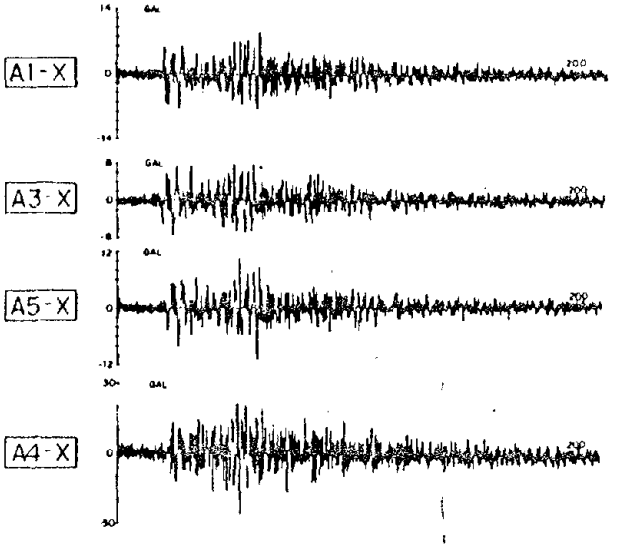

Acceleration in the axis direction

Figure 3.23

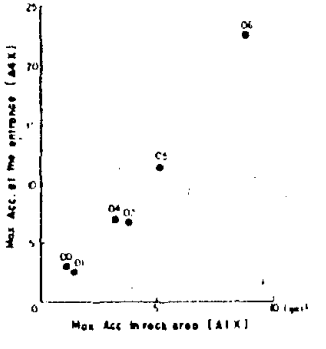

Acceleration amplification at the entrance

Figure 3.24

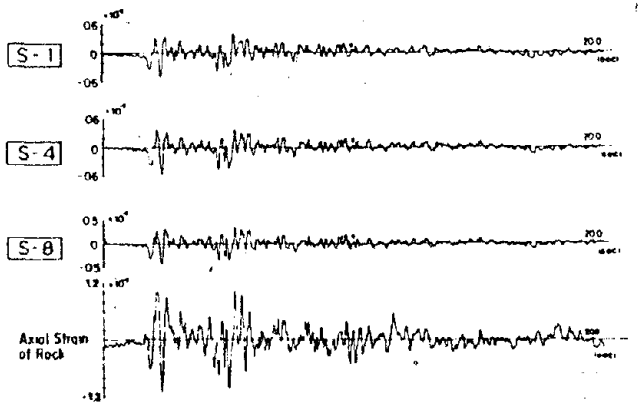

(a) axial strain of tunnel and rock

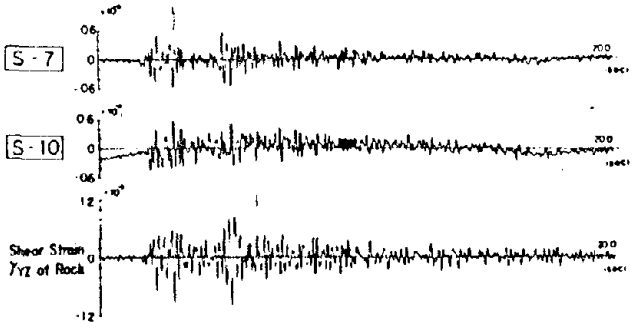

(b) circumferential strain at 45 degrees point of arch and shear strain of rock

Strain of tunnel and rock

Figure 3.25

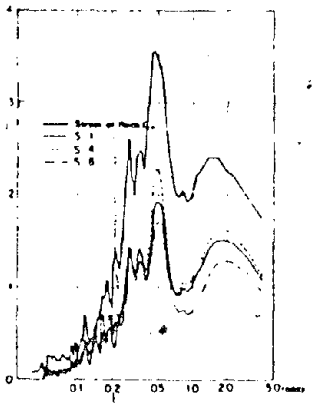

(a) axial strain of tunnel and rock

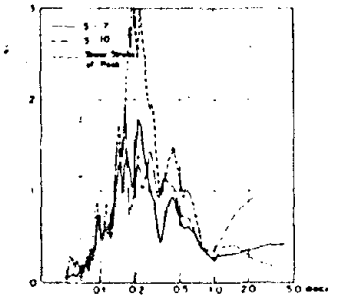

(b) circumferential strain and shear strain

Power spectra of strain

Figure 3.26

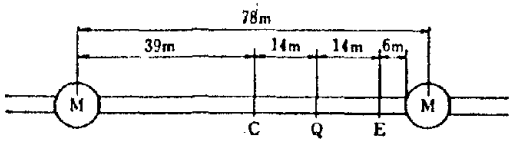

Figure 3.27

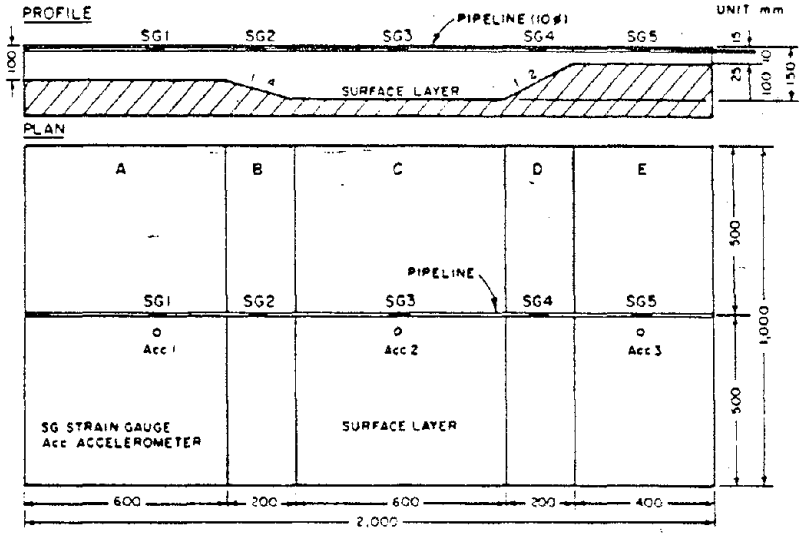

Figure 3.28 Scale Model for the Vibration Test

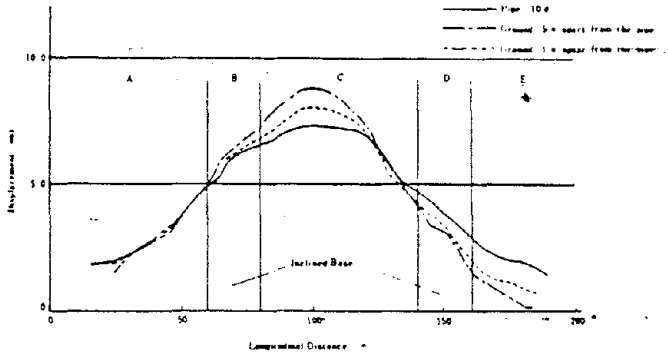

Response Displacement of Pipe and Ground:
Sinusoidal Excitation by 5.64Hz and in
the Axial Direction

Figure 3.29

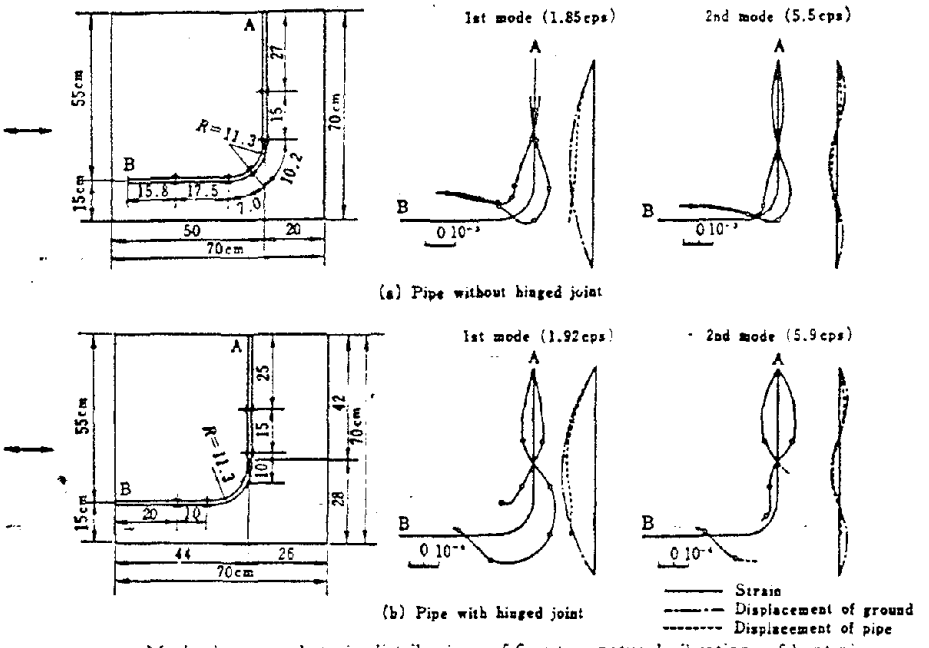

Mode shapes and strain distributions of first two natural vibrations of bent pipe.

Figure 3.30

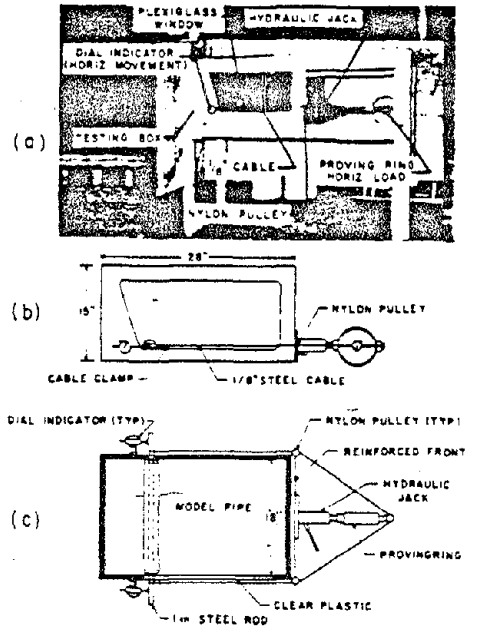

Testing Apparatus: (a) General View of Set Up; (b) and (c) Side and Plan Views of Testing Box (1 in. = 25.4 mm)

Figure 3.31

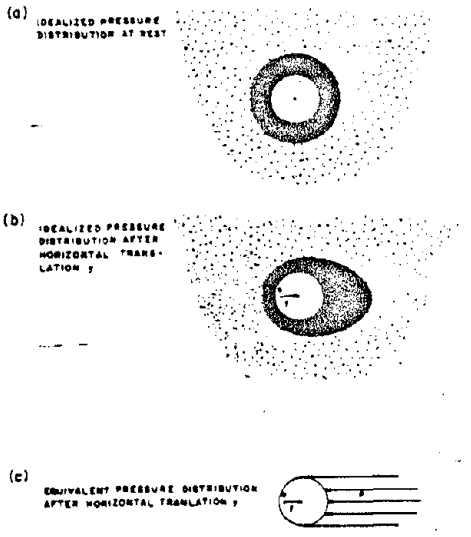

Soil Pressure Around Rigid, Buried Conduit

Figure 3.32

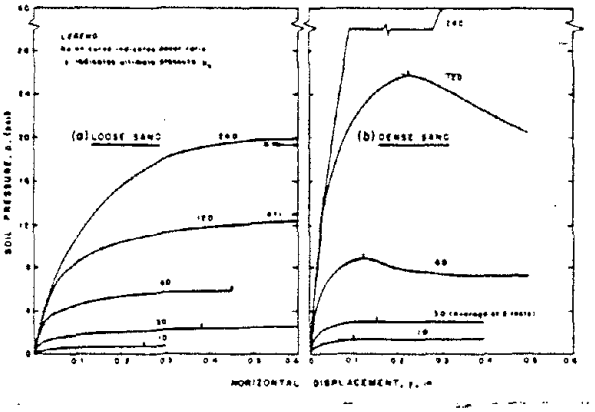

p-*y* Curves for 1 in. Model Conduit Embedded in (*a*) Loose Carver Sand; (*b*) Dense Carver Sand (1 in. = 25.4 mm, 1 psi = 6.89 kN/m²)

Figure 3.33

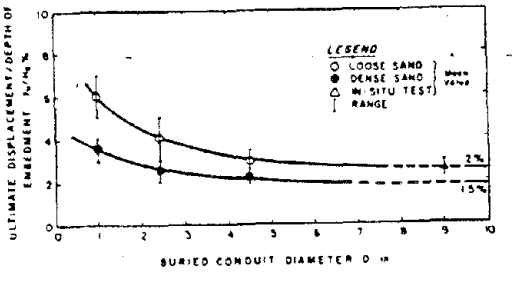

Variations of Y_u/H_r with Diameter of Buried Pipe

Figure 3.34

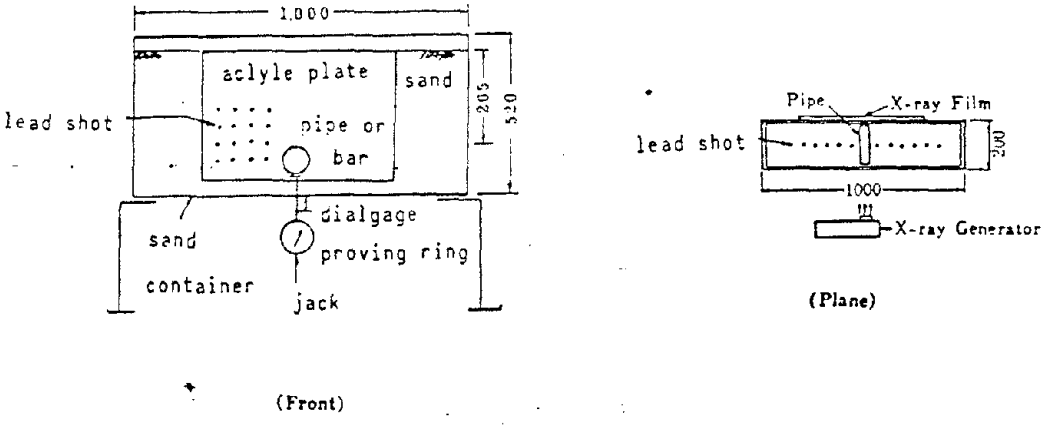

Figure 3.35 Test Installation

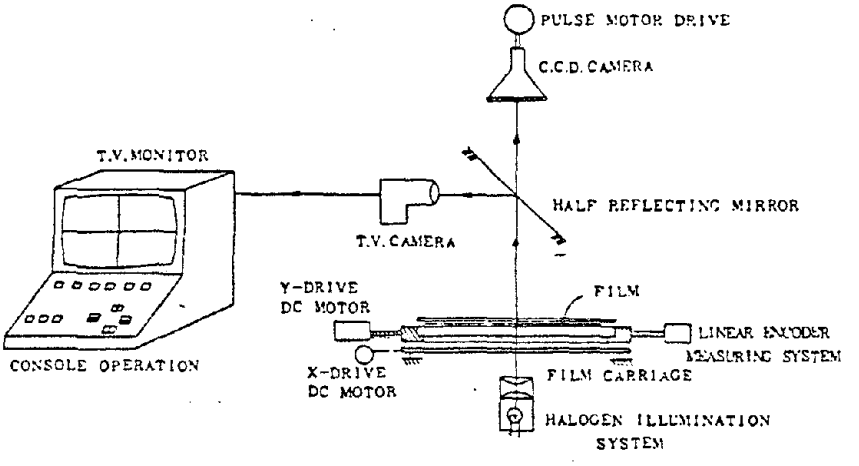

Line Diagram of the Computer Controlled X-ray Film Reader.

Figure 3.36

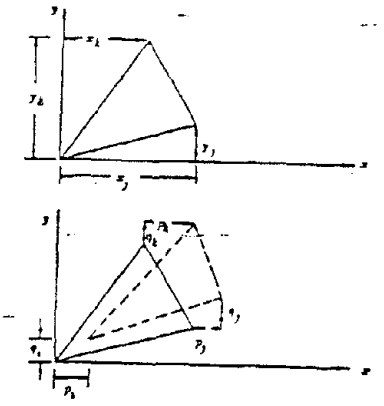

Strain Analysis with Employing
Constant Strain Triangle

Figure 3.37

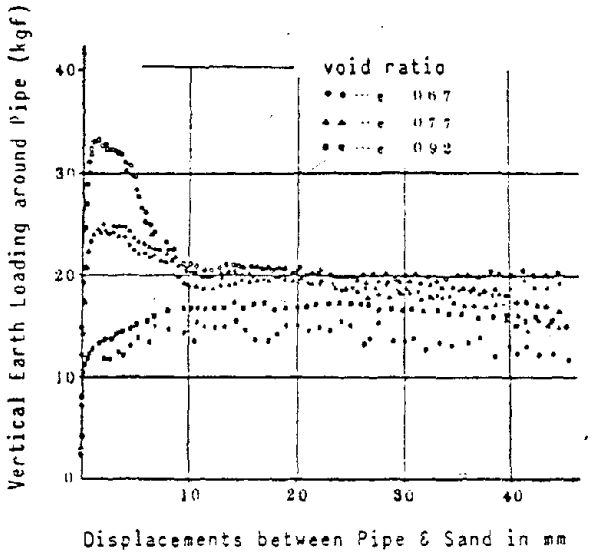

Earth Pressure around a Pipe
due to its Lifting

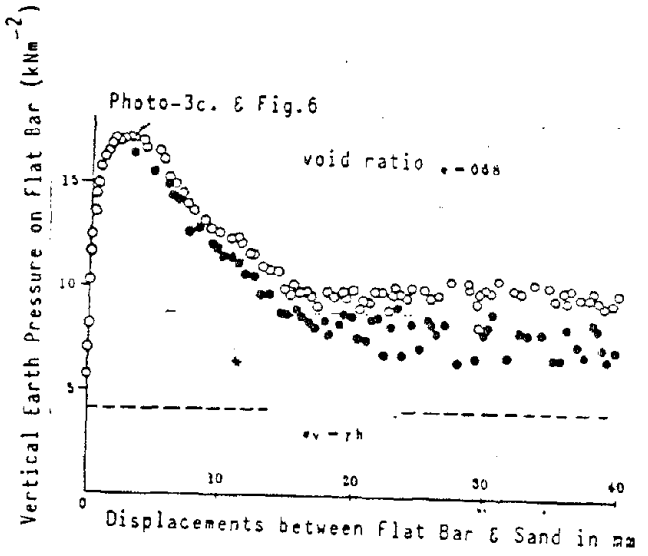

Earth Pressure on a Flat Bar
due to its Lifting

Figure 3.38

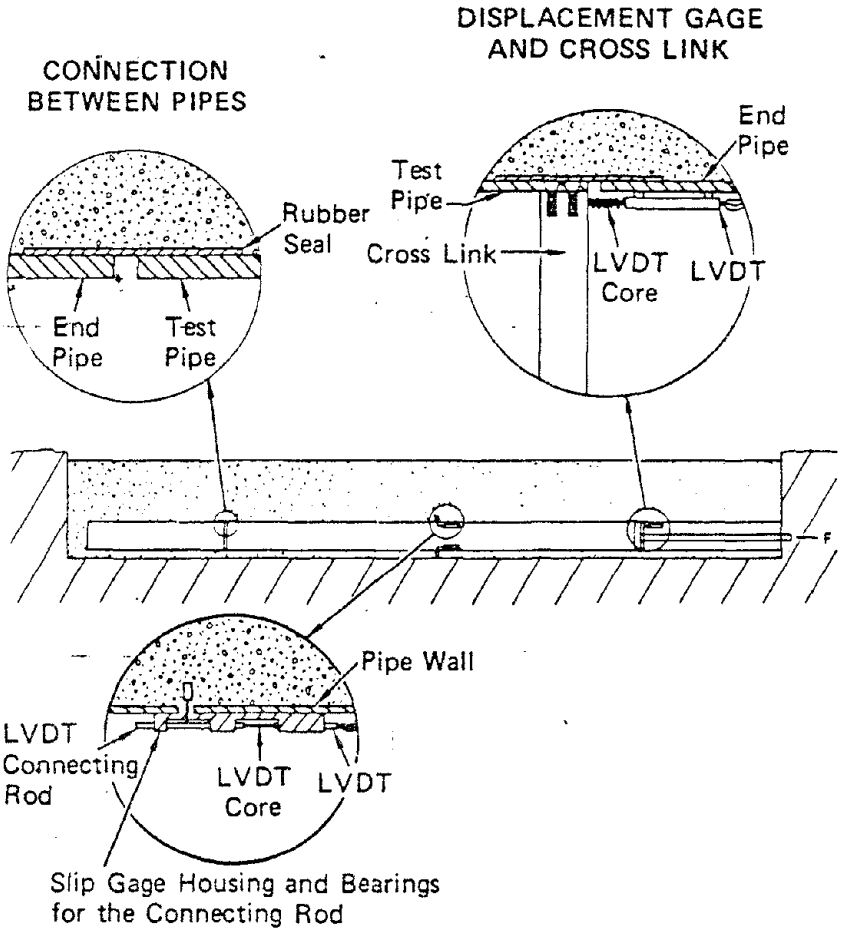

Figure 3.39 Details of Experimental Set-up

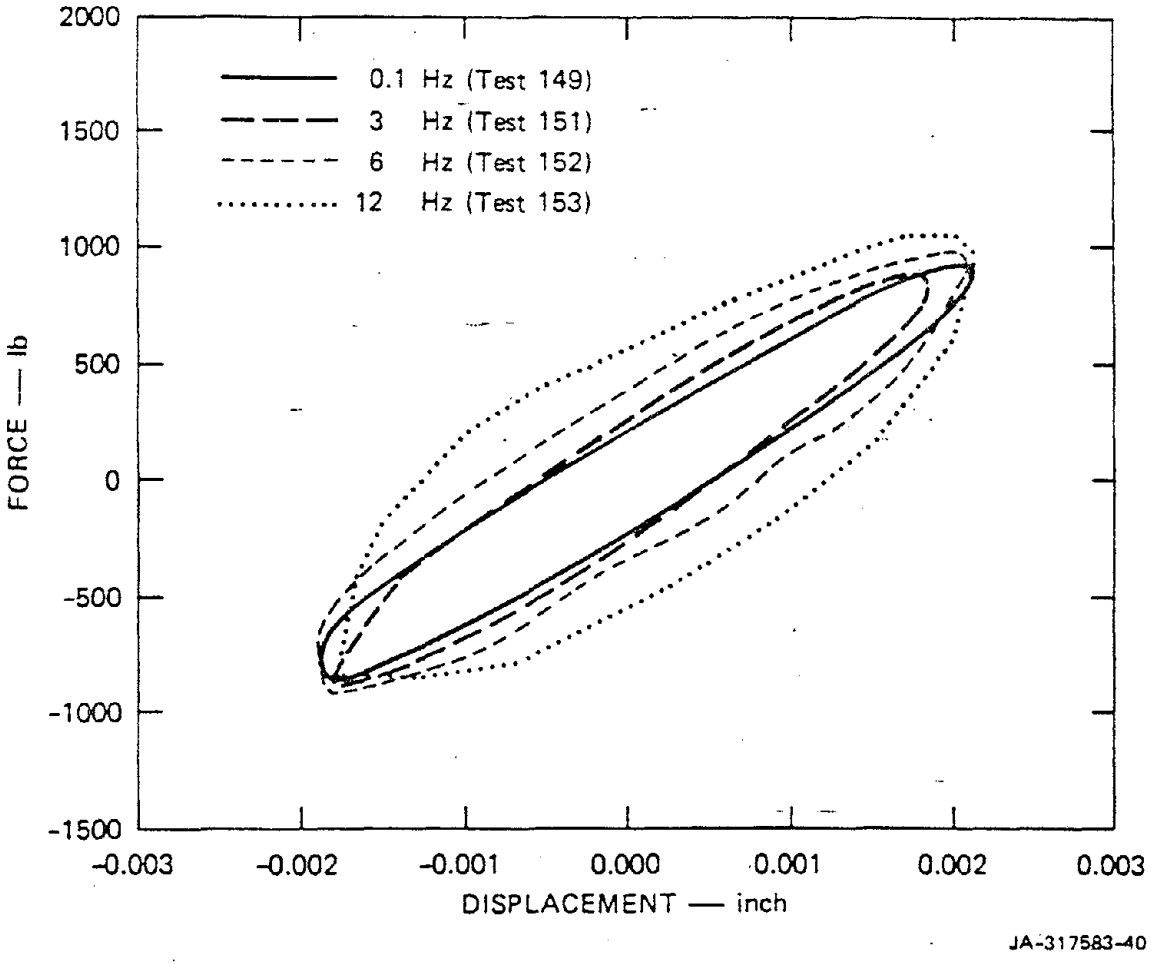

Figure 3.40 TESTS PRODUCING SMALL DISPLACEMENTS AND NO SLIP AT DIFFERENT FREQUENCIES

(5-foot-long pipe, 12-inch sand cover)

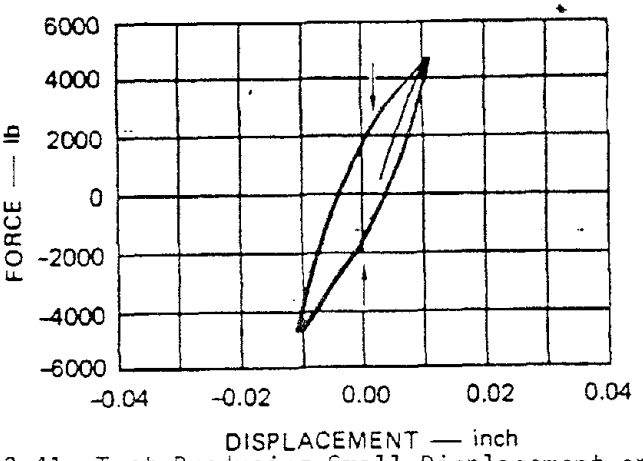

Figure 3.41 Test Producing Small Displacement and Small Slip at a Low Frequency

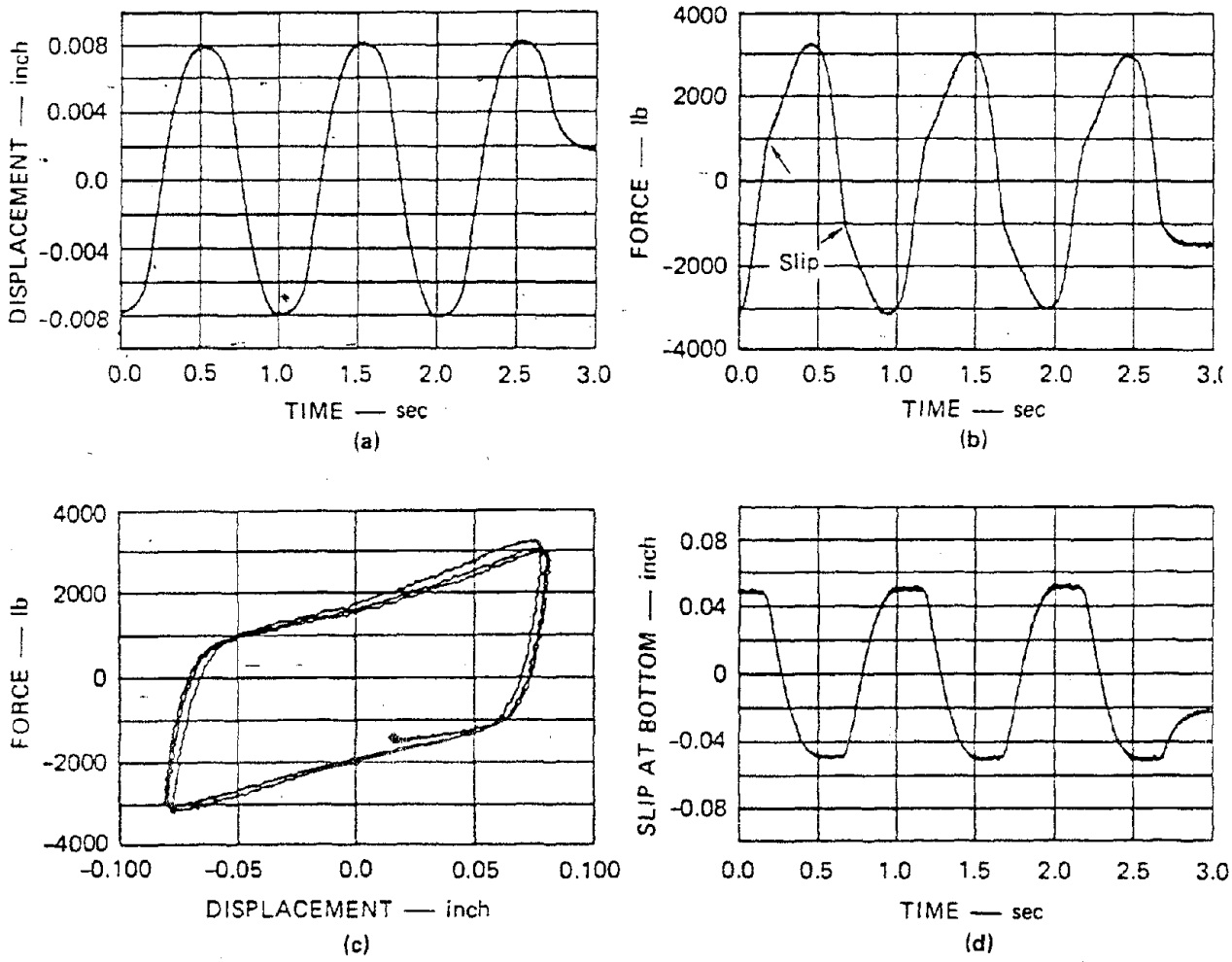

TEST PRODUCING LARGE DISPLACEMENT AND LARGE SLIP AT A LOW FREQUENCY

(Test No. 134, 1.0 Hz, 5-foot-long pipe, 12-inch sand cover)

Figure 3.42

DETAIL OF EXPERIMENTAL APPARATUS

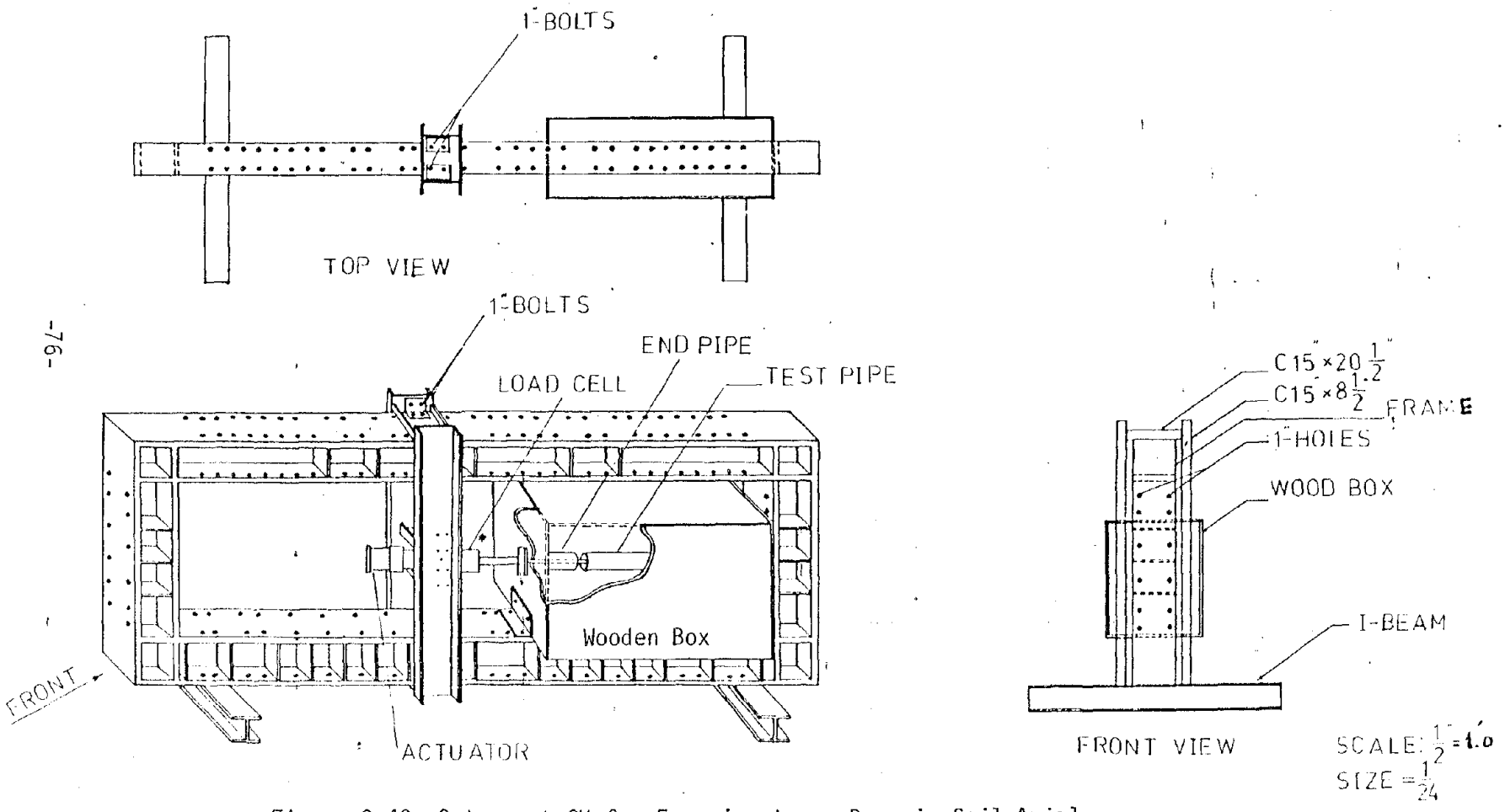

Figure 3.43 Set-up at OU for Experiments on Dynamic Soil Axial Resistance to Pipe Motion

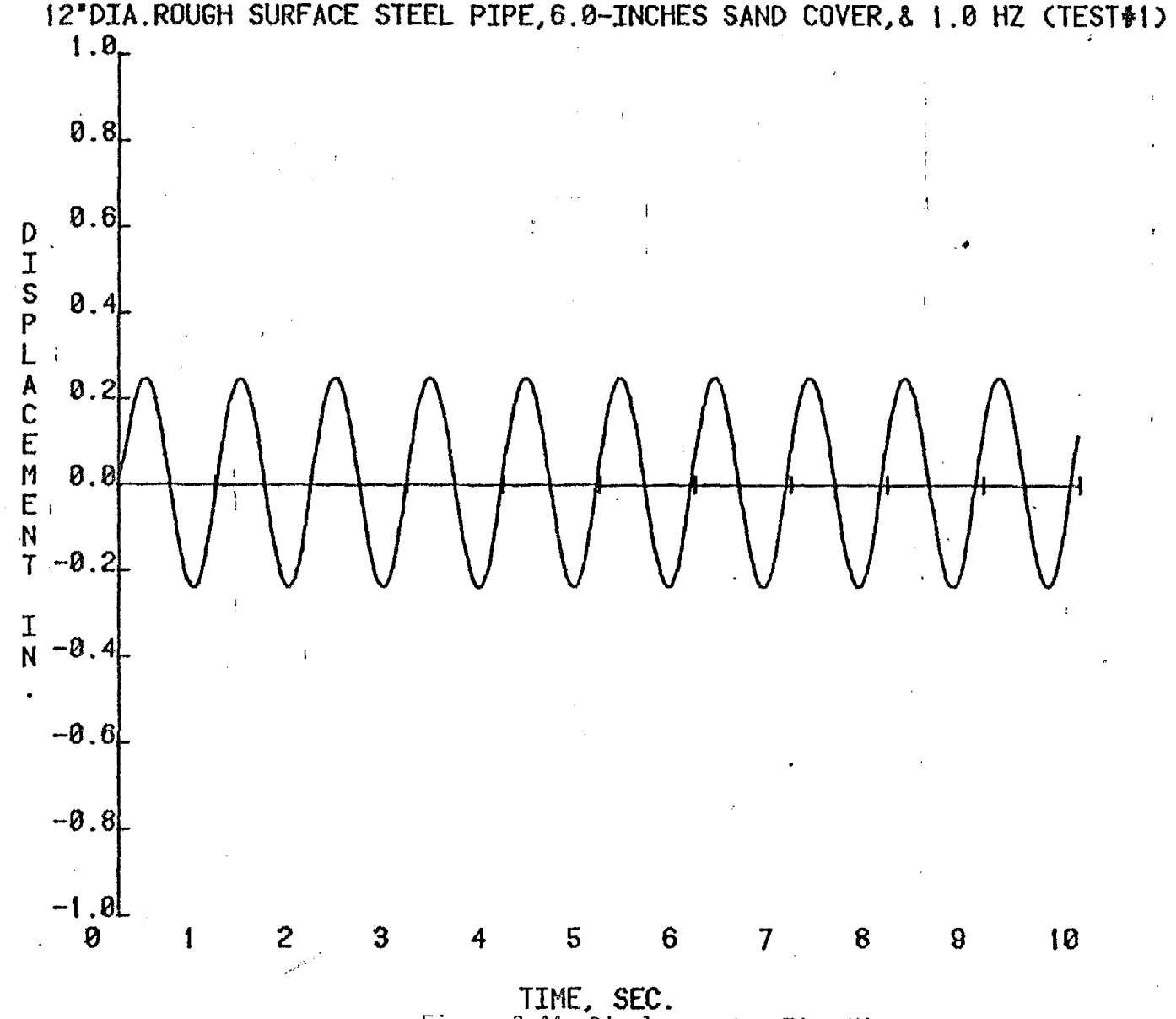

Figure 3.44 Displacement - Time History

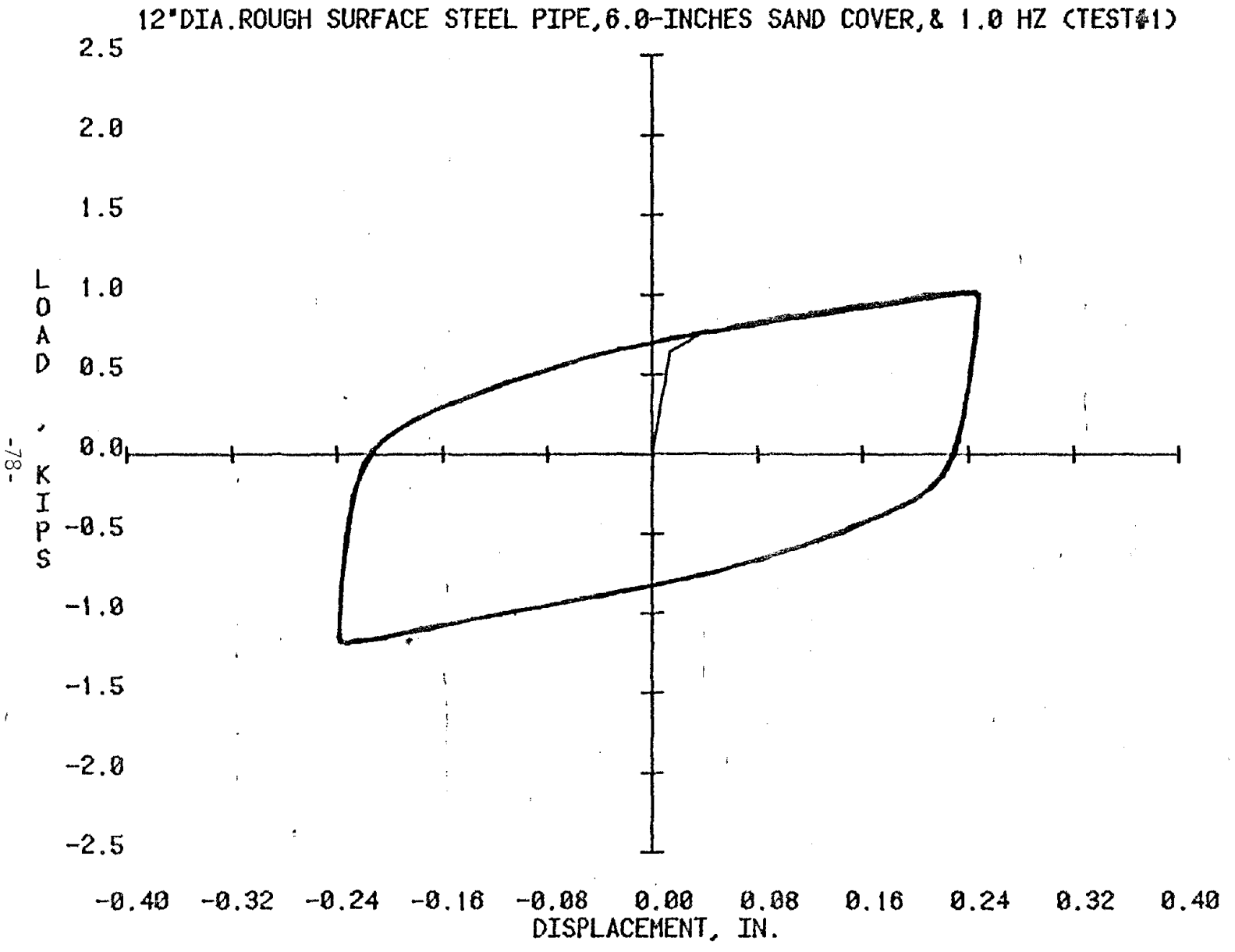

Figure 3.45 Load Displacement Relationship

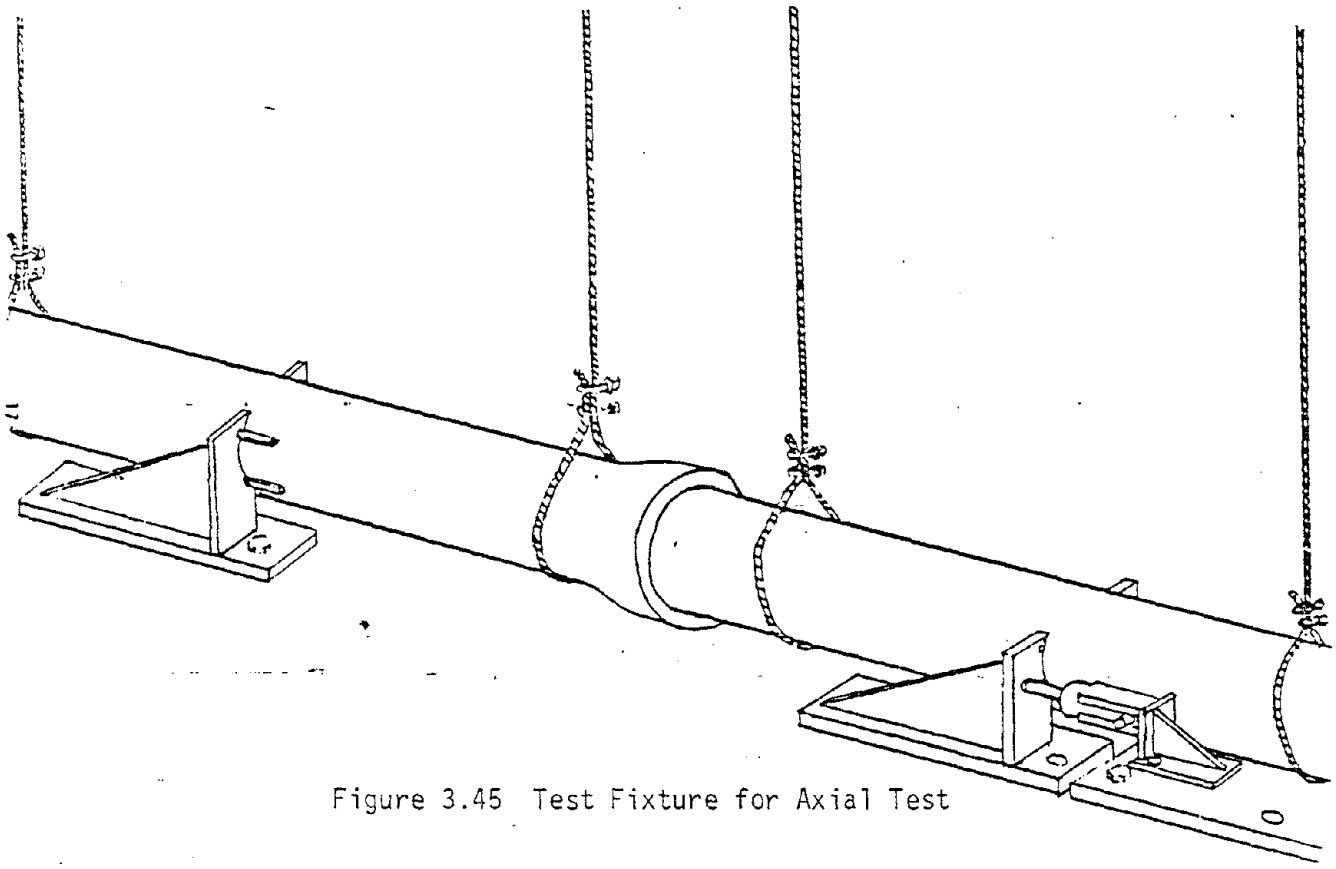

Figure 3.45 Test Fixture for Axial Test

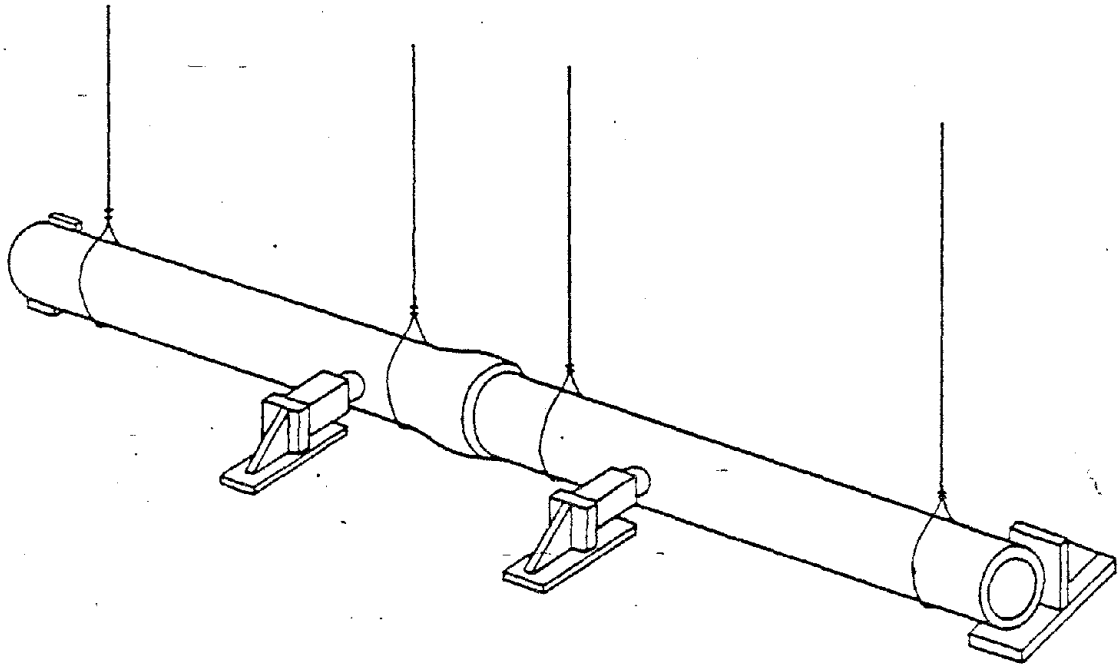

Figure 3.47 Bending Test Set-up

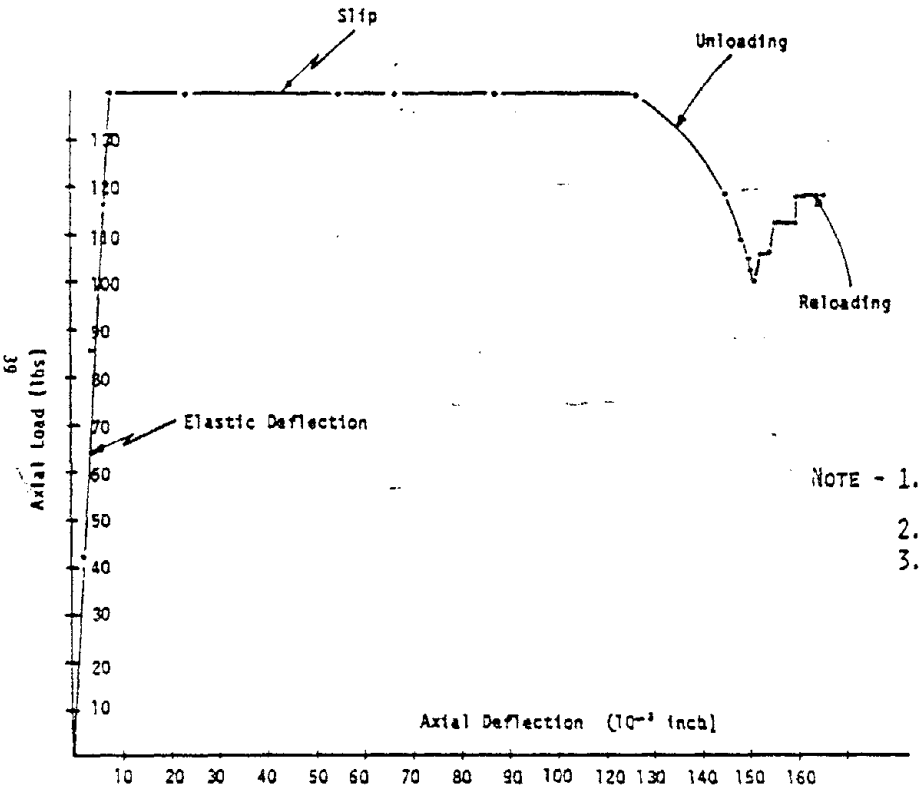

NOTE - 1. ALL DATA POINTS ARE AT 60 SEC INTERVAL.
2. PULL OUT LOAD = 139 LB (INITIAL.
3. " " " = 110 LB (RECYCLE

Figure 3.48 Load Deflection for 8" ϕ Cast Iron Pipe

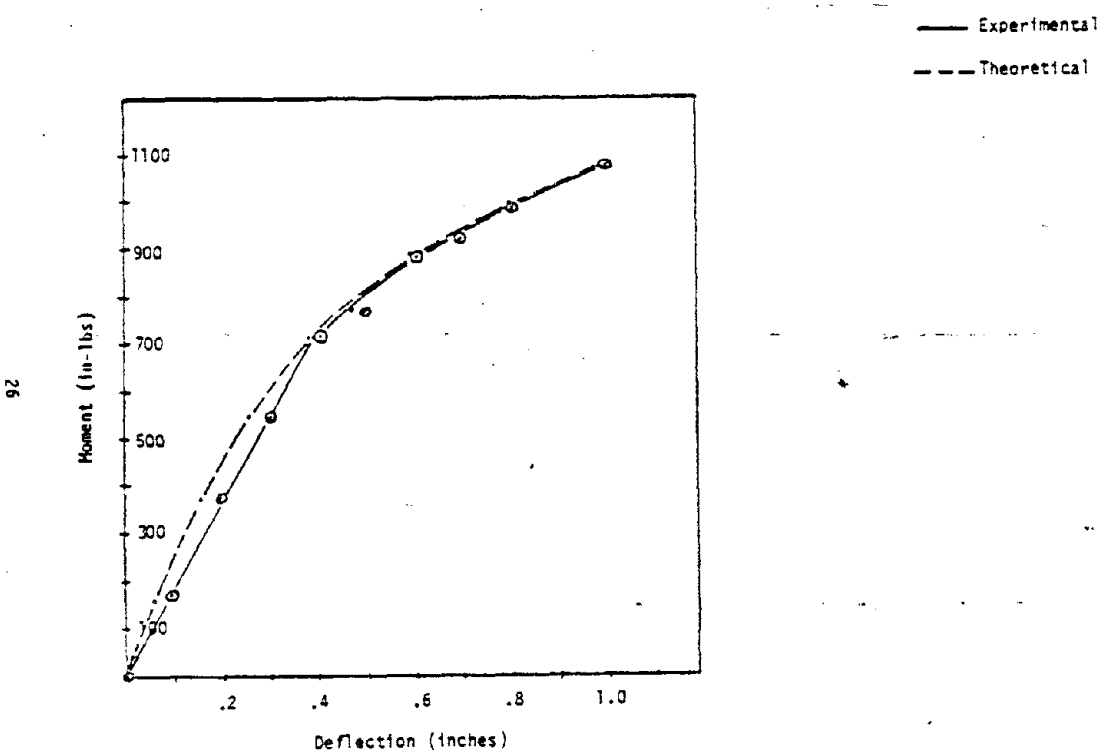

Figure 3.49 Joint Moment-Deflection (Experimental-Theoretical)

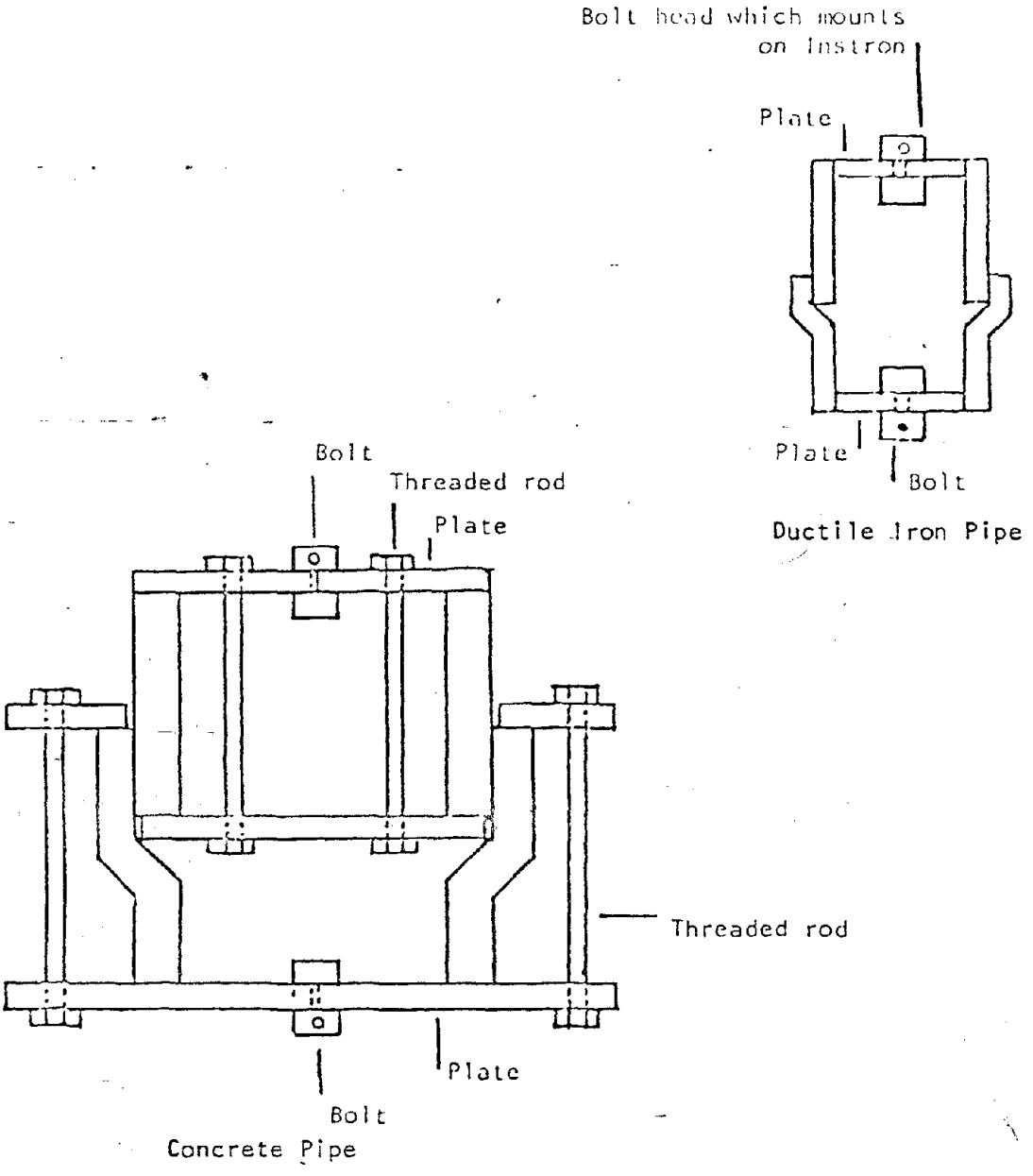

Figure 3.50 Schematic of Pipe Stub - Testing Machine Connections

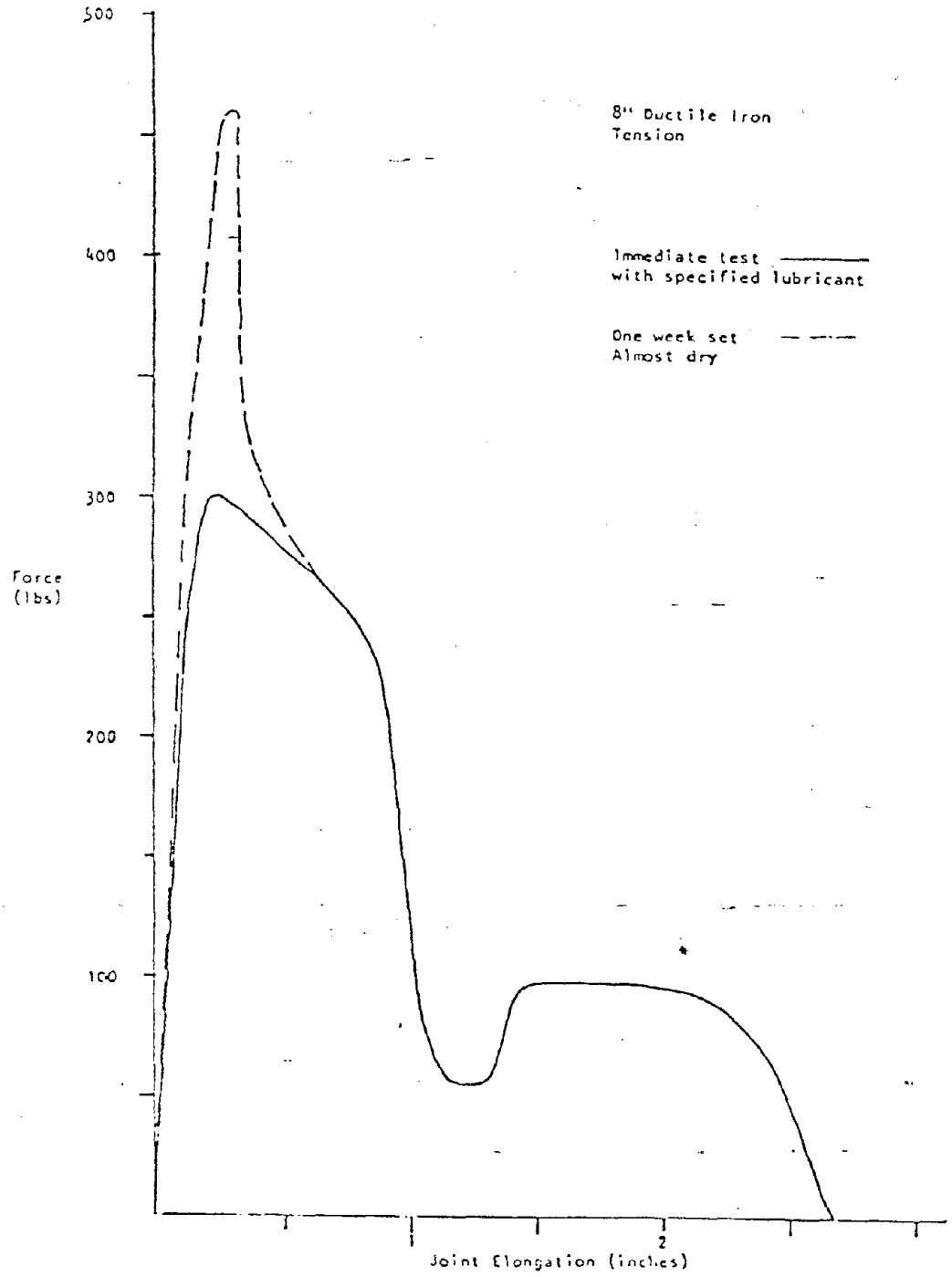

Figure 3.51 Composite Graph, 8 inch Ductile Iron Pipe Joint, Tension

CHAPTER IV

ABOVE-GROUND LIFELINE SYSTEMS

4.1 Introduction

Considerable earthquake research has been initiated and conducted by many organizations during the past several years in order to refine structural analyses, response predictions, building codes and specifications. This has provided the engineer with some background and capabilities necessary to design and construct modern structures to resist force developed during periods of moderate to strong earthquakes. Most of this research has been primarily in the field of building construction. However, the fields of bridge, pipeline and nuclear power plant construction have recently begun to receive some attention.

In general, the above-ground lifeline system covers the above-ground pipeline, highway, railway, electrical transmission line and long span bridges, etc. The seismic responses of above-ground lifeline system during earthquake is quite similar to that of below ground lifelines described in Chapter III. Again, either the field investigation of past damages observed during earthquake or experimental study conducted in a laboratory can be applied to obtain the seismic behaviors of the above-ground lifeline. Note that in this Chapter the seismic study on above-ground pipelines is confined to the damages only because very few data are available.

Various experiments conducted to investigate the dynamic response of above-ground lifeline during excitation were classified as: (1) Seismic observations during earthquakes; (2) field tests of full-scale structure; and (3) model tests on shaking table. Those above experimental methods will be presented in the following sections.

4.2 Seismic Observation

4.2.1 Bridges

In order to understand the behaviors of bridges during earthquakes, many seismic observations[40] have been conducted by installing seismographs on bridges and on the ground sites near bridges. Figure 4.1 and 4.2 show the accelerograms recorded from Shin-Katsushika Bridge and Hirai Bridge respectively during the Higashi Matsuyama earthquake (July 1, 1968, M=6.1). The epicentral distance for both bridges were about 60 km.

For soil condition, a thick layer of medium-grained sand is underlaid beneath the site of Shin-Katsushika Bridge, and the Hirai Bridge is supported on the thick layers of fine sand and silt. Some measurement during earthquake were listed in Table 4.1.

According to the observed records, the natural vibrations were occurring on the bridges during the earthquake. The maximum acceleration at girders are 40% greater than that of ground site. Note that the major vibration periods of the bridges observed during the earthquake are considerably longer than the natural periods obtained from vibration tests.

From comparison of two accelerograms as shown in Figure 4.1 and 4.2, it is observed that the amplitude of vibration recorded from Shin-Katsushika Bridge is much greater than that of Hirai Bridge although their epicentral distances are almost same. The influences on the amplitudes of vibrations may be due to the different ground soil conditions between these two bridge sites. Qualitatively it is, in general, apparent that deep deposits of soft soils tend to produce ground surface motions having predominantly long-period characteristics, with the result that they produce their maximum effects on long-period structures. As mentioned previously, the Shin-Katsushika Bridge is supported

on the thick soft layers of fine sand and silt.

Figure 4.3 shows the relationship between maximum accelerations on the ground and those at the tops of piers. The investigation on maximum accelerations was based on the observations recorded from the strong motion seismographs those installed at bridges scattered over entire country of Japan. Twenty-eight bridges were investigated. Among those bridge sites, the soil conditions are varying from cohesive soil to soft rock. Many types of pier foundations such as footing, caisson and pile foundation etc. were chosen during designing and construction. Except three bridges of them, the heights of piers were generally less than 10m above ground surface.

From Figure 4.3, it is possible to recognize a trend: the maximum acceleration at the tops of piers was much higher than that on the ground level. The magnification ratio of maximum acceleration of pier top to that of the ground level was high up to 3 when ground accelerations were small; but the ratio became smaller if the ground acceleration increased. The ratio was about 1.5 as maximum ground acceleration increased to about 100 gal.

Kuribayashi and Iwasaki[32] have also conducted an investigation to observe the seismic responses of Ochiai bridge during the swarm of earthquakes at Matsushiro within the period of mid 1965 to April of 1966. From obtained records, the Matsushiro earthquakes seem to show the characteristics of relatively short period from 0.1 to 0.2 seconds. But the natural period of the bridge is 0.35 seconds and the damping ratio is about 10% during the free vibration along the bridge axis. The relationship between the response at bridge top and ground acceleration was shown in Figure 4.4. It is obvious that the rate of increase of the maximum response acceleration tends to decrease in accordance with the increase of the absolute maximum value of the ground

acceleration. Thus a regression equation was used to express the above relation. The equation is

$$A_s = 8.33\sqrt{A_g} \quad , \text{ in gal.} \tag{4.1}$$

where A_s represents absolute maximum response accelerations on the superstructure, and A_g represents absolute maximum ground accelerations.

It is apparent that the magnification of seismic response on superstructure of bridge is significant during ground excitation induced by earthquake.

4.2.2 Above-Ground Pipelines

In examining recent studies[23,24] on dynamic responses of pipelines during seismic excitation, it shows that many investigations on buried pipelines were conducted to observe their seismic behaviors (including damage) in the field or in the laboratory; but very few attentions were paid to the above-ground pipelines. Based upon the past damage reports observed during earthquakes, a description was presented herein to describe the possible failure modes and seismic responses of above-ground pipelines.

The response of a structure or element is dependent on its strength, damping characteristics, and the stress-strain or load-deformation relationship for the structure or element considered. For above-ground pipelines the motion of the ground is imparted to the pipe through the piers or supports under the pipe. The deformation of these supports must be considered to avoid tipping or tilting. Of course, liquefaction of the foundation material, or landslide under the support can mean loss of that support.

Consideration must also be given to the relative motions arising from faults crossing the pipeline. Vertical and horizontal displacements of several feet might occur where fault motions take place, and might cause various failure on above-ground pipelines such as buckling, rupture and bending, etc.

In liquefiable zone, it is also very important to ensure that liquefaction does not result in failure or large relative movement of these supports. This consideration requires that the pile supports extend through the liquefaction zone and are founded in competent soil beneath. With properly designed support structures, above ground placement of the pipeline generally represents a desirable method of crossing liquefaction regions from a seismic standpoint.

4.3 Field Tests

Performing actual tests on full-scale structures is the only sure way of assessing the reliability of various assumptions employed in formulating mathematical or finite element models of structures. It is also the most reliable way of determining the parameters of major interest in structural dynamics problems, such as natural frequencies, mode shapes, and damping.

A number of tests on full scale of above-ground lifelines, especially for highway bridges, have been performed to investigate the dynamic behaviors of above-ground lifeline. For instance, for investigating of dynamic responses of bridges, wind and earthquake were the usual source of excitation; but the occurrence of wind/earthquake is unpredictable and out of control. There are so far two other means to induce vibration during test, they are: (1) High-speed vehicular traffic, and (2) quick-release pullback.

4.3.1 Ambient Vibration Tests of Suspension Bridges[1,2,3]

In this investigation, a structural measuring technique using vehicular traffic-induced vibrations was developed for full-scale testing of suspension bridges. The technique incorporates new experimental procedures, improved

deployment and orientation of sensing instruments, and high resolution of the measured data. It has been applied to the Vincent-Thomas Suspension Bridge at Los Angeles Harbor to determine natural frequencies and mode shapes of vertical, torsional, and lateral vibrations and also to estimate the damping of the structure.

The Vincent-Thomas Bridge (Figures 4.5 and 4.6) was constructed in the early 1960's across the Main Channel of Los Angeles Harbor from San Pedro to Terminal Island. Its superstructure consists of a 1,500 ft. (458 m) center span, two 506.5 ft. (155 m) side spans and the width is 52 ft. (16 m). The cable has a vertical sag of 150 ft. (46 m) at the center of the main span. The suspended structure consists of two stiffening trusses, trussed floor beams, and a lower chord wind bracing of K-truss type. The tower legs (336 ft. (103 m) high) have sections of cruciform design.

The uncoupled vibrational modes of a suspension bridge may be classified as vertical, torsional, and lateral (Figure 4.7).

The measurements of the dynamic characteristics of the bridge were carried out with the following instruments.

1. Kinemetrics SS-1 Ranger Seismometer - Eight short-period (close to 1 sec), velocity-type transducers were used to measure motions caused mainly by traffic. Four of them were used to simultaneously measure vertical (seismometers A and B) and lateral (seismometers C and D) motions (Figure 4.5) and were moved to various cross sections of the stiffening structure (Figure 4.6). Four reference seismometers (RA, RB, RC and RD) were permanently located at reference points on cross section R. They were oriented in directions corresponding to seismometers A, B, C, and D.

2. Kinemetrics SC-1 Signal Conditioner - Two four-channel signal conditioner were used to amplify, filter, and simultaneously control the eight outputs from the seismometers. Each channel of the signal conditioners is adjustable to provide displacement, velocity, or acceleration outputs. During the tests, all frequencies higher than 3 Hz were filtered out. The two signal conditioners utilized an AC power source in the tower leg.

3. HP 3960A Instrumentation Tape Recorder - The amplified and filtered signals were recorded on two four-channel tape recorders.

4. HP 7418A Oscillographic Recorder - The measurements taken during the tests were monitored on an eight-channel Oscillographic recorder enabling an immediate visual inspection of the bridge response during each measurement.

5. Kinemetrics DDS-1103 Electronic Analog-Digital Converter - In the dynamic laboratory, the recorded analog signals on the tapes were digitized for computer processing, using an analog-to-digital converter.

The Measuring Procedures are depicted as follows.

1. Installation - The recording instruments, consisting of the signal conditioners, the tape recorders, and the oscillographic recorder, were placed in a traffic lane close to the tower leg. The eight seismometers were first placed at the reference station for calibration. They were connected to the recording instruments by means of electrical cables.

2. Operation - Since the natural frequencies of the seismometers are in the range of the measured frequencies and since the natural period and damping are different for each instrument, the transfer functions of the instruments are not identical. Consequently, relative calibration must be made at all the frequencies of interest. To achieve this, the instruments were alined side by side at one location (Station R). Four seismometers (A, B, RA, and RB) were in the vertical direction and the other four seismometers

(C, D, RC, and RD) were in the lateral direction.

3. Recording - The recording began after several minutes of visual monitoring of the vibrations (by the oscillograph recorder), during which fine adjustments were made. Vertical as well as lateral vibrational motions were recorded for about 10 minutes during the first calibration run. Then seismometers A, B, C, and D were deployed, each with its reference seismometer, as in Figure 4.5, where the adjustment and recording repeated. The foregoing procedures were then repeated for stations 2-16 (Figure 4.6). In all tests, the velocity circuits of two signal conditioners were used to measure the motion due to higher modes since these enhance the higher frequencies of the motion. There was very little wind during the 2 days of tests, so the vibrations of the bridge were mainly caused by vehicular traffic.

After recording the experimental data, a Fast Fourier Transform was then computed for each seismometer record. The spectral were next smoothed with one pass of a Hanning Window (1/4, 1/2 and 1/2 weights). This smoothing facilitates selection of the natural frequencies and, thus, identification of associated modes of vibration. Phase spectral were used to determine the sign (in-phase or 180^{o} out-of-phase) of the model amplitudes.

To determine the mode shape, the smoothed spectral amplitude of the response at a given station was divided by the smoothed spectral amplitude of the simultaneously recorded response at the reference station. In this way, an amplitude was obtained proportional to the mode shape amplitude at that station for a given frequency of vibration; relative calibration was made at all frequencies of interest. Repeating this procedure for all stations where measurements were made, the mode shape amplitudes were determined. The phase of the response was compared to that of the reference instrument to determine

the sign of the modal amplitude. The frequency resolution was 0.0037 Hz, which proved to be high resolution.

The mode shapes and natural frequencies determined by the ambient tests of the Vincent-Thomas Suspension Bridge are compared in Figure 4.8, to those obtained by finite element analysis[1,2]. Figure 4.8 shows only an example of five types of vibrations which including the symmetric and anti-symmetric for both of vertical and torsional vibrations, and symmetric for lateral vibration.

Figure 4.9, which summarizes the comparison between the computed and measured frequencies and modes for vertical, torsional, and lateral vibrations shows quite good agreement, thus confirming the validity of the method of dynamic analysis developed for suspension bridges and also the reliability of the measurements.

Estimated damping values from ambient vibration tests could be obtained by the method of half-power bandwidth of the Fourier spectrum peaks; but it is unlikely that an accurate estimate will be obtained. Several factors contribute to errors in the computed damping values: (1) The vibration of the bridge is nonstationary random process; (2) the presence of adjacent peaks in the spectrum, either due to closely space model peaks or due to spectral overlap, can cause difficulty in estimating damping values; and (3) for some of the modes, it is difficult to find a spectral peak whose width can be properly measured.

Finally, this comparison between measured and computed natural frequencies and mode shapes suggests for future earthquake-resistance analyses that computed values can, indeed, be representative of the real structure.

4.3.2 Quick-Release Pullback Technique for Highway Bridges

The body of experimental knowledge regarding the transverse response of full scale highway bridges from both the static and dynamic point of view is in its infancy. Most of tests on full scale bridges have been performed to measure only the vertical static and dynamic response of highway bridges.

Douglas et al.[17,18] have examined the dynamic behaviors of a concrete bridge subjected to extensive dynamic field tests at Rose Creek. This symmetrical bridge (Figures 4.10 and 4.11) is a 400-foot long reinforced concrete box girder bridge supported by four single column piers. The piers and abutments are supported on pile foundations because the soil profile consists, in general, of a layer of soft clay over a layer of stiff clay on dense sand and gravel. The deck is supported on the abutment foundations by five elastomeric bearing pads. At the abutments, the only mechanism which is effective in transmitting lateral and longitudinal loads from deck to the abutments consists of the elastomeric pads.

During tests, the experimental dynamic excitations were produced by pulling on the bridges with two D-8 crawler tractors and simultaneously quick releasing the cable tensions. Mechanical quick-release hooks were developed with electrical solenoid triggers to achieve simultaneous quick release of the cables. Twenty five thousand pound cable tensions were used during the course of these experiments. Vertical motions were caused by running a loaded sand truck off small ramps.

Accelerometer vibration data were recorded on FM tape for analysis. Mode shapes and natural frequencies were obtained by using the Fourier transform of the recorded field acceleration data. Damping estimates were calculated by using a moving window Fourier transform.

From the quick-release pullback data the first four mode shapes were identified. These are presented in Figures 4.12 and 4.13. The black dots represent the experiment values and the vertical bars represent cases uncertainties in the measurements. From the sand truck vertical motion data the first, third and fourth mode shapes were identified and first five natural frequencies were obtained (Table 4.2). Damping estimates in vertical modes 1, 3, 4 and 5 were also listed in Table 4.2. The first five transverse natural frequencies were also found along with estimates of the modal damping ratios listed in Table 4.2.

An analytical model was used to confirm the dynamic performance of the bridge. A lumped mass space frame model was developed by breaking the bridge deck into elements five feet long and the columns into five elements. The SAP IV program was used for carrying out dynamic response calculations for the 106 member space frame. Table 4.2 shows that agreement between the experimental frequencies and calculated frequencies is excellent considering the small number of parameters used in the model. In Figures 4.12 and 4.13 the experimental mode shapes are given as the solid black dots. The solid lines represent the mode shapes obtained from the analytic model. Agreement is also good.

A remark of conclusion on the field test of quick-release pullback method was described as follows:

1. The quick-release pullback-dynamic tests and vertical motion tests were very effective for purposes of identifying the significant structural dynamic characteristics of the bridge at Rose Creek.

2. From this study, it is apparent that soil structure interaction effects can greatly affect the distribution of seismic loads in bridges, and

the methods described herein are effective in experimentally identifying the in situ foundation compliances.

3. The experimental techniques were effective in identifying the structural properties of the reinforced concrete members.

4. The Rose Creek experimental results suggest that these methods may be useful in indicating whether concrete bridges have been overloaded during their lifetime.

4.4 Laboratory Testings (Model Test)

4.4.1 Dynamic Model Studies of Bridges

Godden and Aslam[22] have conducted an experimental model test to examine the dynamic response of the Ruck-A-Chunky Bridge crossing the Middle Fork of the American River in Northern California (Figure 4.14).

The purpose of the model study was two fold. Firstly, to verify the accuracy of the analytical procedure being used to determine the seismic response of the bridge. Secondly, to identify behavioral characteristics not considered in the analysis that might affect the design of the structure.

The model was used to study the global behavior of the bridge within the limits of elastic behavior. The design of the model was based on reproducing to scale the following structural quantities: (1) Global geometry: This included the location of all cable anchorages, the neutral axis of the girder, and its center of gravity; (2) cable properties: axial flexibility and weight per foot; (3) girder properties: I_x, I_y, J_z, A, weight per foot, and the appropriate distribution of mass for vertical, horizontal, and torsional vibrations; and (4) damping: the damping characteristics of the model had to be similar to those of the prototype, and neither the design of the model nor the instrumentation could introduce excess damping.

The model and its supporting frame were designed as a system. This was essential to prevent interaction between the two and to ensure that the table motions were accurately applied to the model. In this study, the model scale of 1/200 was selected. The model was constructed on the shaking table which contributed a dynamic excitation to the model. Shaking table tests on a small-scale model structure have certain limitations. The applied ground motions are essentially rigid-body motions in which all points on the ground have the same displacement time history, and there is no simple means of studying the effects of differential ground motion.

Instrumentation in a very flexible model has to be carefully designed; it must not add significant mass, stiffness, or damping to the system, thus it is not possible to use such devices as LVDT to measure dynamic displacements. Eight cable forces were measured by the leaf spring devices. Girder forces were measured at three cross sections: midspan, quarterspan, and at one abutment. Strain gages mounted at these sections were used to deduce gross section forces. Miniature accelerometers were used to measure vertical accelerations of the girder at midspan and at both quarterspans.

In order to establish the accuracy of the model in both static and basic dynamic behavior, two preseismic tests were conducted in which careful comparisons were made between test and computer data.

a) Static Live-Load Test - To check that the static behavior of the bridge model matched the static computer analysis, a uniformly distributed load was applied to the girder to simulate the effect of the prototype 1.47-kips/ft. (21.3-kn/m) static live loading. Loading was applied in four equal increments up to a total of approximately 1.8 times the required live load in order to check on the linearity of response. The resulting predicted prototype data are given in Table 4.3 together with the equivalent computed values.

In comparing these two sets of data it should be remembered that the computer analysis was based on linear theory using an equivalent straight line approximation for the cable. The two sets of data show very close agreement.

b) Dynamic Tests - To check that the dynamic behavior of the model matched the computed values, natural frequencies and mode shapes were studied. Natural frequencies were measured in two ways: (1) Multiple impacting, and (2) forced vibration. Multiple impacting along the girder was done by hand and the response of the system was studied by a real-time spectra analyzer. Forced vibration tests were done by using a small electric motor driving an eccentric mass attached at different points along the girder. Results of the forced vibration tests, together with the equivalent computed data, are given in Table 4.4 indicating a high degree of correlation. Correlation became closer with high modes that are less cable dependent. Later it was found that the seismic response of the bridge is dominated by the first few modes, and particular by the first.

c) Damping - System damping in the model was measured by free decay response in different modes. Mode 1 damping was measured at 0.09% of critical, and mode 3 at 0.25%. These are extremely low values and indicate the potential for low damping in a structure of this kind.

After two preseismic tests, a shaking table test was conducted to investigate the dynamic response of the model. The shaking table used has two independent components of motion: one horizontal and the vertical. For one set of tests the bridge was mounted so that it could be shaken in the horizontal x (or y) direction. In this position it could also be shaken in the vertical z direction and the x (or y) and z components could be applied simultaneously. Each motion was applied in incremental intensity so that the

linearity of dynamic response could be studied both by the form of the time-history response and also by maximum values.

The table motions were derived from an artificial earthquake with a 15-sec duration motion with horizontal and vertical peak accelerations of 0.12 g and 0.08 g, respectively. All data were recorded at 100 samples/sec. In addition, a movie was made of the response of the bridge so that cable vibrations, girder motions, and the expansion joint response could be observed.

The intensive study of the model, both with and without a midspan expansion joint, and a comparison of measured and computed response data for the continuous bridge led to the following observations:

1. This particular design is very effective in resisting all horizontal components of ground motion due to its continuity and the horizontal curvature of the girder. All horizontal motion tests produced very small response (Figure 4.15).

2. The primary response of the bridge is due to the vertical component of ground motion (Figure 4.16), and for the motions applied it was largely first mode response.

3. A comparison of measured and computed response for identical ground motions indicates that although the analysis neglects cable vibrations and is based on linear theory, this is quite accurate enough for design purposes (Table 4.5).

4. Cable vibrations, though clearly visible under all conditions of ground motion, have little effect on the gross behavior of the bridge.

5. The ground motions applied in this study were "rigid body" table motions. Differential ground motions were not studied.

Kuribayashi et al.[33] have also conducted two vibration tests of bridge models by using a large shaking table. The purposes of the tests are to study the dynamic response characteristics of Katashina-gawa Bridge in Kan-etsu Expressway and of a continuous girder bridge in Metropolitan Expressway during earthquakes.

Katashina-gawa Bridge is a curved truss bridge supported on high piers (R = 2200 m, maximum height of pier = 69 m); and the bridge in Metropolitan Expressway is a 12-span continuous girder bridge with hinged support on each pier. Several vibration tests of these two bridge models have been conducted by using a large shaking table (6m x 8m) at Public Works Research Institute, Japan.

Based on the results observed from the model tests, Kuribayashi et al.[33] made conclusions as follows:

1. Vibration modes of Katashina-gawa Bridge model subject to oblique direction excitations were same as those subject to longitudinal or transverse direction excitations. Responses induced by oblique direction excitation were smaller than that induced by longitudinal or transverse direction excitations. In this respect, it is adequate to only consider the effects on the bridge structures due to longitudinal and/or transverse excitations.

2. There is an appreciable effect on the vibration modes of Katashina-gawa Bridge model due to the curvature of bridge girder; but the influence is small enough to be neglected in the earthquake-resistant design.

3. As to the model the bridge in Metropolitan Expressway, its dynamic responses were larger than those of simple support bridge. But its characteristics of dynamic responses were not so complicated as those of the

other type bridges, and it could be estimated precisely by dynamic analysis of mathematical model.

4.4.2 Qualification Test of Communication Equipment

Determining the true earthquake resistance of equipment through calculation alone frequently is relatively difficult because of the mechanical complexity, as well as because of the nonlinear and inelastic response of some individual components. On the other hand, testing on a hydraulic shaker programmed to match the seismic motions at the equipment support points evaluates the design and allows modifications before field use.

A qualification test should be used to prove in equipment. Synthesized time history waveforms can be prepared that closely resemble actual earthquake motions in a building and match the response spectrum of the various earthquake zones.

When testing is performed it is preferrable that the equipment or component and its supporting medium simulate as closely as possible that actually used in practice. Tests employed on the hydraulic shaker at the Bell Laboratories, Whippany employ a large concrete block located directly over the shaker machine to simulate the actual floor construction. The equipment is connected to the block in exactly the same fashion as in the field, employing all of the specified hardware bolts, shims, and other fasteners to hold the test item in place.

Foss[19,20] concluded that communications equipment in building will experience earthquake motions that may be considerably different from those occurring in the ground. In-building equipment response will be dictated by

the motions of the attachment points to the structure. It is believed that the attachment point motions are influenced by the following factors such as soil interaction at the building foundation, building stiffness and mass distribution, and damping characteristics. The amplification of seismic motion within building is expected during excitation. Note that the average building acceleration amplification is decreased with increasing ground motion; and that the vertical motions in the ground with accerations up to three-quarters of those in the horizontal direction must be considered.

Table 4.1

Earthquake Vibration of Bridges.

			Name		
			Shin-Katsushika	Hirai	Yoshida-Ōhashi
Maximum acceleration (gal)	Parallel to axis	Ground	40	100	25
		Girder	56	140	38
		Ratio	1.40	1.40	1.50
	Perpendicular to axis	Ground	40	65	
		Girder	50	65	
		Ratio	1.25	1.00	
Major period (sec)	Parallel to axis	Ground	unknown	0.70	
		Girder	0.48	0.80	
	Perpendicular to axis	Ground	0.93	0.40	
		Girder	0.21	0.67	
Vibration Test	Parallel to axis	Natural period (sec)	0.36	0.42*	0.29
		Damping factor	0.066	0.129*	0.110

* Vibration test of Hirai Bridge conducted in condition of girder not loaded on piers.

Table 4.2

FREQUENCIES AND DAMPING RATIOS

Direction	Mode	Expt. Freq. HZ	Th. Freq. HZ	Damping Range	Avg. Damping	No. of Damping Estimates
TRANSVERSE	1	2.7	2.8	1.8 - 2.4	2.1	8
	2	3.8	3.7	4	4	2
	3	5.5	5.7	1.0 - 2.5	1.9	6
	4	8.7	8.4	3.4 - 5.0	4.3	4
	5	11.5	11.7	-	-	-
VERTICAL	1	2.3-2.9	2.7	4.8 - 9	6.5	12
	2	3.5	3.5	-	-	-
	3	4	3.9	1.2 - 2.7	1.8	8
	4	7.6	7.8	1.2 - 2.3	1.7	8
	5	8.1	8.2	1.0 - 2.3	1.5	8

Table 4.3

Measured and Computed Response for Static Live Load

Quantity (1)	Model prediction (2)	Computer (3)
Midspan deflection, in feet	2.75	2.67
Cable forces, in kips		
SI: 1	102	106
7	75	81
12	11	15
SO: 1	136	127
7	120	121
12	37	42
NI: 7	78	84
NO: 7	112	105
Vertical moment in girder, in kip-feet		
Midspan	7,430	7,954
25 ft north of quarterspan north	8,490	6,141
6.25 ft from north abutment	−32,200	−31,900

Note: 1 ft = 0.305 m; 1 kip = 4.45 kN; 1 kip-ft = 1.36 kN · m.

Table 4.4

Measured and Computed Natural Frequencies

Frequency (Hz)		Mode Shape			
Computed*	Model†	Vertical		Horizontal	Torsional
		Symmetrical	Antisymmetrical		
f_1 = 0.265	0.257				
f_2 = 0.363	0.354				
f_3 = 0.537	0.523				
f_4 = 0.807	0.809				
f_5 = 1.00	1.07				
f_7 = 1.16	1.19				
f_6 = 1.14	1.38				
f_8 = 1.58	1.62				
f_9 = 1.74	1.90				
f_{10} = 2.07	2.20				
	2.82				

* Mass lumped at 80 sections, straight-line reduced modulus cable approximation
† Mass lumped at 26 girder sections (at cable connection points), no approximation for cable mass or sag

Table 4.5

Measured and Computed Response for Shaking Table Test

Quantity (1)	Model Prediction		Computer	
	Maximum (2)	Minimum (3)	Maximum (4)	Minimum (5)
Midspan deflection, in feet	3.00	−3.75	4.06	−4.23
Cable forces, in kips				
SI: 1	115	−150	156	−163
7	77	−70	76	−70
12	17	−14	9	−9
SO: 1	144	−175	186	−195
7	110	−93	112	−104
12	26	−19	21	−22
Vertical moments in girder, in kip feet				
Midspan	16,920	−26,580	22,600	−26,120
25 ft north of quarterspan north	13,490	−10,420	6,468	−7,711
6.25 ft from north abutment	23,620	−30,680	28,110	−24,620

Note: 1 ft = 0.305 m; 1 kip = 4.45 kN; 1 kip-ft = 1.36 kN · m.

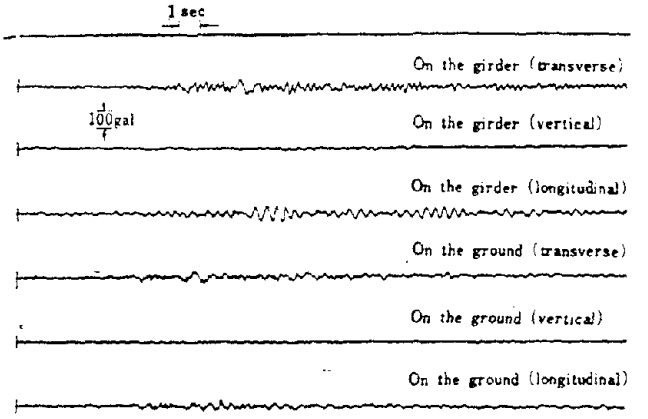

Fig. 4.1 Acceleration of Shinkaisushika Bridge due to earthquake on 1 July 1968.

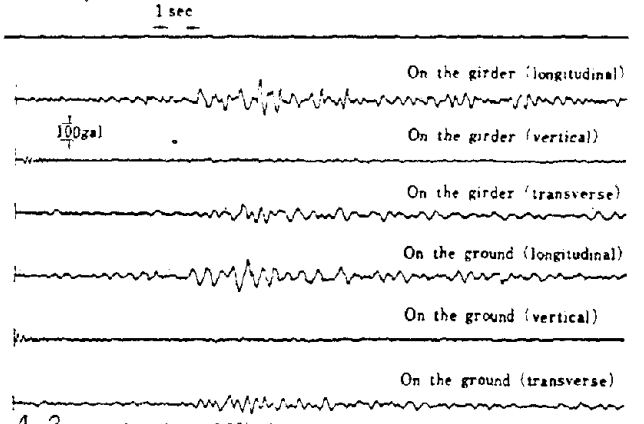

Fig. 4.2 Acceleration of Hirai Bridge due to earthquake on 1 July 1968.

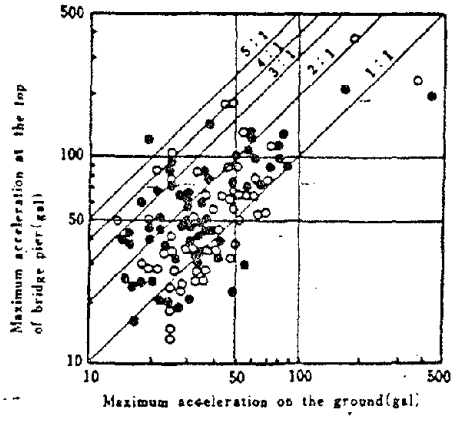

Fig. 4.3 Relation between maximum acceleration of the ground and at the top of the bridge pier (after Mr. E. Kuribayashi).

●: In the direction of bridge axis.

○: In the direction perpendicular to bridge axis.

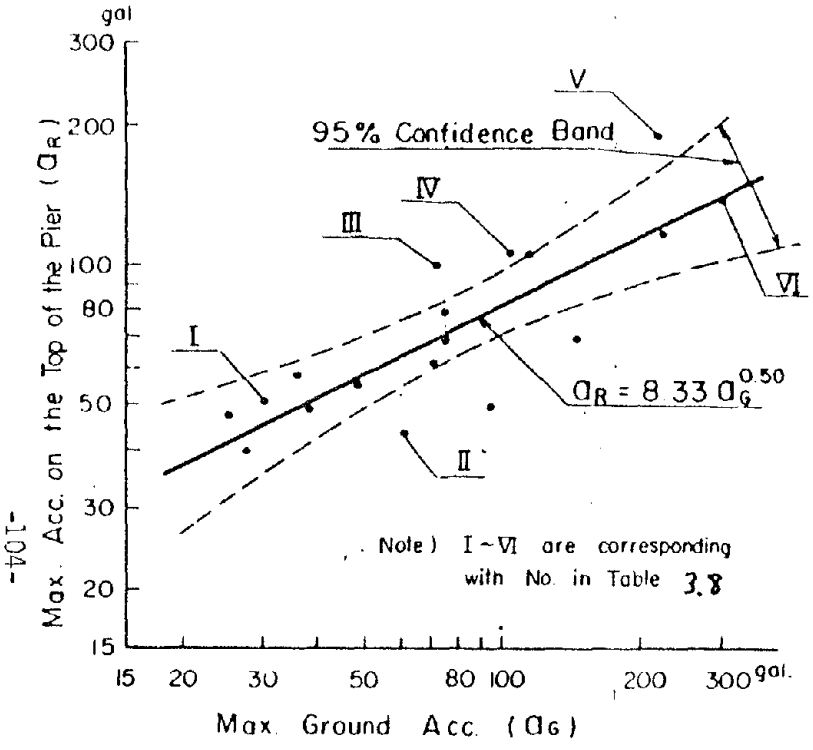

Relation Between Ground Accelerations and Response Accelerations Observed at the Ochiai Bridge
(Longitudinal Direction)

Figure 4.4

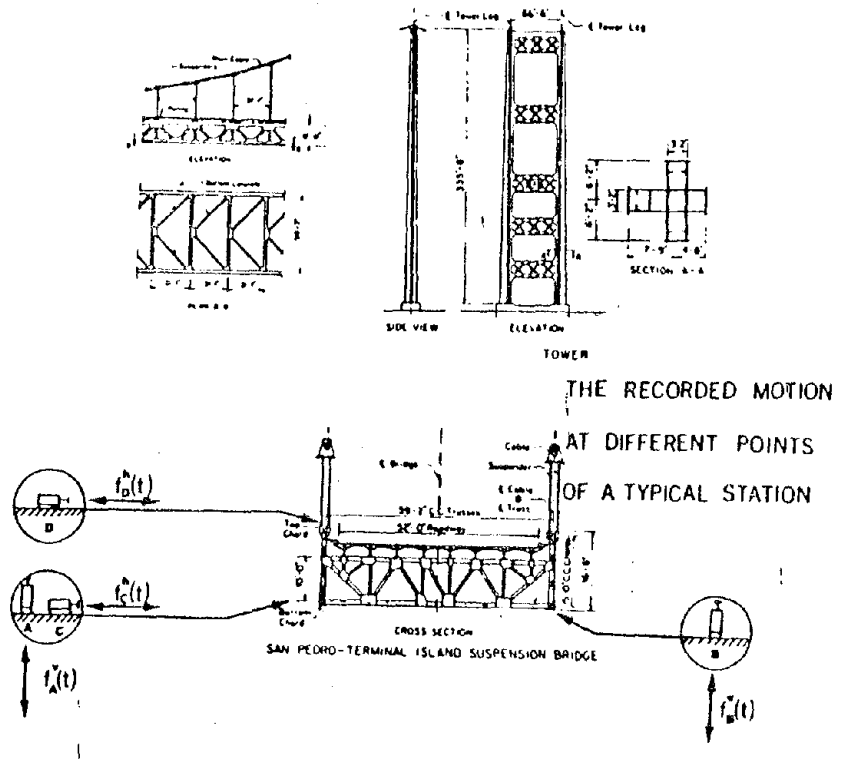

Structural Details and Deployment of Seismometers on Typical Cross Section
(1 ft = 0.305 m; 1 in. = 25.4 mm)

Figure 4.5

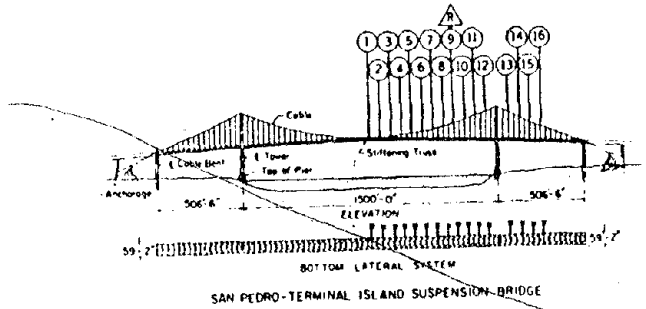

SAN PEDRO-TERMINAL ISLAND SUSPENSION BRIDGE

Measurement Stations (1 ft = 0.305 m; 1 in. = 25.4 mm)

Figure 4.6

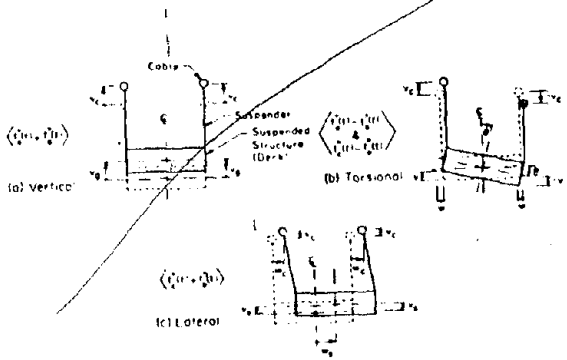

Types of Vibrational Motion in Suspension Bridges

Figure 4.7

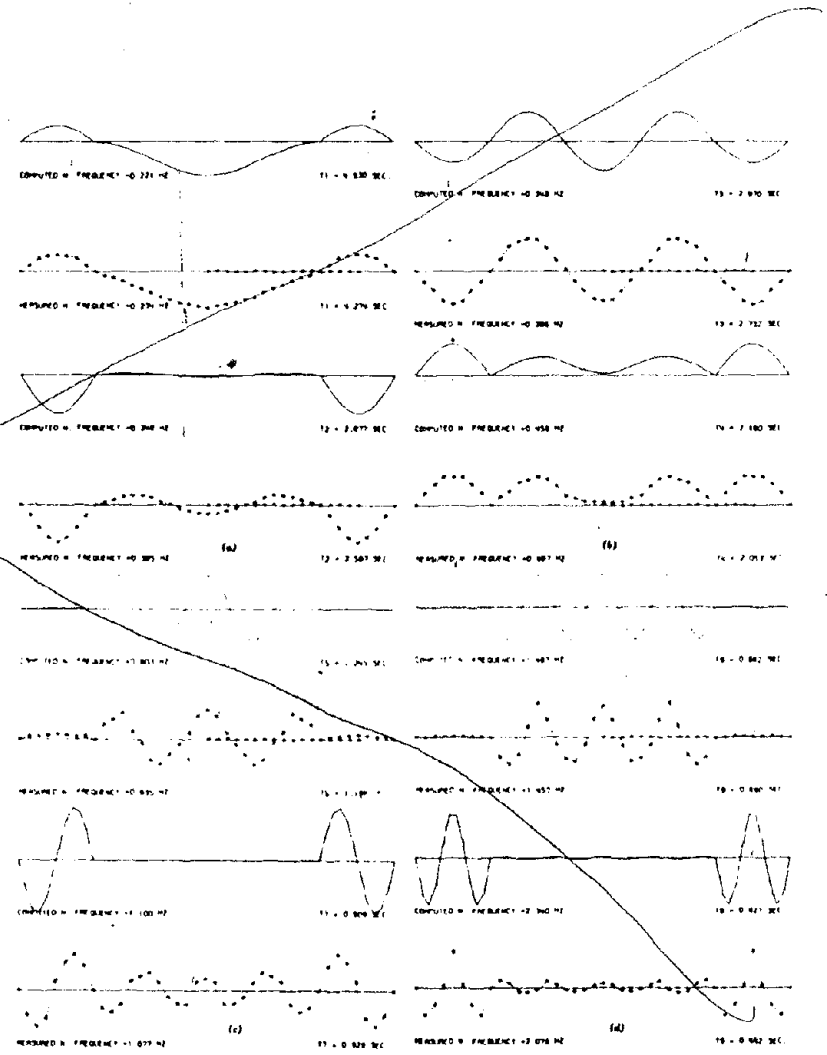

Ambient Vibration Tests for San Pedro-Terminal Island Suspension Bridge—Symmetric Vertical Vibration

Figure 4.8

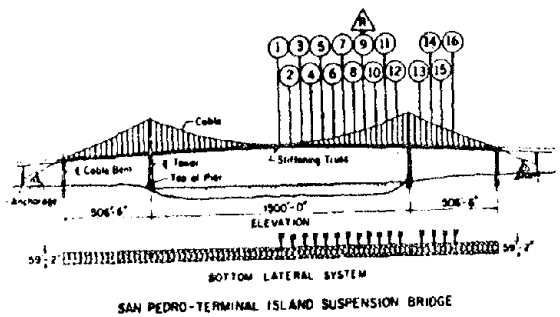

SAN PEDRO-TERMINAL ISLAND SUSPENSION BRIDGE

Measurement Stations (1 ft = 0.305 m; 1 in. = 25.4 mm)

Figure 4.6

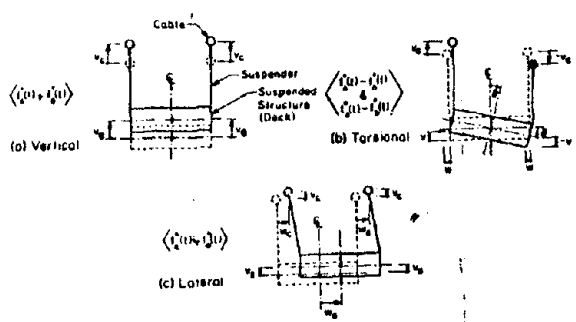

Types of Vibrational Motion in Suspension Bridges

Figure 4.7

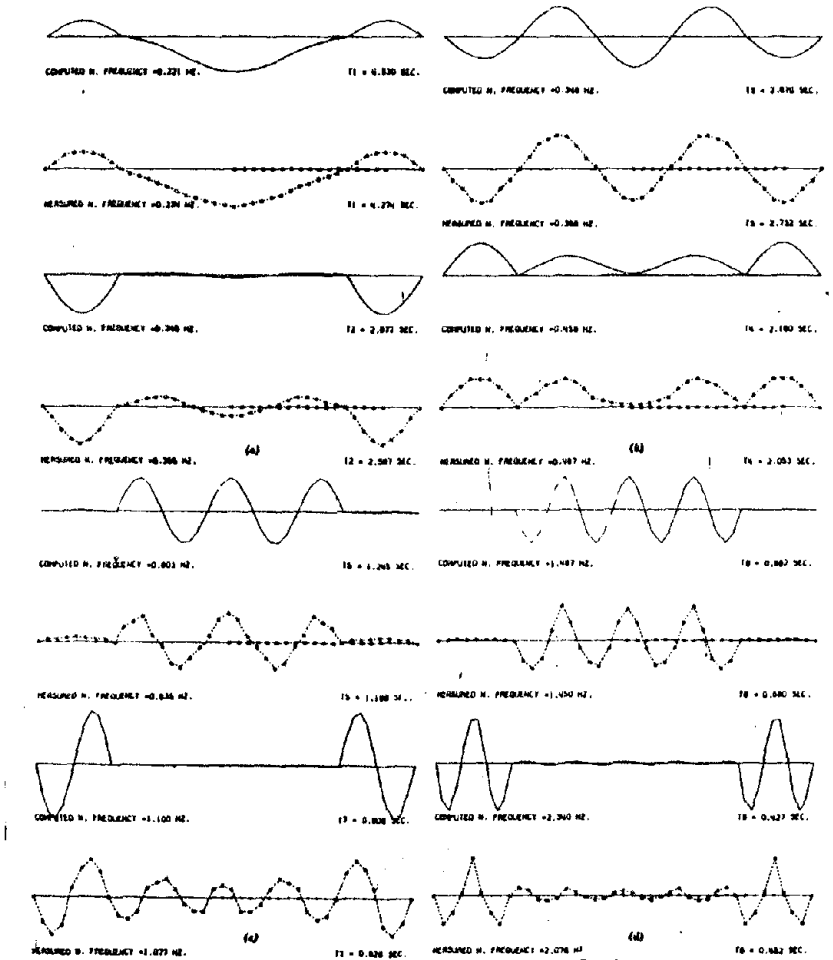

Reproduced from best available copy.

Ambient Vibration Tests for San Pedro-Terminal Island Suspension Bridge—Symmetric Vertical Vibration

Figure 4.8

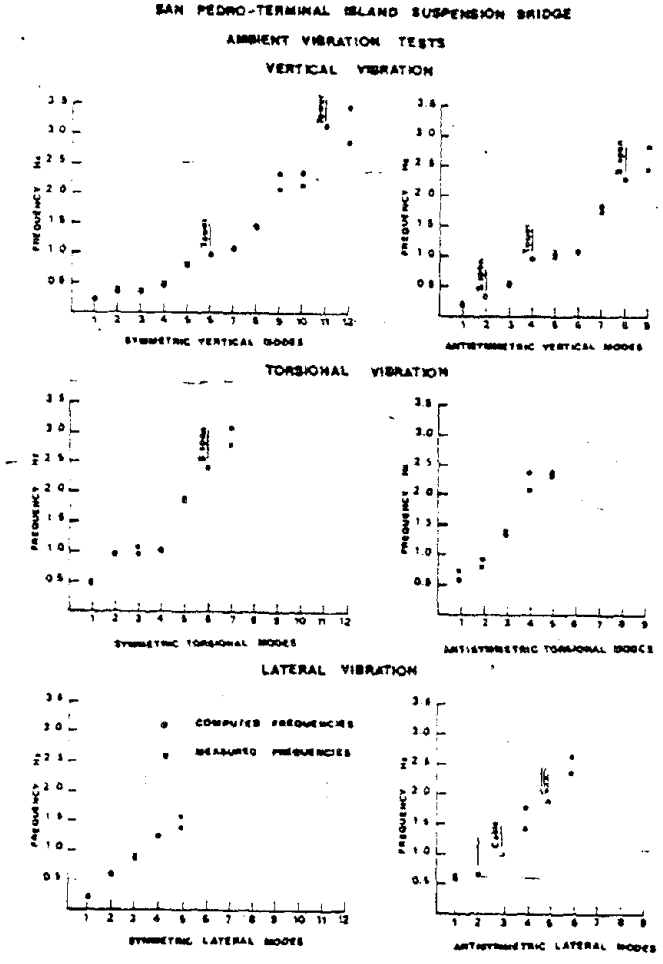

Comparison between Computed and Measured Frequencies for Vertical, Torsional, and Lateral Modes of Vibration

Figure 4.9

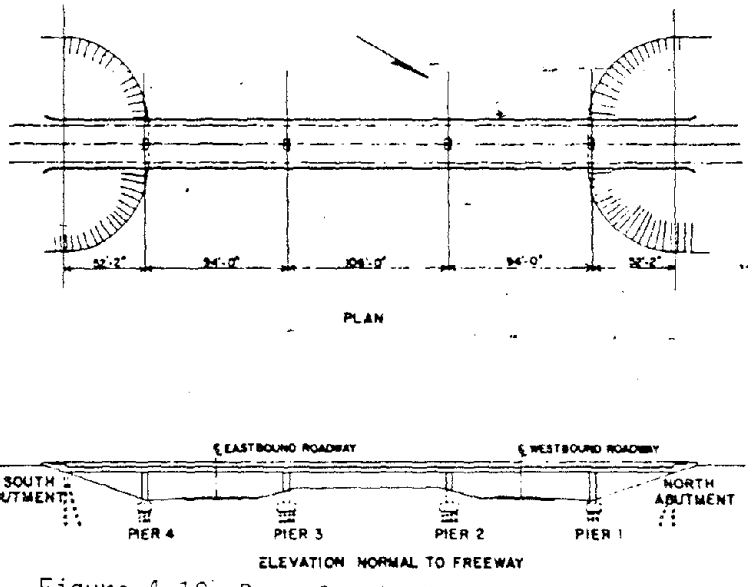

Figure 4.10 Rose Creek Plan and Elevation

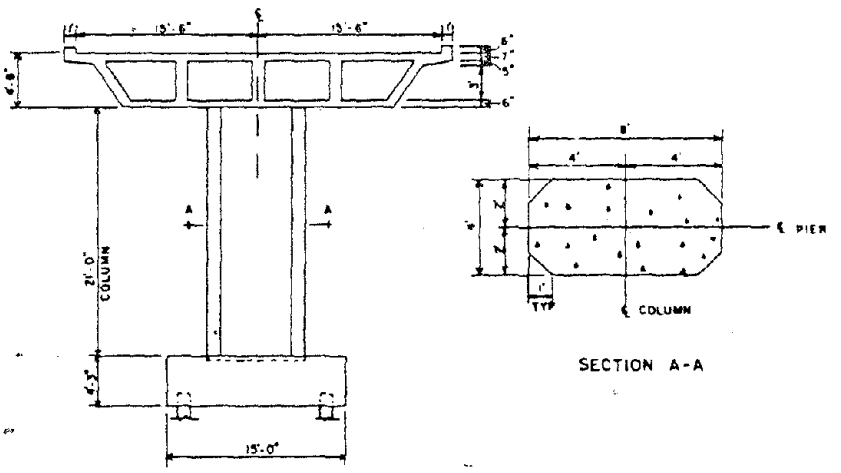

Rose Creek Typical Pier

Figure 4.11

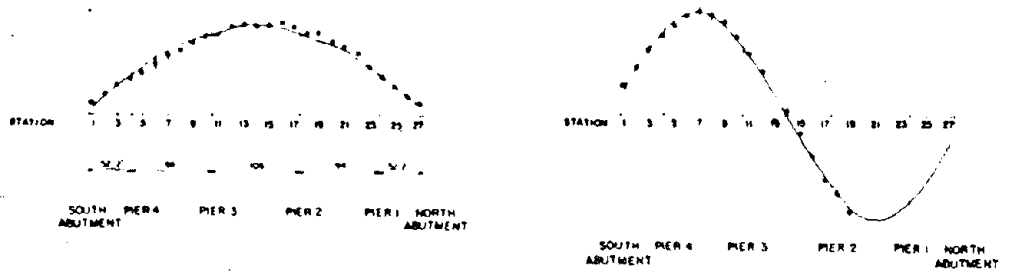

Rose Creek Transverse Mode Shapes 1 and 2

Figure 4.12

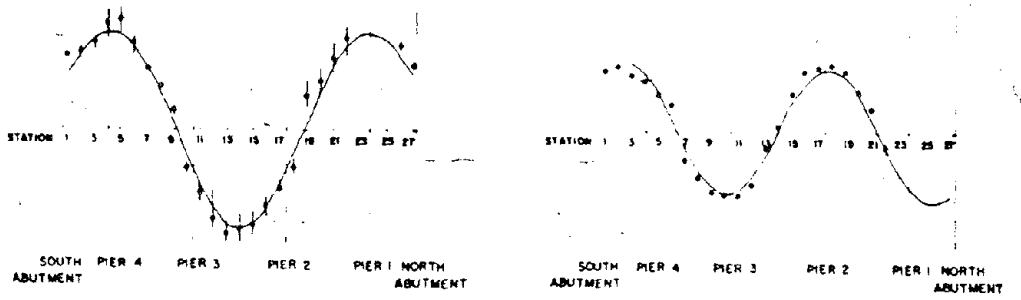

Rose Creek Transverse Mode Shapes 3 and 4

Figure 4.13

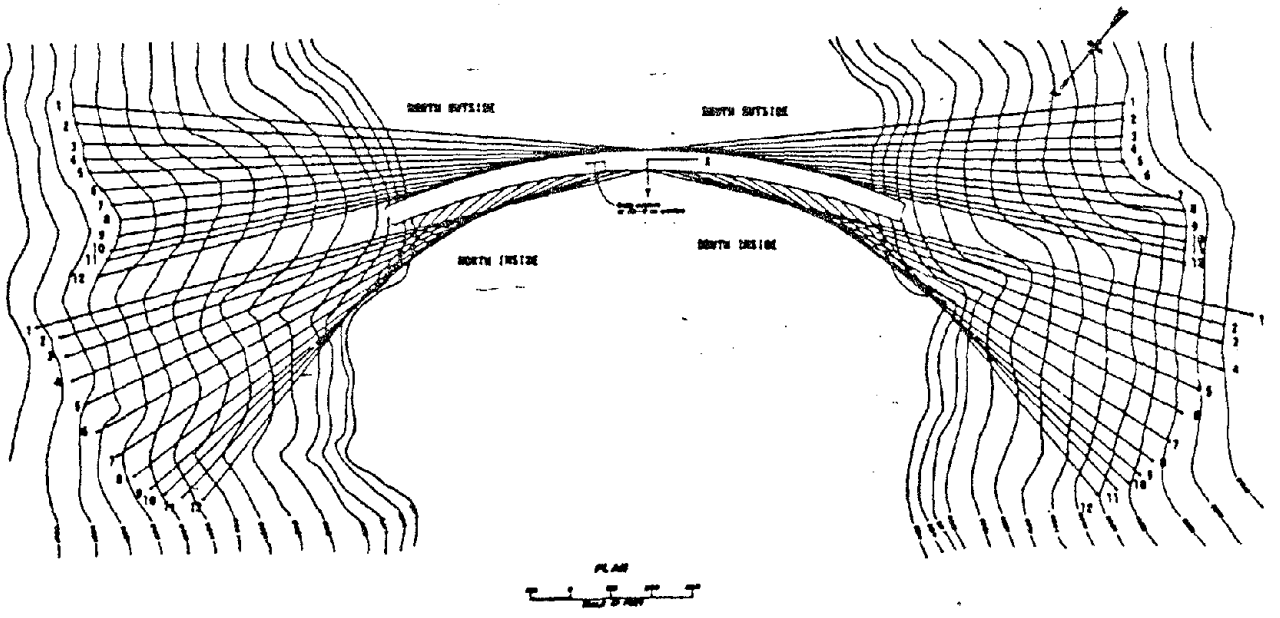

Layout of Prototype Bridge (1 ft = 0.305 m)

Figure 4.14

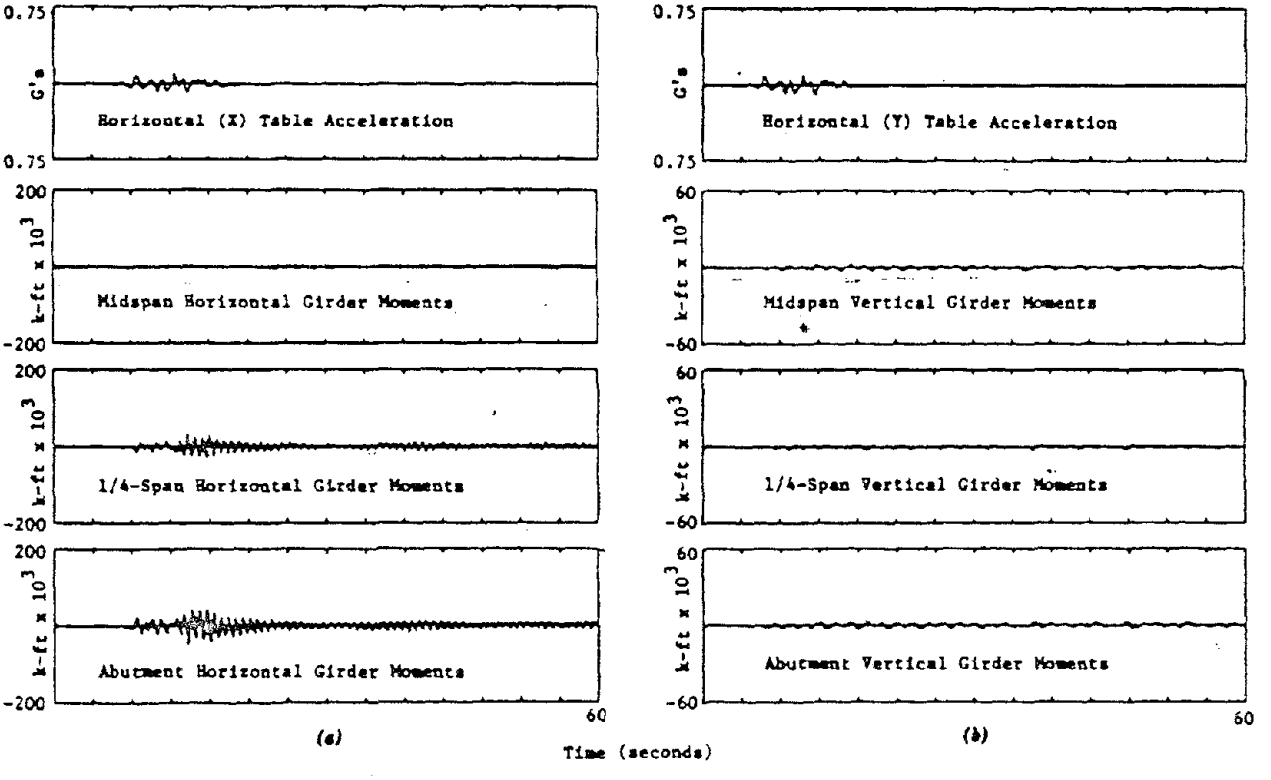

Response to Horizontal Table Motion: (a) *X* Direction; (b) *Y* Direction (1 kip-ft = 1.36 kn · m)

Figure 4.15

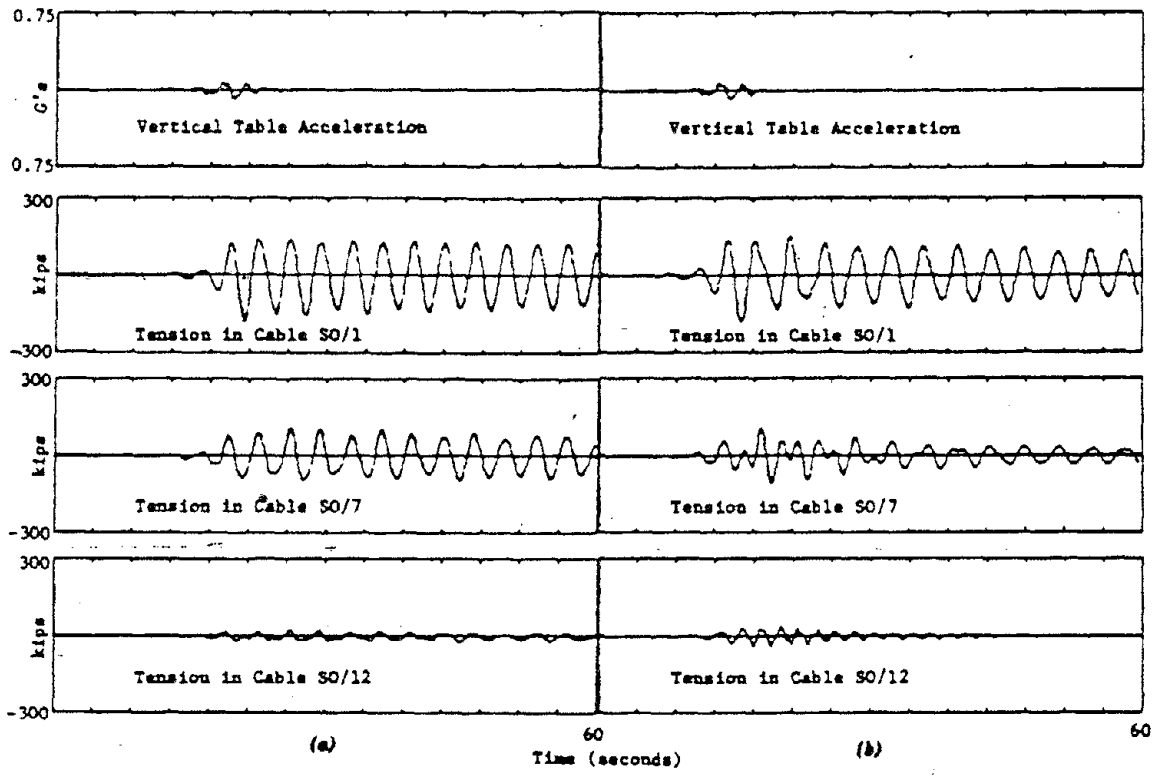

Response to Vertical Table Motion of: (a) Continuous Bridge; (b) Bridge Midspan Expansion Joint (1 kip = 4.45 kN)

Figure 4.16

CHAPTER V

SUMMARY

This report summarizes and discusses the available experimental methods that are needed to evaluate the performance of above- and below-ground lifeline systems.

Since both above- and below-ground lifeline systems are affected by the ground motions, the studies of ground motion characteristics are discussed first in Chapter II. At the present time, the methods to study the ground motions are dense lineal, plane and three dimensional strong motion arrays. Lifeline systems, either above- or below-ground are generally extended to a long distance above or slightly below surface of the ground, a dense lineal array, say less than or up to 50 m apart would be sufficient to define the ground motion input for any lifeline system.

Chapter II evaluates below ground lifeline systems. Active field testing methods, passive field testing methods, laboratory testing methods, as well as influential parameters are described. Active field testings which emphasize more on ground motion generation include explosions, moving loads, vibrators, air-gun and board striking (shear) process, and pile driving. Passive field testings on buried pipelines, tunnels, communication lines, are introduced. Finally, the influential parameters mostly to buried lifeline systems, such as lateral and longitudinal soil resistance characteristics and joint resistant behavior are discussed.

For above-ground lifeline systems shown in Chapter IV, seismic observations, field testings, and laboratory (model) testing of bridges, above-

ground pipelines, and communication lifelines are presented. In general, above-ground lifeline systems can be evaluated by a multiple system table system, which is not available at this time in the United States. Very limited data on above-ground lifeline experiments are available.

REFERENCES

1. Abdel-Ghaffar, A.M., "Dynamic Analyses of Suspension Bridge Structures", EERL 76-01, Earthquake Engineering Research Laboratory, California Institute of Technology, Pasadena, Calif., 1976.

2. Abdel-Ghaffar, A.M., "Dynamic Analyses of Suspension Brdige Structures and Some Related Topics", Thesis presented in partial fulfillment of the requirements for the degree of Doctor of Philosophy, Cal. Inst. Tech., Pasadena, Calif., 1976.

3. Abdel-Ghaffar, A.M. and Housner, G.W., "Ambient Vibration Tests of Suspension Bridge", Journal of the Engineering Mechanics Division, ASCE Vol. 104, No. EM5, Oct., 1978, pp. 983-999.

4. Ariman, T and M. Hamada, "Experimental Investigations on Seismic Behavior of Buried Pipelines", Proc. of Current State of Knowledge of Lifeline Earthquake Engineering, ASCE/Oakland, Aug. 1981.

5. Audibert, J.M.E., N.W. Lai and R.G. Bea, "Designing Subsea Pipelines To Resist Instabilities - Part 3", Pipeline & Gas Journal, June, 1980, pp. 49-53.

6. Audibert, J.M.E. and K.J. Nyman, "Coefficients of Subgrade Reaction for the Design of Buried Piping", Proc. of the Second ASCE Specialty Conference on Structural Design of Nuclear Plant Facilities, New Orleans/LA., Vol. 1A, Dec., 1975, pp. 109-141.

7. Audibert, J.M.E. and Nyman, K.J., "Soil Resistant Against Horizontal Motion of Pipes", Journal of the Geotechnical Engineering Division, ASCE, Vol. 103, No. GT10, Oct., 1977.

8. Berkke, T.L., "Seismic Instrumentation of Transportation Tunnels in California", Report No. FHWA-RD-77-138, Federal Highway Administration, August 1977.

9. Bertken, T.G., "State-of-the-Art Review Earthquake-Resistant Design of Transportation Lifelines", Proc. of Current State of Knowledge of Lifeline Earthquake Engineering, ASCE/LA, Aug. 1977.

10. Bolt, B.A., Penzien, J., and Tsai, Y.B., "Preliminary Results From the Strong-Motion Accelerograph Array in Taiwan", EERI Newsletter, September 1981, pp. 24-27.

11. Boore, D.M., Hsieh, L.L., Iwan, W.D., Peng, K.Z. and Teng, T.L., "USA-PRC Cooperative Project on Strong Ground Motion", Proc. of the US-PRC Bilateral Workshop on Earthquake Engineering, Harbin, China, Aug. 1982, pp. A-1-1 to A-1-12.

12. Bruce, J.R. and Lindberg, H.L., "Earthquake Simulation using Contained Explosions", Proceedings of the Specialty Conference on Dynamics Response of Structures, ASCE/Atlanta GA. Jan. 1981, pp. 111-125.

13. Bruce, J.R., Lindberg, H.L., and Abrahamson, "Simulation of Strong Earthquake Motion with Contained-Explosion Line Source Arrays", Final Report to NSF, Dec. 1979.

14. Chrostowski, J., et al., Simulating Strong Motion Earthquake Effects on Nuclear Power Plants Using Explosive Blasts, UCLA-ENG-7119, Nuclear Energy Laboratory and Earthquake Engineering and Structures Laboratory, University of California at Los Angeles, Feb. 1972.

15. Colton, J.D. et al., "Measurement of Dynamic Soil-Pipe Axial Interaction for Full-Scale Buried Pipelines Under Field Laying Conditions", Preparation for Publication in the International Journal of Earthquake Engineering and Soil Dynamics.

16. Das, B.M., "Pullout Resistance of Vertical Anchors", J. of the Geotechnical Engineering Division, ASCE, Vol. 100, No. GT1, Jan., 1975, pp. 87-91.

17. Douglas, B.M., "Quick Release Pullback Testing and Analytical Seismic Analysis of Six Span Composite Girder Bridge", Report No. FHWA-RD-76-173, Federal Highway Administration, Offices of Research and Development, Washington, DC.

18. Douglas, B.M., Drown, C.D. and M.L. Gordon, "Experimental Dynamics of Highway Bridges", Proc. of the 2nd Specialty Conference on Dynamic Response of Structures: Experimentation, Observation, Prediction, and Control, Atlanta, Jan/1981 pp. 698-712.

19. Foss, J.W., "Protecting Communications Equipment Against Earthquake", Proc. of U.S.-JAPAN Seminar on Earthquake Engineering Research with Emphasis on Lifeline Systems, Tokyo, Japan, Nov/1976.

20. Foss, J.W., "Communications Lifelines in Earthquakes", Proc. of Current State of Knowledge of Lifeline Earthquake Engineering, ASCE/LA, Aug. 1977.

21. Getza, J.L., "Joint Resistance Characteristics of Under Pipes", Unpublished M.S. Thesis, Department of Civil Engineering, Renssdaer Polytechnic Institute, May 1980.

22. Godden, W.G. and M. Aslam, "Dynamic Model Studies of Ruck-A-Chucky Bridge" J. of the Structural Division, ASCE, Vol. 104, No. ST12, Dec. 1978, pp 1827-1844.

23. Hall, W.J., and Newmark, M.N., "Seismic Design Criteria for Pipelines and Facilities", Journal of the Technical Councils of ASCE, Vol. 104, No. TCI Nov., 1978, pp. 91-107.

24. Hamada, M., "Earthquake Observation and Numerical Analysis of Underground Storages", Recent Advances in Lifeline EArthquake Engineering in Japan, ASME, pvp - 43, Aug., 1980 pp. 121-127.

25. Higgins, C.J., K.B. Simons, and S.F. Pickett, "A Small Explosive Simulation of Earthquake-like Ground Motions", Proc. of the ASCE Geotechnical Engineering Division Specialty Conference, Pasadena, CA, June, 1978, pp. 512-529.

26. Higgins, C.J., and G.E. Triandafilidis, "The Simulation of Earthquake Ground Motions with High Explosives", Sixth World Conference on Earthquake Engineering, New Delhi, India, Jan. 10-14, 1977.

27. Idriss, I.M., "Characteristics of Earthquake Ground Motions", Proceedings of the ASCE Geotechnical Engineering Division Specialty Conference, Vol. III, June 19-21, 1978, Pasadena, CA pp. 1151-1265.

28. Iwan, W.D., ed., "Strong-Motion Earhtquake Instrument Arrays", Proc. of the International Workshop on Strong-Motion Earthquake Instrument Arrays, Honolulu, May 1978.

29. Jalalvand, F., "Soil-Pipe Surface Friction Characteristics of Buried Pipes", Unpublished Project Report, School of Civil Engineering and Environmental Science, University of Oklahoma, August 1982.

30. Kennedy, R.P., Darrow, A.C. and Short, S.A., "Seismic Design of Oil Pipeline Systems", Journal of the Technical Councils of ASCE, Vol. 105, No. TCI, April, 1979, pp. 119-134.

31. Kubo, K, Katayama, T., and Ohashi, A., "Present State of Lifeline Earthquake Engineering in Japan," Proceedings of ASCE Current State of Knowledge of Lifeline Earthquake Engineering, Aug. 1977, pp. 118-133.

32. Kuribayashi, E., and T. Iwasaki, "Observed Earthquake Responses of Bridges", Proc. of 4th World Conference of Earthquake Engineering, 1969.

33. Kuribayashi, E., O. Ueda and R. Hagiwara, "Vibration Tests of Bridge Models Using a Large Shaking Table", 13th Joint Meeting of U.S.-Japan Panel on Wind and Seismic Effects, UJNR Tsukuba, Japan, May, 1981.

34. Narita, K., "Study on Pipeline Failure Due to Earthquake", Proc. of U.S. Japan Seminar on Earthquake Engineering Research with Emphasis on Lifeline Systems, Tokyo, Japan, Nov/1976.

35. Nasu, N., S. Kazama, T. Morioka and T. Tamura, "Vibration Test of the Underground Pipe with a Comparatively Large Cross-Section", Proceedings of the 5th World Conference on Earthquake Engineering, Rome 1974, pp. 583-592.

36. Nishio, N., T. Ukaji and K. Tsukamoto, "Experimental Studies and Observation of Pipeline Behavior During Earthquakes", Recent Advances in Lifeline Earthquake Engineering in Japan, ASME, pvp-43, Aug. 1980, pp. 67-76.

37. Nishio, N., K. Yoneyama, N. Takagi and K. Shimomura, "Strain Analysis of Soils around a Buried Pipe by X-Ray Technique", Proc. of 15th and 16th Annual Conference of JSSMFE, June 1980 and 1981.

38. Niyogi, BK. and J.S. Sethi, "Testing and Analysis of Buried Piping Under Applied Loads", Pressure Vessels and Piping Conference, San Francisco, CA, June, 1979, pvp-34, pp. 153-160.

39. Ohta, Y, N. Goto, H. Kagami and K. Shiono, "Shear Wave Velocity Measurement during a Standard Penetration Test", Earthquake Engineering and Structural Dynamics, Vol. 6, 1978, pp. 43-50.

40. Okamoto, S., "Introduction to Earthquake Engineering", John Wiley and Sons, Inc., New York, NY, 1973.

41. Okamoto, S. and C. Tamura, "Behavior of Subaqueous Tunnels During Earthquakes", Earthquake Engineering and Structural Dynamics, Vol. 1, 1973, pp. 253-266.

42. Okubo, T., Iwasaki, T., and Kawashima, K, Dense Instrument Array Program to the Public Works Research Institute and Preliminary Analysis of Some Records, 13th Joint Meeting of U.S.-Japan Panel on Wind and Seismic Effects, U.J.N.R., Tsukuba, Japan, May 1981.

43. Seed, H.B. and I.M. Idriss, "Influence of Soil Conditions on Ground Motions During Earthquakes", Journal of the Soil Mechanics and Foundation Division, ASCE, Vol. 95, No. SM1, Jan., 1969, pp. 99-137.

44. Singhal, A., "Experiments on Pipeline Joints", ASME PVP Conference, Paper #80-C2/PVP-70, Aug. 1980.

45. Suzuki, H., "Seismometer Array Observation Along A Gas Pipeline During the Miyagi-Ken-Oki Earthquake", Recent Advances in Lifeline Earthquake Engineering in Japan, The 1980 Pressure Vessels and Piping Conference, ASME, PVP-43, pp. 61-66.

46. Tokyo Electric Power Co. and Taisei Corporation, "Report on Aseismic Design of Buried Pipeline of Fuel Transportation", March 1979.

47. Wang, L.R.L., "Seismic Evaluation Model for Buried Lifelines", Proc. of the ASCE Specialty Conference on Lifeline Earthquake Engineering, Oakland, CA, Aug. 1981, pp. 335-347.

48. Wang, L.R.L., Kawashima, K, Yeh, Y.H. and Aizawa, K., Study of Ground Strains from Strong Motion Array Data for Lifeline Application, Technical Report No. LEE-003, NSF Grant No. CEE-8025172, Fears Structural Engineering Laboratory, University of Oklahoma, Dec. 1981.

49. Wang, L.R.L. and O'Rourke, M.J., "An Overview of Buried Pipelines Under Seismic Loading", Journal of Technical Council on Earthquake Engineering of ASCE, Vol. 104, No. TC-1, Nov. 1978 pp. 121-130.

50. Wataru, Y., "Vertical Earth Pressure on a Pipe in the Ground", Soils and Foundations, JSSMFE, Vol. 16, No. 2, June 1976.

51. Wootton, T.M., "State of California Strong Motion Instrumentation Program", The Current State of Knowledge of Lifeline Earthquake Engineering, Proceedings of Technical Council on Lifeline Earthquake Engineering Specialty Conference, 1977, pp. 378-382.

List of Technical Reports on Lifeline Earthquake Engineering

Sponsored by the National Science Foundation
Award No. CEE-8025172 and CEE-8209241

No. 1. Leon Ru-Liang Wang, Tadayoshi Okubo, Eiichi Kuribayashi, Toshio Iwasaki and Osamu Ueda
Lifeline Earthquake Engineering Literatures in Japan
October, 1982

No. 2. Leon Ru-Liang Wang
Tsukuba Science City and Its Magnificent Civil and Earthquake Engineering Research Facilities
November, 1982

No. 3. Leon Ru-Liang Wang, Kazuhiko Kawashima, Yaw-Huei Yeh and Koh Aizawa
Study of Ground Strains from Strong Motion Data for Lifeline Application
December, 1981

No. 4. Leon Ru-Liang Wang
Field Investigation and Analysis of Buried Pipelines Under Various Seismic Environments
June, 1982

No. 5. Leon Ru-Liang Wang and Yaw-Huei Yeh
Seismic Performance Evaluation of Lifelines
November, 1982 (Final Report for Award No. CEE-8025172)